INSTITUT FRANCAIS DE RECHERCHE SCIENTIFIQUE POUR LE DEVELOPPEMENT EN COOPERATION

Centre ORSTOM de Nouméa

PROGRAMME NATIONAL D'ETUDE DE LA DYNAMIQUE DU CLIMAT

TOGA - PACIFIQUE TROPICAL

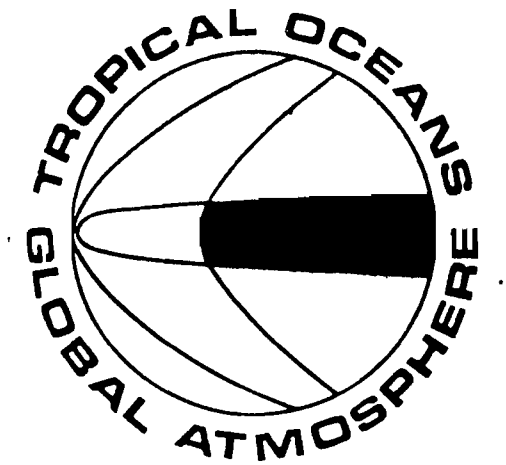

Rapport scientifique A S P 19.84.132

VALIDATION D'UN MODELE DU PACIFIQUE TROPICAL A L'AIDE DE DONNEES XBT MOUILLAGES CHAINES A THERMISTANCES

J. PICAUT *

avec la collaboration de :

M. J. McPHADEN **, A.J. BUSALACCHI ***, S. P. HAYES **

G. RAYMOND ****, R. TOURNIER *, J. MARCHAND *

Octobre 1987

* Centre ORSTOM de Nouméa , Nouvelle Calédonie

** NOAA / PMEL , Seattle , U.S.A.

*** NASA / Goddard Space Flight Center , Greenbelt , U.S.A.

**** University of Washington , Seattle , U.S.A.

SOMMAIRE

INTRODUCTION

Ces travaux de recherches ont reçu une aide finançière du PNEDC (Programme National d'Etude de le Dynamique du Climat) de 59.010F hors TVA pour les années 1985-1986. Ils font partie intégrante du programme international TOGA (Tropical Ocean and Global Atmosphere) dont les buts, rappelons le, sont les suivants:

- déterminer jusqu'à quel niveau la prédictabilité du système océans tropicaux-atmosphère globale est possible et en comprendre les mécanismes.

- étudier la possibilité de modéliser le système couplé océan-atmosphère dans le but de prévoir ses fluctuations.

- fournir les connaissances scientifiques de base pour développer et améliorer les réseaux d'observations et de transmission de données en vue de la prédiction du climat.

De part l'importance du phénomène ENSO (El Nino-Southern Oscillation) dans le Pacifique Tropical, la majorité des efforts de la communauté scientifique internationale porte en fait sur cette région Pacifique.

C'est donc sur la partie équatoriale de l'Océan Pacifique que nous avons mis en oeuvre un programme de recherches correspondant aux thèmes majeurs de TOGA et basé sur une collaboration très étroite avec plusieurs équipes américaines. Ce programme se partage en fait en deux opérations:

- La première utilise l'ensemble des données XBT du Pacifique Tropical pour valider un modèle numérique à partir de données XBT et accessoirement de niveau moyen.

- La deuxième consiste à mettre en place des mouillages équipés de chaînes à thermistances pour suivre en temps réel les variations thermiques de la bande équatoriale. Cette dernière opération n'ayant été vraiment financée côté français qu'à compter de fin 1986, il ne sera fait état, dans le présent rapport que des techniques de mouillages et de brefs résultats.

VALIDATION D'UN MODELE DU PACIFIQUE TROPICAL

Par validation, on entend une évaluation quantitative des comparaisons modèle-observations. Le modèle considéré est forçé par plusieurs jeux de vent afin de déterminer dans quelles limites les différences modèle-observations sont dues à des erreurs dans les champs de vent. Ce travail s'est fait en collaboration étroite avec M.J.McPhaden du NOAA/PMEL (Pacific Marine Environmental Laboratory), A.J.Busalacchi de NASA-Greenbelt et l'aide de G.Raymond de l'Université de Washington

à Seattle et de R.Tournier, allocataire de recherche MRES (Ministère de la Recherche et de l'Enseignement Supérieur) au Centre ORSTOM de Nouméa.

Notre propre travail, au Centre ORSTOM de Nouméa, a constitué surtout à mettre en place une véritable banque de données de température de subsurface. En effet, une première analyse objective des 16000 XBT, collectés par le groupe SURTROPAC (SURveillance TRansOcéanique du PACifique) du Centre ORSTOM de Nouméa depuis 1979, a montré que la densité spatio-temporelle de ces données est très insuffisante pour espérer construire un champ de température régulièrement réparti dans tout le Pacifique Equatorial. Même en se limitant aux trois principaux rails moyens de navigation, centrés dans l'ouest, le centre et l'est du Pacifique, la densité temporelle s'est encore avérée trop irrégulière pour espérer construire des séries temporelles assez complètes le long de ces trois rails moyens. De multiples demandes auprès des centres de recherche et banques de données de différents pays ont permis de réduire ce problème, en doublant le nombre total de profils XBT au voisinage de ces trois rails. La mauvaise qualité d'une partie de ces observations nous a contraints à mettre au point tout un ensemble de tests de validation, afin de construire, à partir d'une méthode d'analyse objective adaptée, des séries temporelles continues de la structure thermique le long de ces trois rails moyens, de 0 à 400m de profondeur. Les hauteurs dynamiques correspondantes ont été enfin calculées à partir des relations T-S moyennes issues du fichier climatologique de Levitus.

Ces préparations et analyses de données, ont été faites essentiellement à Nouméa. L'utilisation intensive de la messagerie électronique TELEMAIL et de nombreuses rencontres scientifiques (R.Tournier et J.Picaut à Seattle en novembre 1985, A.J.Busalacchi et M.J.McPhaden au Centre ORSTOM de Nouméa en novembre 1986, rencontre commune à la suite de la réunion de travail de l'US-TOGA à Honolulu en août 1986, J.Picaut à Seattle et Greenbelt en mai et août 1987 nous ont permis de coordonner efficacement la partie observation de ce programme avec ses parties modélisation et validation effectuées essentiellement aux Etats Unis. Les trois produits de vent forçant ce modèle ont été préparés, analysés et interpolés par M.J.McPhaden et G.Raymond à Seattle et A.J.Busalacchi a mis au point et fait tourner un modèle linéaire à quatre modes verticaux à Greenbelt. La partie validation proprement dite a été terminée à Seattle. Ce programme a donné lieu à deux articles qui ont été soumis à "Journal of Geophysical Research".

Le premier article montre que 25 à 50% de la variance du signal saisonnier, de la topographie dynamique de surface, peut être expliquée par la dynamique linéaire. Cet article met aussi en évidence l'imprécision des champs de vent actuels pour espérer reproduire avec précision les observations à travers les modèles numériques.

Le deuxième article s'attache par contre aux erreurs propres à la répartition géographique des données. En effet, il a été nécéssaire de supposer toutes les données XBT, encadrant de manière large un rail de navigation moyen, comme concentrées sur ce rail idéal. Il apparait que les distorsions, ainsi introduites, rendent caduque toute étude sur les XBT à une échelle inférieure à la période semi-annuelle.

MOUILLAGES CHAINES A THERMISTANCES

La deuxième partie de notre programme de recherches, implique directement S.P.Hayes du NOAA/PMEL de Seattle et son équipe de techniciens. Elle s'apparente plus aux programmes de réseaux d'observations en temps réel et fait appel à des techniques modernes de transmission par satellite de données issues de bouées ATLAS (Autonomous Temperature Line Acquisition System), équipées de chaînes à thermistances et de capteurs de vent.

Le besoin pour des séries continues de température de sub-surface et de vent à partir de mouillages a été reconnu et incorporé dans la planification du programme TOGA. Un réseau TOGA-TAO (Thermal Array for the Ocean) a été déployé au cours des premières années du programme TOGA. Il consiste principalement en lignes méridiennes de bouées ATLAS à 165°E, 140°W et 110°W, relevées à l'occasion des campagnes océanographiques régulières américaines, françaises et chinoises. En plus du suivi en temps réel du phénomène d'El Nino, les objectifs plus particuliers de ce réseau peuvent se résumer ainsi:

- améliorer la description des vents de surface dans la zone équatoriale

- saisir la variabilité basse fréquence de la structure thermique des couches proches de la surface dans les régions du guide d'ondes équatoriales.

- étudier le forçage local de vent en mesurant simultanément la distribution méridienne du champ de vent et la structure thermique des couches de sub-surface.

- étudier les effets des forçages éloignés et les ondes équatoriales en utilisant les mesures du champ thermique pour déterminer les propagations horizontales et verticales et les structures méridiennes.

- suivre le contenu thermique des couches de surface et le relier aux interactions air-mer.

- déterminer des indices de variations des transports géostrophiques zonaux et méridiens.

- fournir une description en temps réel des champs de vent et des couches de sub-surface dans des régions clés du Pacifique Tropical.

- permettre aussi d'affiner les expériences de validation de modèle comme la nôtre à l'aide de séries temporelles continues de température des couches de sub-surface et éventuellement assimiler ces séries temporelles dans ces modèles.

Dans le présent rapport nous présenterons le déroulement des opérations franco-américaines du réseau TAO le long du méridien 165°E et succintement les premiers résultats, la partie technique étant explicitée dans le rapport de stage au NOAA/PMEL de J.Marchand en décembre 1985.

VALIDATION D'UN MODELE DU PACIFIQUE TROPICAL

I. Comparisons of Observed and Simulated Mean Seasonal Cycles in Tropical Pacific Surface Dynamic Height and Sea Level

M.J. McPhaden[1]
A.J. Busalacchi[2]
J. Picaut[3]

[1]Pacific Marine Environmental Laboratory
National Oceanic and Atmospheric Administration
7600 Sand Point Way NE
Seattle, WA 98115-0070

[2]Laboratory for Oceans
NASA/Goddard Space Flight Center
Greenbelt, MD 20771

[3]Office de la Recherche Scientifique et Technique Outre Mer
Noumea, New Caledonia

Contribution No. 971 from NOAA/Pacific Marine Environmental Laboratory

Abstract

We examine simulations of the mean seasonal cycle in the tropical Pacific using a multi-vertical mode linear numerical model forced with FSU, SAWIN and FNOC surface wind stress products for the period 1979-1981. The model is run to equilibrium for each of four vertical modes and results are summed. Simulated mean seasonal cycles in dynamic height and sea level are then compared to observed variations based on XBT and tide guage data for the same 1979-1981 period.

All simulations show characteristic features of the mean meridional ridge/trough structure in surface topography. However, north and south equatorial ridges at 20°N and 20°S are much higher than observed, only weak equatorial ridges are generated near 4°N, and none of the simulations exhibits a significant equatorial trough. These discrepancies are due principally to limitations in model physics and in the wind forcing.

Observed and modeled mean seasonal variations in surface height are on the order of a few centimeters. Coherence estimates of 0.5-0.7 were found between the models and the observations for the 1 cycle per year harmonic which dominates the seasonal cycle over most of the tropical Pacific. This suggests that 25-50% of the variance in the observed seasonal surface height can be accounted for by linear dynamics given current estimates of the surface wind field. In a longitudinal sense, the eastern Pacific (south of 5°N) is the most poorly modeled due to weak local wind forcing, errors in wind analyses and model phase speeds tuned to the central and western Pacific. Latitudinally, variability in the equatorial zone (5°N to 5°S) is modeled better than either to the north or to the south because of the ocean is more sensitive to noise in the wind field at higher latitudes.

1. Introduction

Most model hindcasts of tropical Pacific Ocean variability have been restricted to the study of El Niño events. Busalacchi and O'Brien (1981), Busalacchi *et al.* (1983), and Busalacchi and Cane (1985) examined the sea level response of a linear model to estimates of wind field variability for specific years encompassing several major El Niños between 1961 and 1983. Cane (1984) used a linear model forced by composited wind anomalies to hindcast average El Niño conditions described in Rasmusson and Carpenter (1982). Quantitative assessments of these simulations were performed by testing the solutions against sea level time series from scattered island and coastal tide gauges. Qualitative comparisons of observed and modeled equatorial current and subsurface temperature time series from the 1982-1983 El Niño event have also been done with a more sophisticated ocean general circulation model (OGCM) (Philander and Siegel, 1985).

In view of the large interannual variability in the tropical Pacific, studies of the weaker mean seasonal cycle have been less frequent. Busalacchi and O'Brien (1980) and Gent (1985) have studied the response of linear models to climatological mean seasonal wind forcing and Philander *et al.* (1987) have done so with an OGCM. It is difficult however to assess the accuracy of these seasonal simulations in part because the climatology of the forcing functions for the models is not necessarily computed over the same period of time as the climatologies of the oceanic data used for comparison. Also, it is not clear to what extent simulations are adversely affected by surface wind stress errors, the magnitude and scales of which are generally not well known (e.g. see Halpern and Harrison, 1982). Furthermore, in evaluating model results, previous studies have relied on tide gauge data, current meter mooring data and/or hydrographic data that tend to be regionally limited in their

distribution. Thus, inferences about model performance are generally confined to point comparisons within a particular region and not the basin as a whole.

The purpose of this study therefore is to quantitatively evaluate simulations of the mean seasonal cycle in the tropical Pacific Ocean on a very broad scale to different specifications of wind stress forcing. The model used is a linear, multi-vertical mode version of the model used in Busalacchi and O'Brien (1980). The period of study will be 1979-1981 for which there are several coincident oceanic and surface wind data sets, as well as a fairly regular seasonal cycle leading into the 1982-83 El Niño. Mean seasonal dynamic height variations derived from an augmented version of the Ship-of-Opportunity (SOP) XBT data set will be compared with the model solutions. The XBT data are concentrated along heavily travelled shipping lanes in the eastern, central and western Pacific. Sea level data from the TOGA Pacific sea level network (Wyrtki, 1985), which is concentrated in the central and western Pacific, will also be used in this study. To permit as broad based a comparison as possible, the model will be forced by the mean seasonal cycle of surface wind stress from three distinct wind analyses for 1979-81; namely the FSU analysis (Goldenberg and O'Brien, 1981), the SAWIN analysis (Sadler and Kilonsky, 1985), and the FNOC analysis (Harrison, 1984). The differences among these wind products and how they affect the oceanic response will be of particular interest.

Results of these model studies have formed the basis for observing system simulation experiments in which the effects of aliased zonal variability have been evaluated (e.g. McPhaden *et al.*, 1987). Our results also provide background for studies of the 1982-1983 El Niño. Knowledge of the seasonal cycle is relevant for a definition of year-to-year anomalies, for a diagnosis

of processes involved in the generation, maintenance and decay of El Niño and for an examination of the phase locking of the El Niño anomalies to the annual cycle.

The plan for this paper is as follows. The oceanic data sets are described in Section 2 and the wind data sets used to force the model are discussed in Section 3. Basin-scale similarities and differences in the three wind products are noted. Model formulation and description of the basin-scale sea level responses to the FSU, SAWIN and FNOC wind fields are presented in Section 4. Intercomparisons between the ocean data and model solutions are discussed in Section 5. The principal result of this work is that about 25-50% of the variance of the mean seasonal cycle in dynamic height and sea level can be accounted for by linear dynamics. Longitudinally, the eastern Pacific (south of 5°N) is the most poorly modeled due to weak local wind forcing, errors in wind analyses and model phase speeds tuned to the central and western Pacific. Latitudinally, variability in the equatorial zone (5°N to 5°S) is better modeled than either to the north or to the south because of the ocean is more sensitive to noise in the wind field at higher latitudes. We also find that relative to the observed mean sea surface topography, simulated mean topographies exhibit a number of major discrepancies which can be related to limitations in model physics and in the wind forcing.

2. Oceanic Data

a. Ship-of-Opportunity XBT Data

In June 1979, The Office de la Recherche Scientifique et Technique Outre Mer (ORSTOM) of Noumea, New Caledonia and Scripps Institution of Oceanography (SIO) organized an XBT Ship-of-Opportunity (SOP) Program in the tropical Pacific Ocean (Donguy and Meyers, 1987). The program became fully operational.

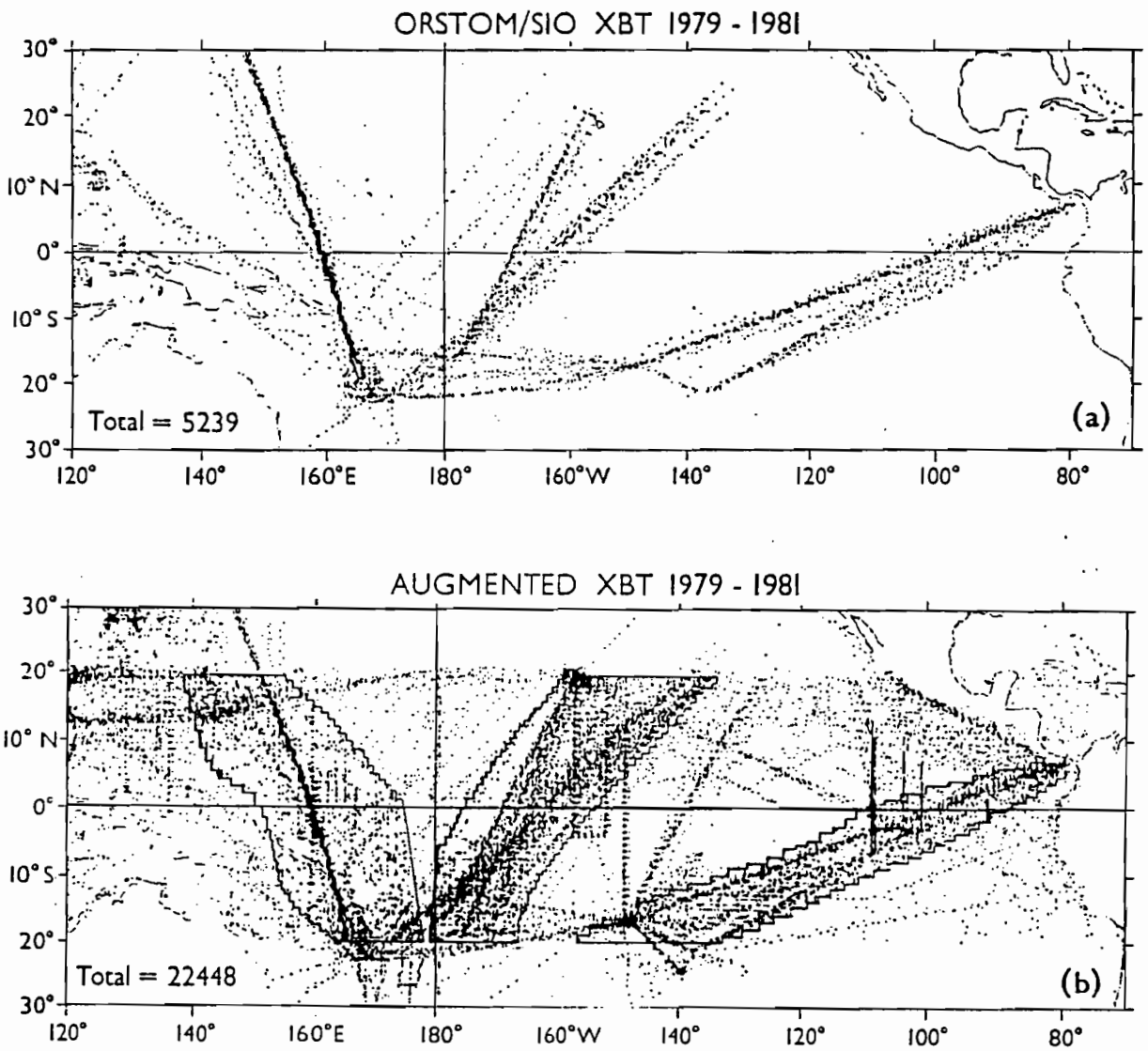

Fig. 1. Distribution of XBT data in the tropical Pacific for the period 1979-1981. a) Data from the ORSTOM/SIO Ship-of-Opportunity program; b) augmented XBT data set used in this study. Shaded areas in (b) indicate groupings of XBT data in the eastern, central and western Pacific.

in September 1980 between 20°N and 20°S and now provides XBT data routinely along several merchant ship lines as shown on Fig. 1a. However, there have been many gaps of 1 month or longer and several degrees of latitude due to problems with varying ship schedules, XBT supplies and XBT failures. For the purposes of our work and for a more complete analysis over the 1979-85 period, we have augmented the SOP data as much as possible in the region 70°W-120°E, 20°S-20°N. The augmented data set used in this study is shown in Fig. 1b. Details about data sources, quality control and objective analysis to a uniform latitude/depth grid along the three main XBT transects shown in Fig. 1b can be found in Picaut *et al.* (1987). A summary is presented here with special attention on the 1979-81 period of interest in the present study.

Five agencies responded to our requests for additional XBT data: the French Navy Hydrographic and Oceanographic Service (EPSHOM), Japan Oceanographic Data Center (JODC), the U.S. National Oceanographic Data Center (NODC), Commonwealth Scientific and Industrial Research Organization (CSIRO) of Australia and Scripps Institution of Oceanography. We also added some thermal CTD and hydrocast profiles from the ORSTOM-Noumea data base in order to fill notable data gaps as occurred in the first half of 1979. Table 1 shows the number of thermal profiles per agency in our augmented file after elimination of duplicate data. For 1979-1981, we more than quadrupled (to 22448) the number of data available from the ORSTOM/SIO SOP program (5239).

Despite such augmentation in data coverage, data are still mostly concentrated along the main shipping lines. Thus, we have chosen to analyze the data in vertical sections, as Kessler and Taft (1987) did in the central Pacific, rather than to interpolate to a four-dimensional grid. We have grouped the data on a monthly basis without regard to longitude in the three

Table 1. List of sources and numbers of casts of thermal data that contributed to the augmented data set show in Fig. 1b. Sources in addition to the ORSTOM/SIO Ship-of-Opportunity XBT program are the French Navy Hydrographic and Oceanographic Service (EPSHOM), Japan Oceanographic Data Center (JODC), the U.S. National Oceanographic Data Center (NODC), Scripps Institution of Oceanography (SIO), Commonwealth Scientific and Industrial Research Organization (CSIRO), and thermal CTD and hydrocast profiles from ORSTOM-Noumea (ORSTOM).

Agency\ Year	1979	1980	1981	Total
ORSTOM/SIO	792	1902	2545	5239
EPSHOM	816	725	397	1938
JODC	360	112	135	607
NODC	2376	2665	2092	7133
SIO	2430	2562	1401	6393
ORSTOM	981	48	109	1138
Total	7755	8014	6679	22,448

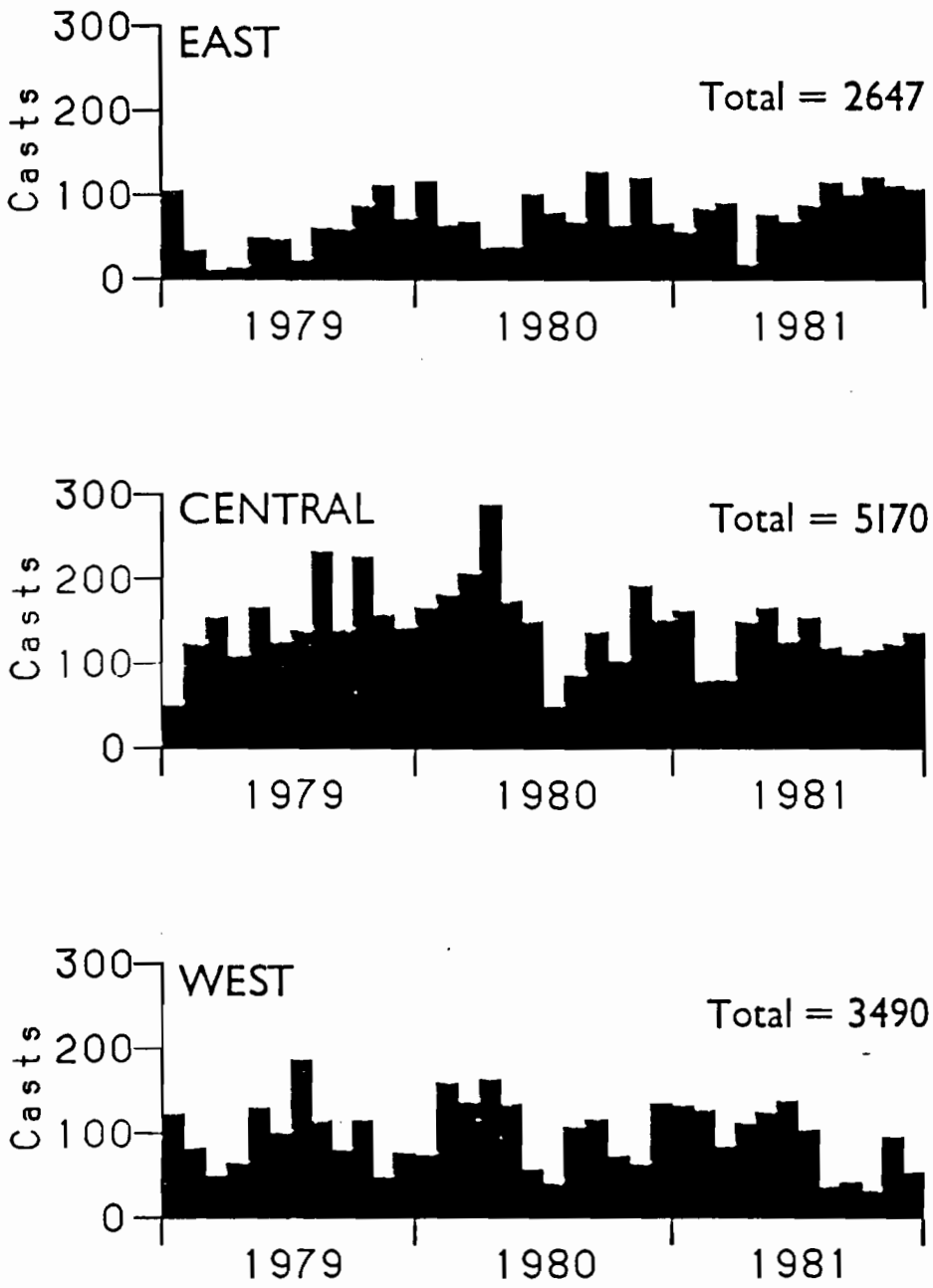

Fig. 2. Data distribution as a function of time in the eastern, central and western Pacific for the augmented XBT data set shown in Fig. 1b.

regions outlined in Fig. 1b in the eastern, central and western Pacific. Each region has been subjectively determined so that there is a minimum of one XBT per month per 1 degree latitude band. The average data density is 2.4, 3.6 and 2.7 XBT/month/degree latitude in the eastern, central and western regions, respectively. The large western region is explained by the fact that after March 1983 the single direct Noumea-Japan track was replaced by two tracks displaced from the main route. The deepest depth considered is 400 m since 76% of the XBTs reach this depth as opposed to only 62% that reach 450 m. Figure 2 shows that the data distribution in time over the three regions is fairly erratic, with a slight trend toward increasing data density in the eastern Pacific and a slight trend towards decreasing data density in the central Pacific.

Several levels of subjective and objective quality control were applied to the temperature data (Picaut *et al.*, 1987) before gridding in latitude and depth. Vertical sections were then smoothed by fitting the data at each depth to least squares determined Fourier components and eliminating all wavenumbers higher than 0.33 cycles per degree of latitude. No smoothing in time was performed on the monthly data.

A dynamic height field relative to 400 db was derived from temperature using a mean T-S relationship from Levitus (1982). This is a simpler scheme than the one used in Kessler and Taft (1987) which made use of observed SOP sea surface salinities. We found that their method does not necessarily improve dynamic height estimates in the western Pacific where the mixed layers in salinity and temperature do not always coincide (Delcroix *et al.*, 1987).

Errors in dynamic height calculations due to the use of a mean T-S relation are probably 1-2 dynamic cm. Grouping the data along transects without regard to longitude probably results in an additional error of

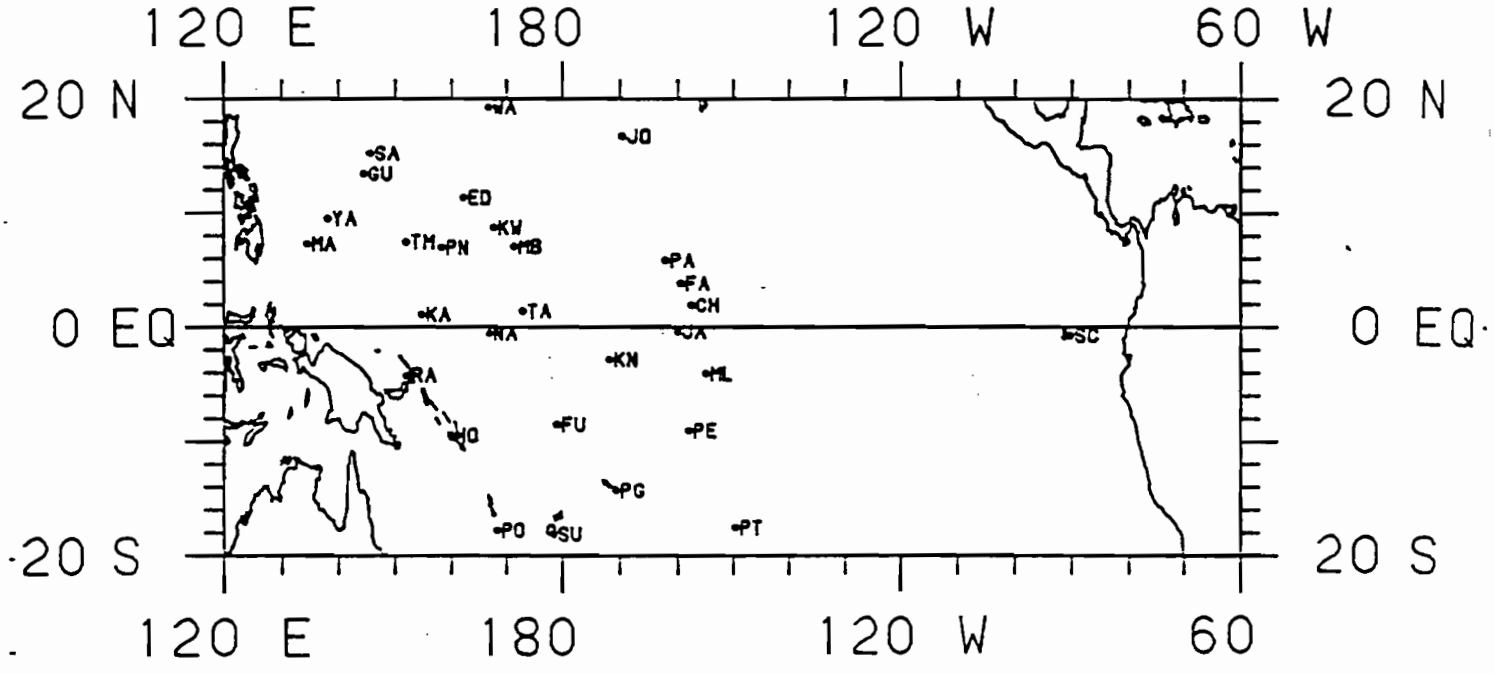

Fig. 3. Distribution of island sea level stations in the tropical Pacific. Islands are Christmas (CH), Enewetok (ED), Fanning (FA), Funafuti (FU), Guam (GU), Honiara (HO), Jarvis (JA), Johnston (JO), Kapingimarangi (KA), Kanton (KN), Kwajalein (KW), Malakal (MA), Majoro (MB), Malden (ML), Nauru (NA), Palmyra (PA), Penrhyn (PE), Pago Pago (PG), Ponape (PN), Port Villa (PO), Papeete (PT), Rabaul (RA), Saipan (SA), Santa Cruz (SC), Suva (SU), Tawara (TA), Truk (TM), Wake (WA), Yap (YA).

2 dynamic cm (McPhaden *et al.*, 1987). This error can be larger where data are separated by more 20 degrees of longitude as occurs poleward of 15°N in the central Pacific. Errors due to aliased internal waves, unstable 20-30 day waves and other high frequency phenomena (e.g. Hayes, 1982; Hayes and McPhaden, 1987) may be 1-2 dyn cm. Estimates of the mean seasonal cycle can also be affected by year-to-year variations. These errors, to the extent that they are random, will be reduced by averaging in latitude and time, so that we expect uncertainties in our mean monthly dynamic heights to be about 2 dynamic cm.

b. Sea Level Data

The shallow thermocline and the baroclinic nature of seasonal variability in the tropics means that sea level and dynamic height relative to 400 db are well correlated in our study region (e.g. Rebert *et al.*, 1985). Thus, we have augmented the XBT data with a complementary data set from the TOGA island sea level network (Wyrtki, 1985) for the period 1979-1981. Tide gauge data were processed to monthly means for each of 29 island stations shown in Fig. 3. Data are concentrated in the western and central Pacific with Santa Cruz in the Galápagos being the only instrumented island east of 150°W. Median record length for all island stations is 33 months and the shortest record is 15 months at Malden Island. Expected error in monthly mean sea level is about 1 cm.

3. Wind Data

Wind data to drive the model have been chosen from the same years used to form the seasonal mean of the XBT and sea level observations, i.e. 1979-1981. This helps to eliminate ambiguities that result from comparing

seasonal means of oceanographic observations taken at one period of time with model solutions forced by climatological winds from another time. Moreover, we have chosen to utilize three wind products to enable an interpretation as to how some of the differences between the model solutions and the observations result from uncertainties in the analyzed wind data.

The model integrations are performed using three wind stress products for which monthly means are currently available for January, 1979 through December, 1981. Two of these data sets are derived from subjective analyses and the third from an operational objective analysis. One subjective analysis is the Florida State University (FSU) analysis of ship wind observations provided by James J. O'Brien. The analysis procedure of transforming individual ship-board observations into wind stress fields on a 2° × 2° grid is described by Goldenberg and O'Brien (1981). Data density is generally adequate for determination of monthly mean wind stress, although ship wind data are very sparse (less than 4 observations per month per 2° latitude by 10° longitude box) in the southeastern tropical Pacific and in a broad area in the equatorial Pacific stretching from the dateline to 110°W. The other subjective analysis is a combination of satellite-observed, low-level cloud motions east of the dateline, ship wind observations, island wind observations, and buoy wind observations performed by James Sadler at the University of Hawaii. This derivation of monthly mean surface winds on a 2.5° × 2.5° grid from satellite observations of low-level cloud drift (referred to hereafter as SAWIN) is described in Sadler and Kilonsky (1985). Cloud motion vectors are extrapolated to the surface using a climatological estimate of boundary layer shear; west of the dateline the analysis only utilizes surface observations, since no cloud motion vectors were available in the western Pacific during 1979-1981. The third data set we use is an

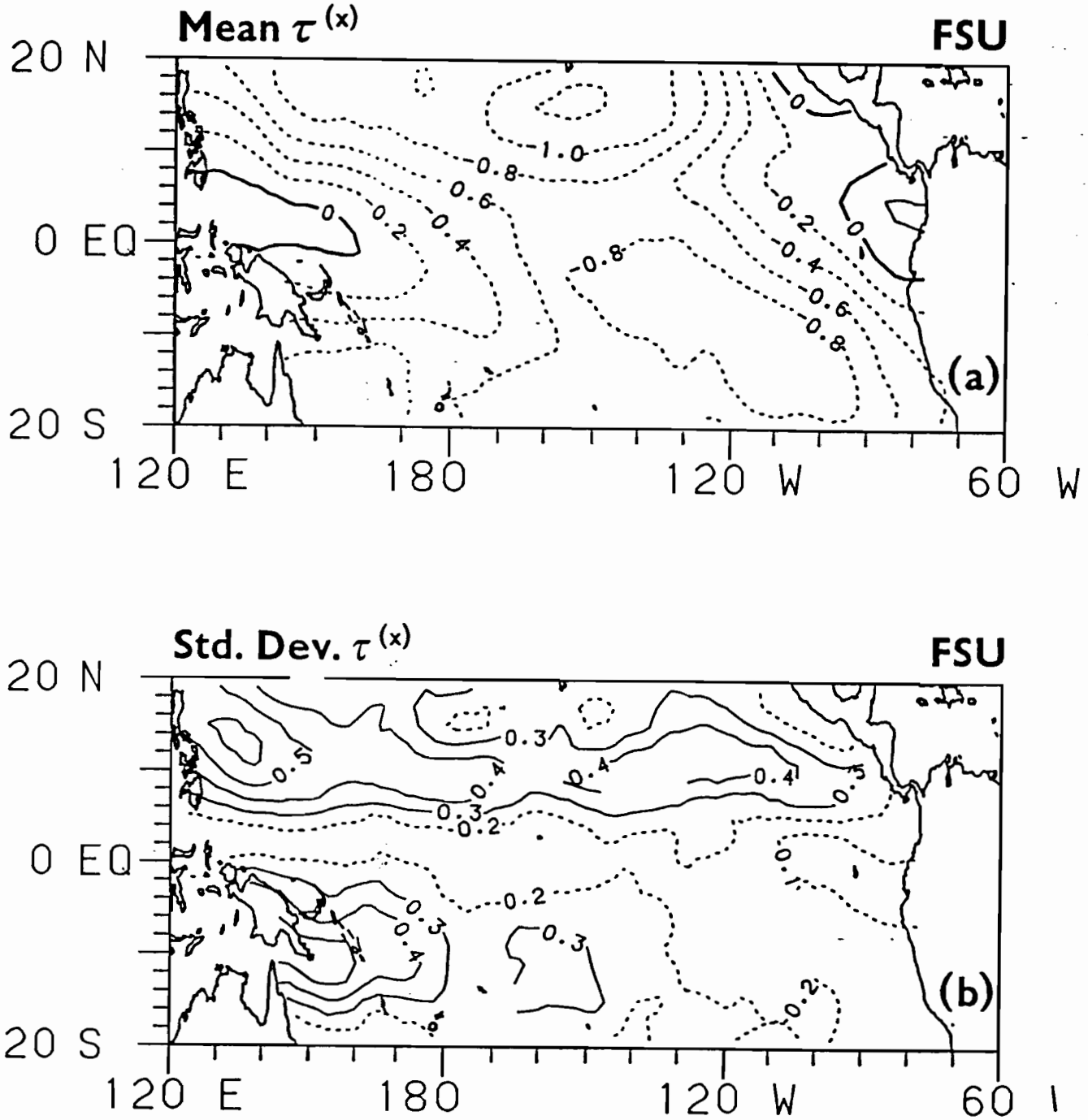

Fig. 4. FSU zonal wind stress a) mean and b) seasonal standard deviation; SAWIN zonal wind stress c) mean and d) seasonal standard deviation; FNOC zonal wind stress e) mean and f) seasonal standard deviation. Contours are in dyne cm^{-2}. Dashed contours in (b), (d) and (f) indicate regions where stress variability is less than 0.2 dyne cm^{-2}.

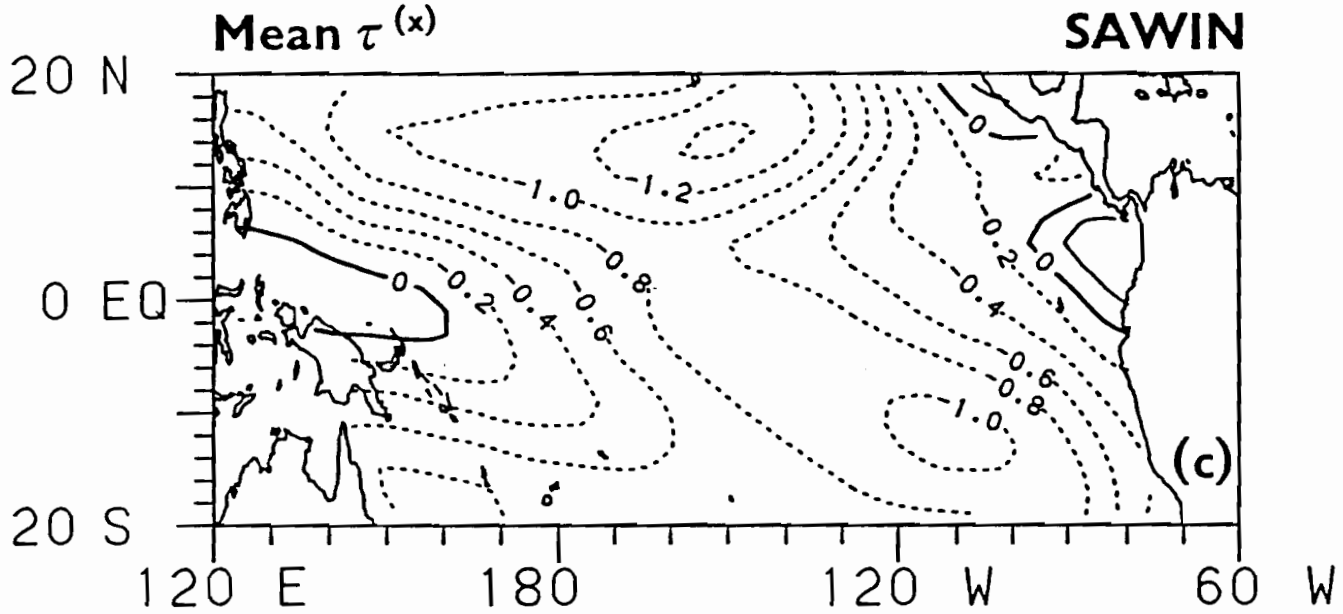
Mean τ (x)
SAWIN
20 N
0 EQ
20 S
120 E
180
120 W
60 W
(c)

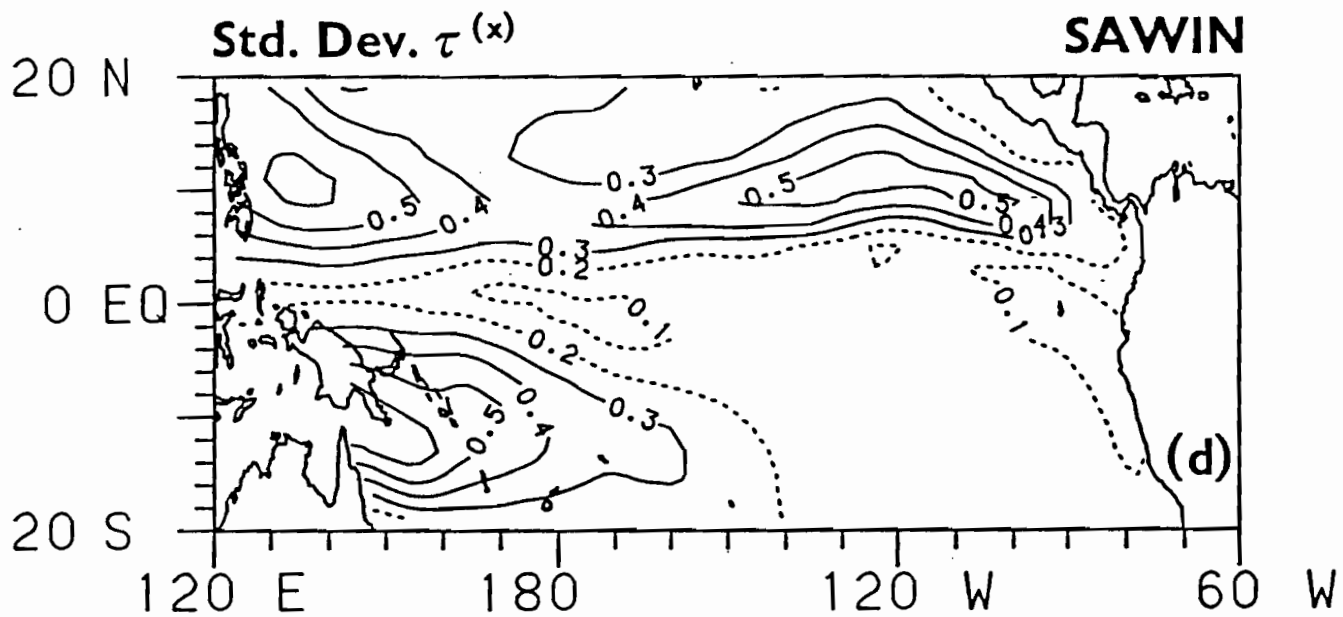
Std. Dev. τ (x)
SAWIN
20 N
0 EQ
20 S
120 E
180
120 W
60 W
(d)

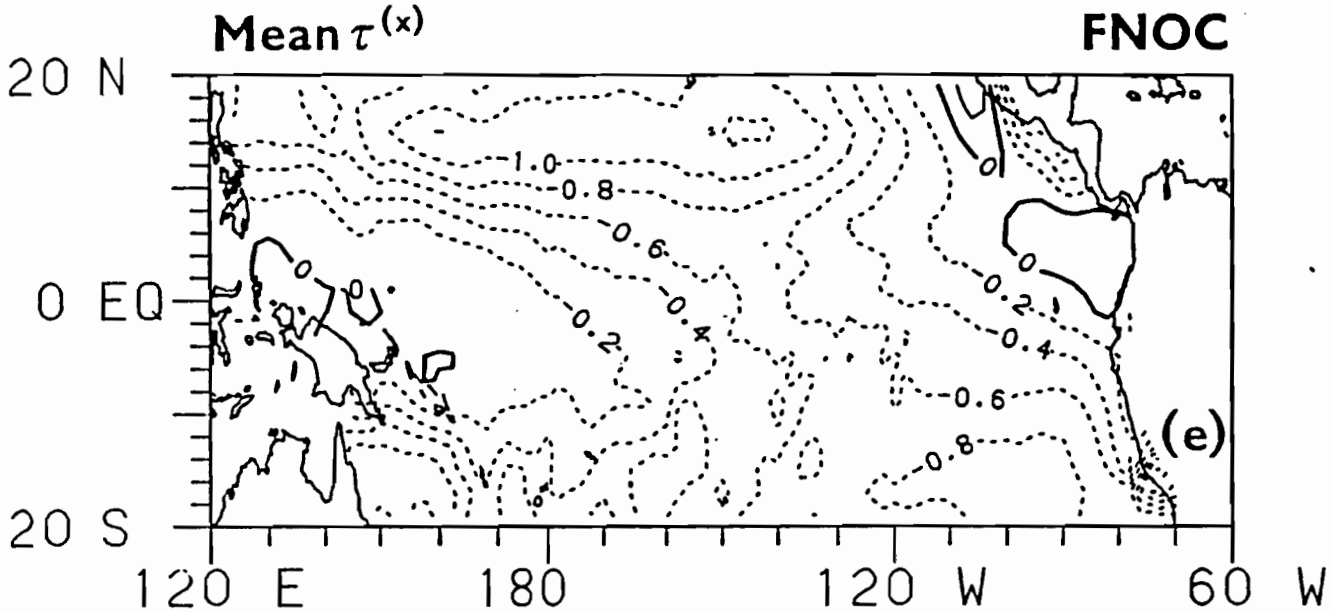
Mean $\tau^{(x)}$
FNOC
20 N
0 EQ
20 S
120 E
180
120 W
60 W
1.0
0.8
0.6
0.4
0.2
0
0.2
0.4
0.6
0.8
(e)

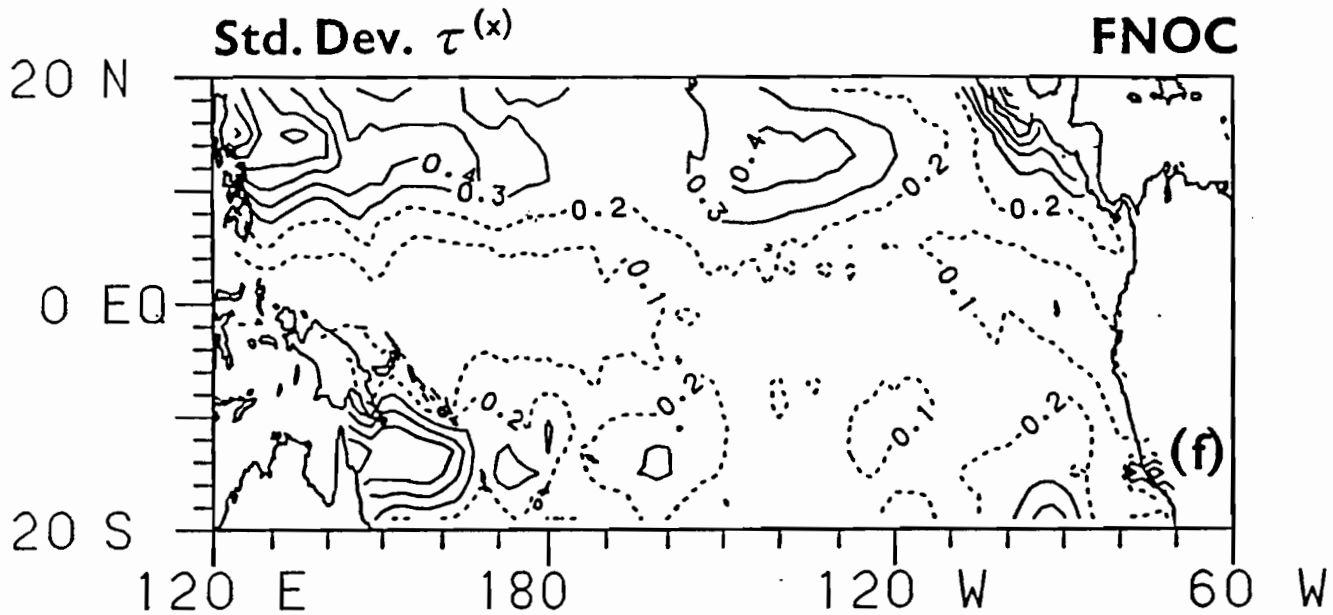
Std. Dev. $\tau^{(x)}$
FNOC
20 N
0 EQ
20 S
120 E
180
120 W
60 W
0.4
0.3
0.2
0.1
0.2
0.3
0.4
0.2
0.1
0.2
0.1
0.2
(f)

objectively analyzed, operational product from the Global Band Analyses of the United States Navy's Fleet Numerical Oceanography Center (FNOC) (Harrison, 1984). An objective analysis based on Cressman (1959) is used on all reports (ship, island, buoy, etc.) in an operational data base for six hour intervals on a 2.5° × 2.5° grid. Detailed comparison of the three wind products for November 1979 appears in Halpern and Harrison (1982).

From each of these wind products the data from 1979-1981 have been used to form the 12 monthly means representing the mean seasonal cycle for this period. In the present study, a constant drag coefficient of 1.5×10^{-3} and constant air density of 1.2 kg m^{-3} are used to convert from wind to wind stress for all three data sets. The uncertainty in the drag coefficient is about 10-20% (e.g. Large and Pond, 1981) implying an amplitude uncertainty in the model response of this amount.

The mean and standard deviation of each seasonal cycle are presented for the zonal wind stress (Fig. 4), meridional wind stress (Fig. 5), and wind stress curl (Fig. 6). Similar large-scale features are found in all the mean zonal wind stress fields (Figs. 4a, c, e) and meridional wind stress fields (Figs. 5a, c, e). The Northeast and Southeast Trade Winds are dominant over most of the basin. Core regions of the Trades lie poleward of 10° whereas weak, mean westerlies are found equatorward of 10° at the extreme ends of the basin. Mean SAWIN easterlies are typically the strongest and FNOC easterlies the weakest; mean FNOC wind stress has the most small-scale structure, particularly within coastal regions, whereas the SAWIN product is the smoothest. The smoothness of the SAWIN product does not necessarily imply that it is a more accurate wind analysis. Rather, it reflects a bias of the analyst to smooth out small scale features in order to emphasize the largest scales of variability. An interesting qualitative difference between the mean

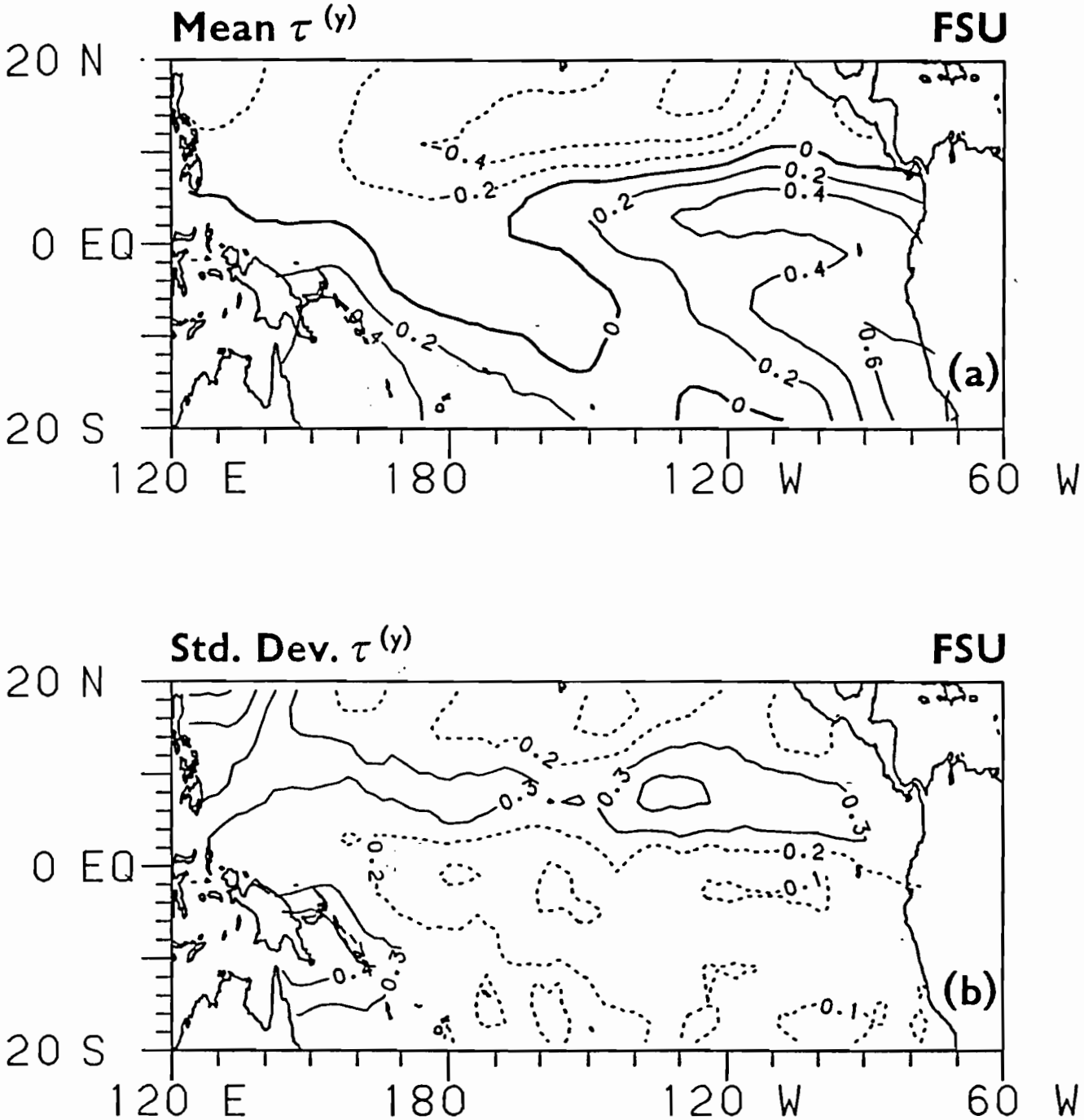

Fig. 5. Same as in Fig. 4, but for meridional wind stress.

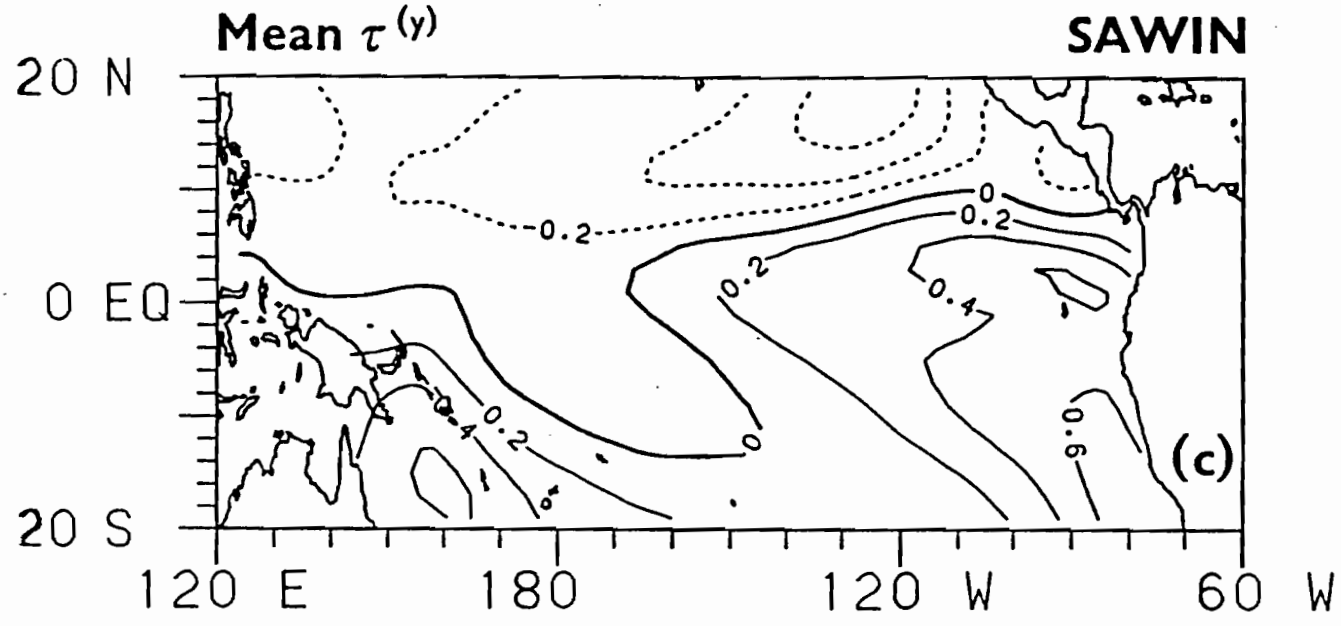
Mean $\tau^{(y)}$
SAWIN
20 N
0 EQ
20 S
120 E
180
120 W
60 W
-0.2
0
0.2
0.2
0.4
0.2
0
0.6
(c)

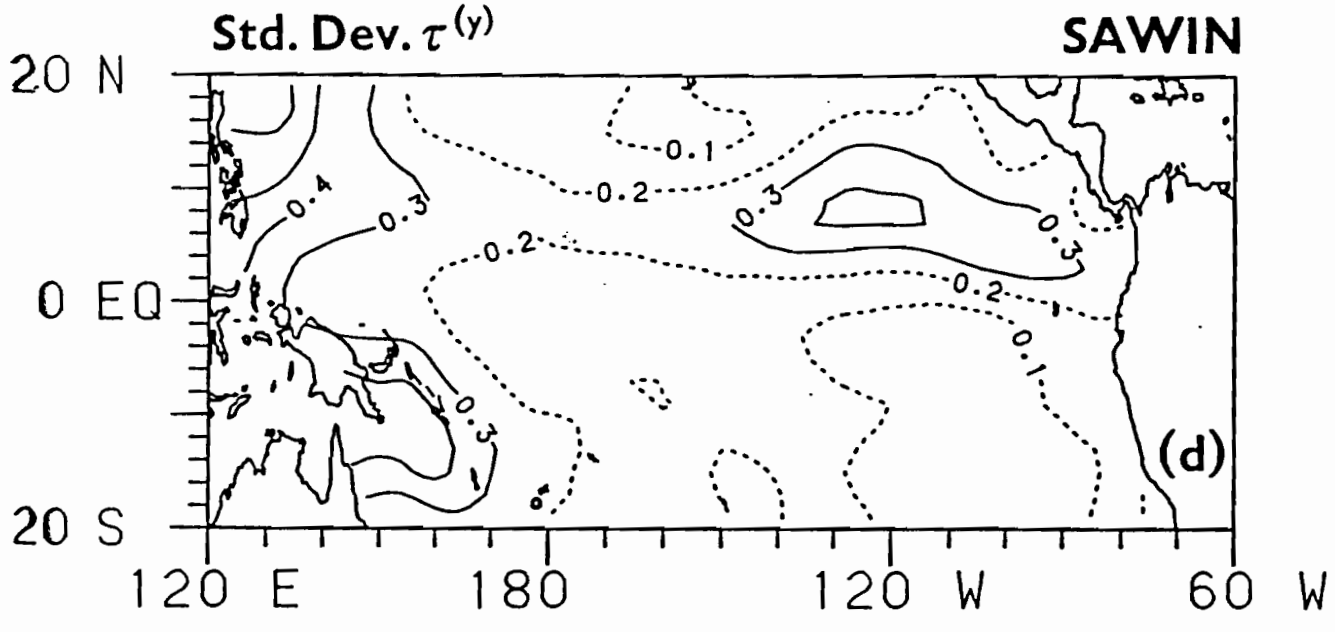
Std. Dev. $\tau^{(y)}$
SAWIN
20 N
0 EQ
20 S
120 E
180
120 W
60 W
0.1
0.2
0.4
0.3
0.2
0.3
0.3
0.2
0.1
0.3
(d)

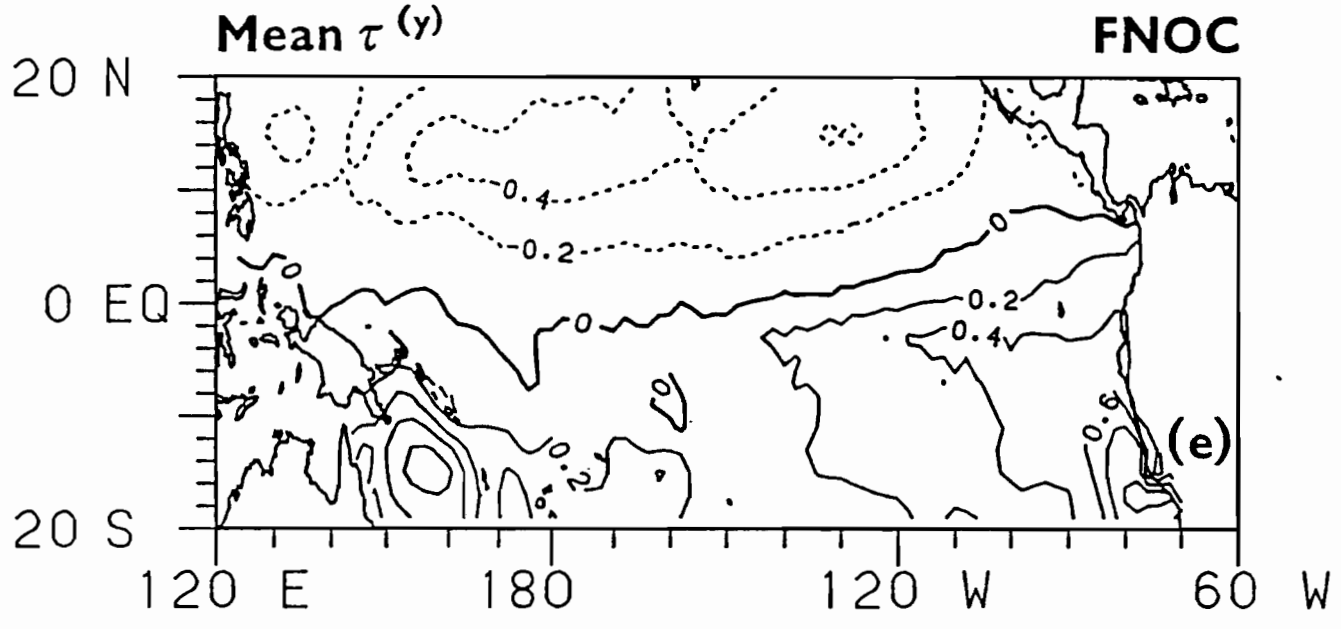
Mean τ (y)
FNOC
20 N
0 EQ
20 S
120 E
180
120 W
60 W
0.4
0.2
0
0.2
0.4
0.6
(e)

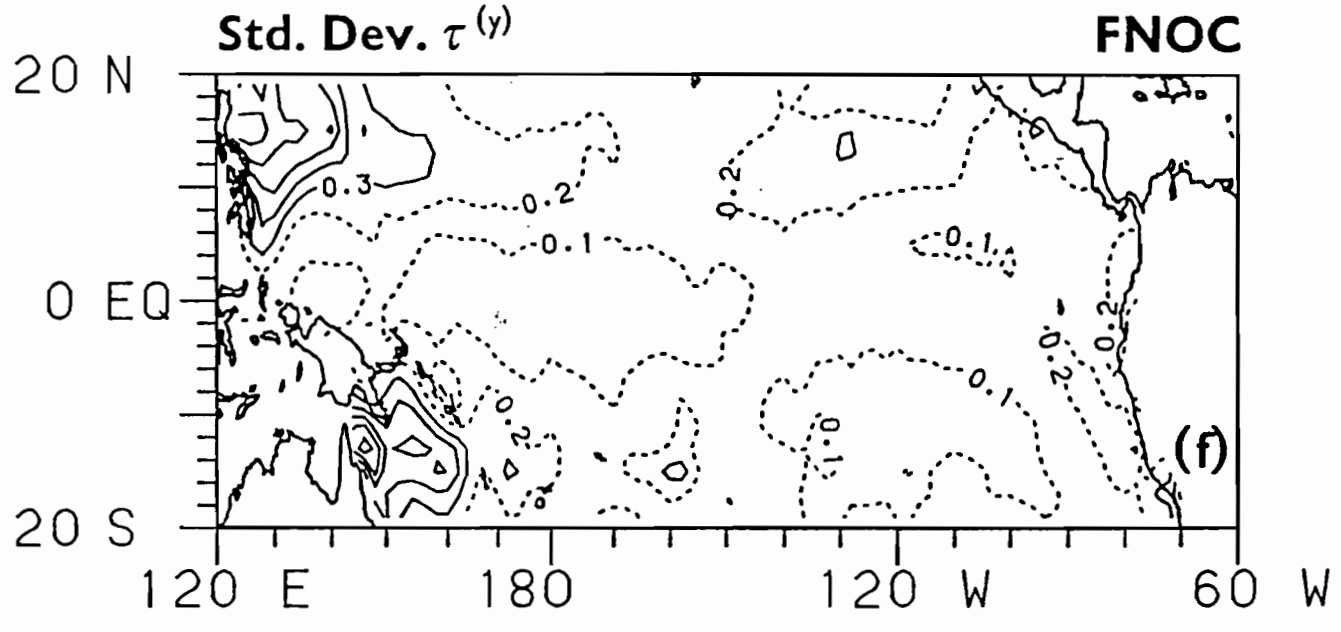
Std. Dev. τ (y)
FNOC
20 N
0 EQ
20 S
120 E
180
120 W
60 W
0.3
0.2
0.1
0
0.2
0.1
0.2
0.1
0.2
0.1
0.2
(f)

meridional winds is the position of the zero contour which, in the eastern and central Pacific, delineates the approximate location of the Intertropical Convergence Zone (ITCZ) between the Northeast and Southeast Trades. In the FNOC winds this contour is several degrees closer to the equator than in the SAWIN or FSU analyses.

The mean FSU and SAWIN curl fields (Fig. 6a and 6c) have similar spatial structures though SAWIN curls are slightly larger and smoother. Both are characterized by a zonal band of positive curl in the northern hemisphere between about 4°N and 12°N; in the southern hemisphere a region of positive curl oriented NW-SE separates two regions of negative curl. The mean curl distribution for the FNOC product (Fig. 6e) is very different. The small-scale structure in the mean FNOC zonal and meridional wind stress fields is amplified in the curl field and tends to obscure the large-scale structure.

The variability of the seasonal cycle for zonal and meridional wind stress is summarized in the maps of the standard deviations in Fig. 4b, d, f and 5b, d, f. The annual excursion of the ITCZ appears as maxima of 0.2-0.4 dynes cm^{-2} between 5°-15°N east of the dateline in these fields. Maxima associated with monsoon variability over the far northwestern and southwestern Pacific are also robust features in all three wind products. In marked contrast, the near equatorial band (5°N-5°S) and the southeastern quandrant of the tropical Pacific exhibit relatively weak seasonal change. As in the mean fields, the FNOC standard deviation plots show more small-scale structure. The SAWIN data generally have larger amplitudes, except near the coasts of Central America, Australia and Southeast Asia where the FNOC winds are significantly stronger. In all three wind fields, sixty to eighty percent of the variability in the seasonal cycle is due to the annual harmonic.

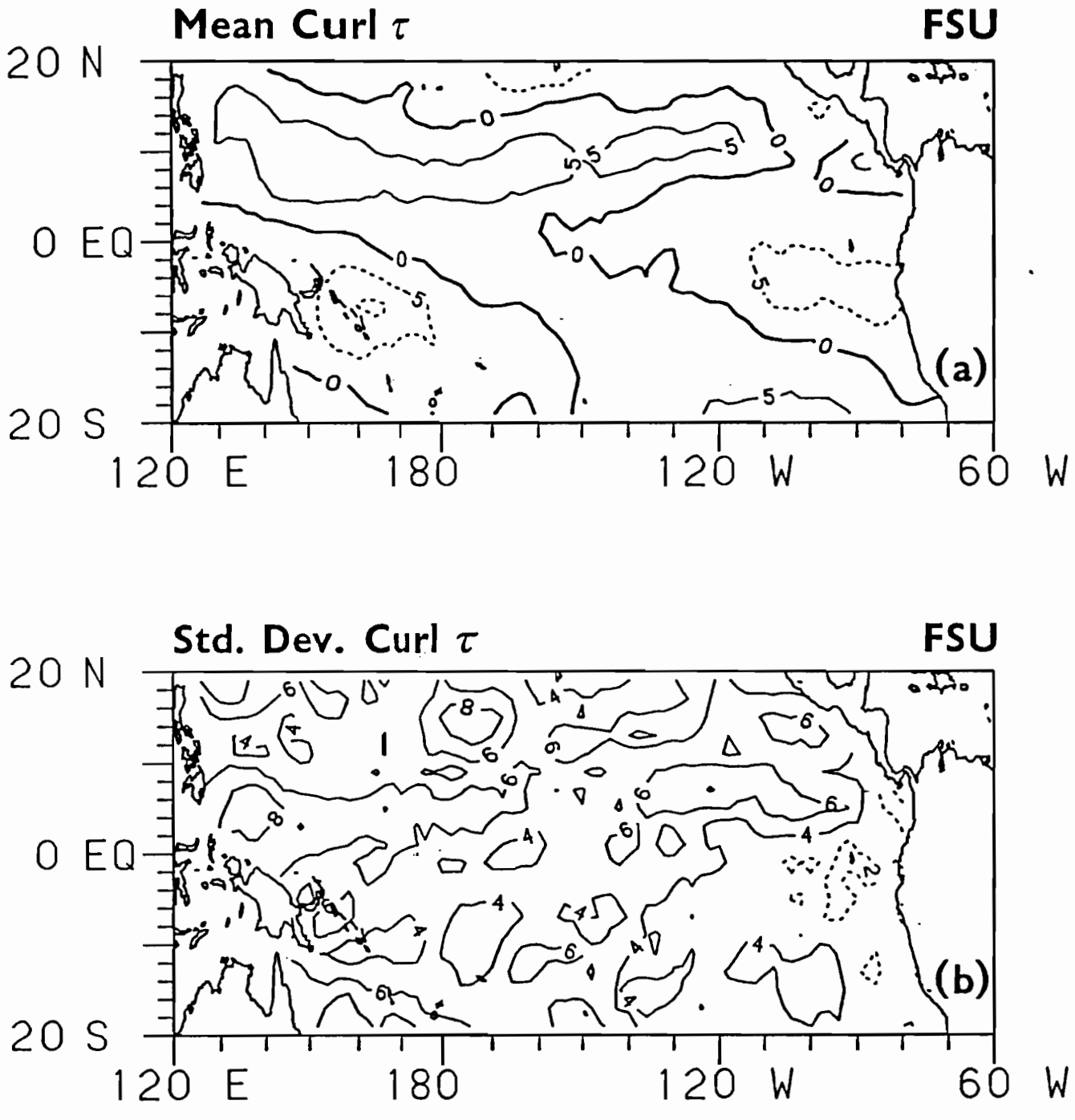

Fig. 6. Same as in Fig. 4, but for wind stress curl (in 10^{-9} dyne cm^{-3}). Dashed contours in (b), (d) and (f) indicate regions where curl variability is less than 2×10^{-9}dyne cm^{-3}.

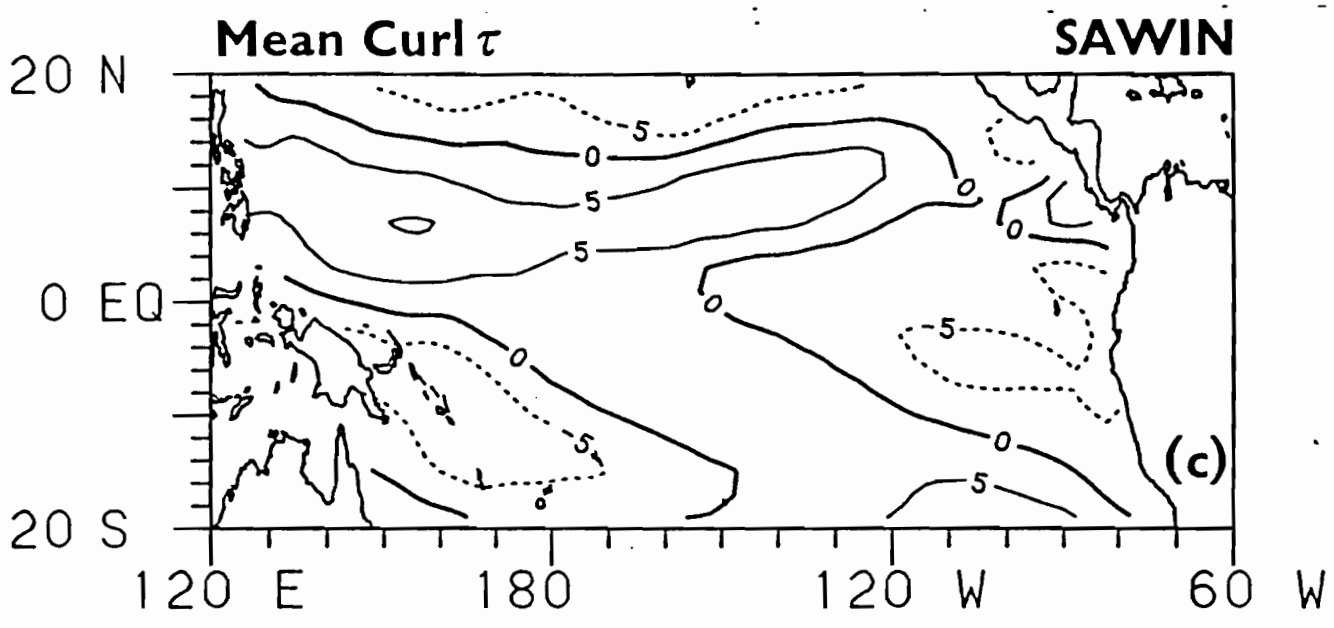
Mean Curl τ
SAWIN
20 N
0 EQ
20 S
120 E
180
120 W
60 W
(c)

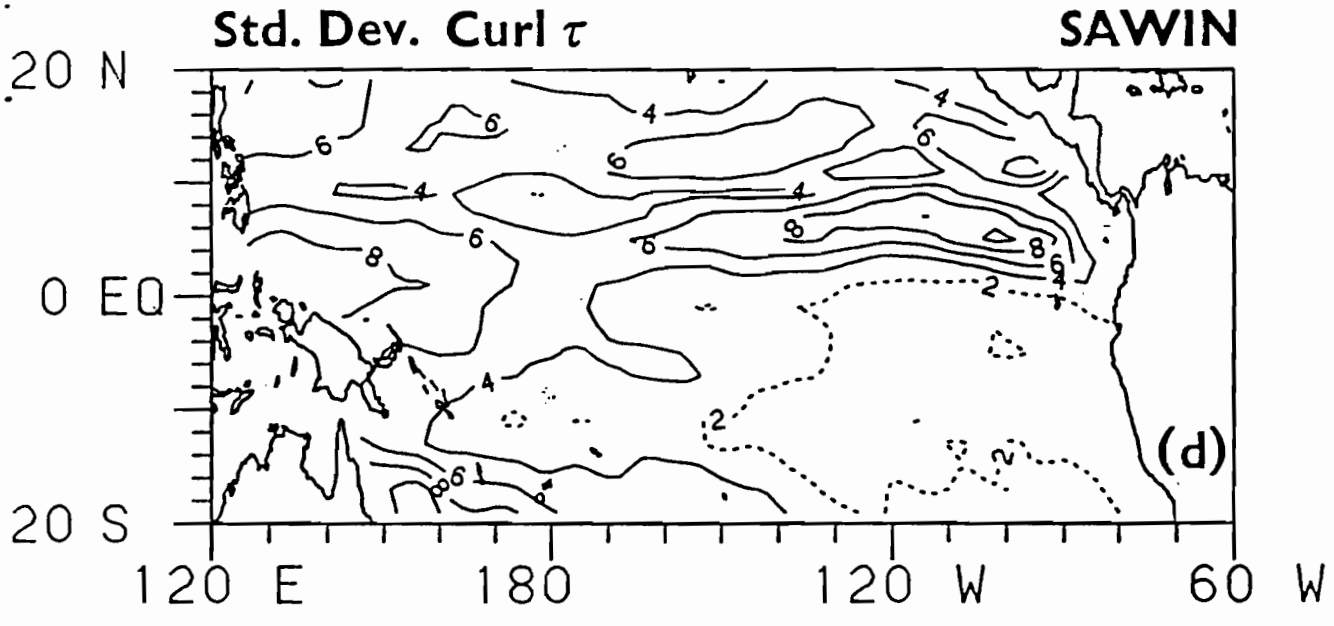
Std. Dev. Curl τ
SAWIN
20 N
0 EQ
20 S
120 E
180
120 W
60 W
(d)

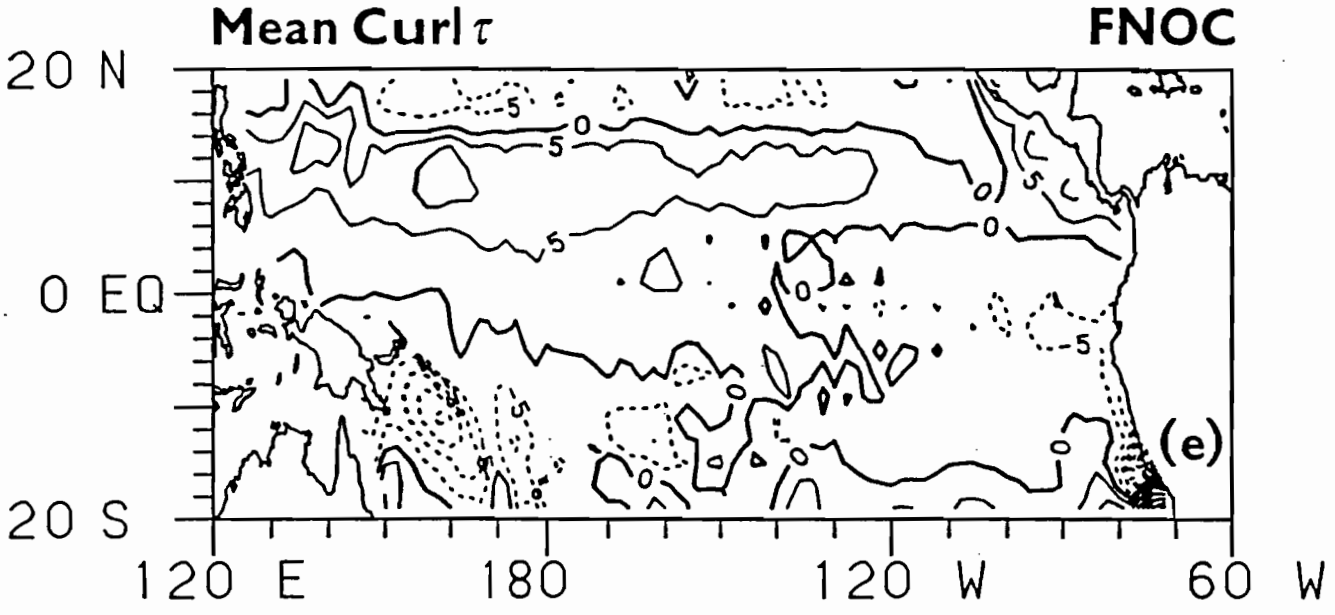
Mean Curl τ
FNOC
20 N
0 EQ
20 S
120 E
180
120 W
60 W
(e)

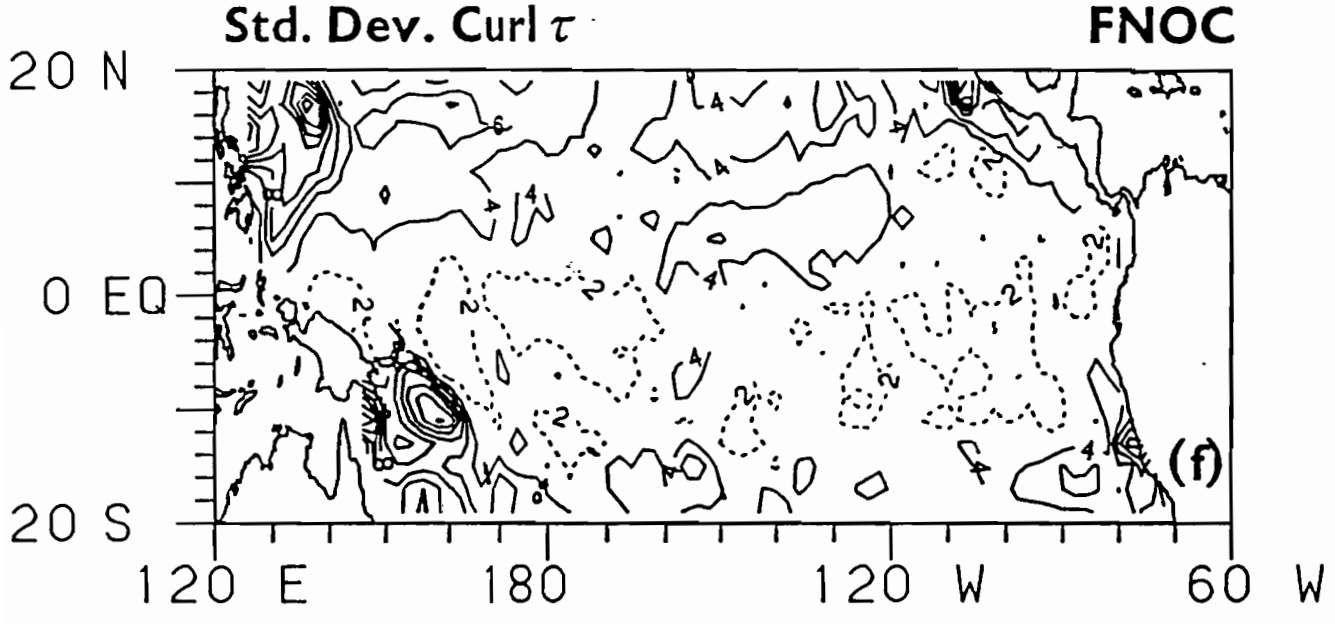
Std. Dev. Curl τ
FNOC
20 N
0 EQ
20 S
120 E
180
120 W
60 W
(f)

As expected, the standard deviations of the wind stress curl (Figs. 6b, d, f) reflect the variability of the individual wind stress components discussed above. The dominant features in the SAWIN curl field are zonally oriented extrema on either side of the mean position of the ITCZ and a broad region of weak curl in the southeastern tropical Pacific. By comparison, the FSU and FNOC curl fields show much greater small scale variability, much (but perhaps not all) of which is noise related. However, the patterns of weak variability in the southeastern quadrant and maxima on either side of the ITCZ in the eastern and central Pacific appear in all three analyses.

4. Modeling Approach

The model used in this study is similar to that employed by Busalacchi and O'Brien (1980). A linear, numerical treatment of the shallow water wave equations is used to analyze the seasonal dynamic response of a model tropical Pacific Ocean to different representations of the surface wind stress. Changes to the previous version of the model include increased horizontal resolution of 40 km between like variables and a horizontal Laplacian friction of 10^7 cm^2 s^{-1}. Sensitivity studies for the value of friction indicate little quantitative difference for changes to a factor of five. The model basin extends from 20°N to 20°S and 126°E to 70°W. Open boundary conditions are applied at the northern and southern boundaries (Roed and Smedstad, 1984) and a no-slip condition is imposed along the idealized coastal boundaries.

Busalacchi and Cane (1985) determined that at least two vertical modes are necessary to simulate sea level amplitudes on seasonal time scales in the equatorial waveguide. Hence, we generated model height field solutions for the four gravest baroclinic modes of a Brunt-Vaisala frequency profile based

on CTD data between 1.5°N and 1.5°S at 179°W as presented by Eriksen *et al.* (1983). This profile was used because it is located in the equatorial wave guide in a region with significant wind stress fluctuations on seasonal and interannual time scales. The internal wave speeds for the four vertical modes are $c_1 = 2.90$ m s^{-1}, $c_2 = 1.77$ m s^{-1}, $c_3 = 1.13$ m s^{-1}, and $c_4 = 0.84$ m s^{-1}. A final solution is found by summing the individual contributions of all four modes. Modes 1 and 2 contribute most significantly to our results as in Busalacchi and Cane (1985).

Due to the range of the wave speeds, the time step of the model is mode dependent. All mode 1 calculations have a 1 hour time step whereas the slower speeds of modes 2-4 permit a 2 hour time step without compromising numerical stability. Similarly, the time required for initial transients to die out during spin-up is mode dependent. Beginning from a state of no motion and in response to the mean seasonal wind stress, an exact repeating seasonal cycle is obtained basin-wide after a spin-up of 12 years for mode 1, 22 years for mode 2, 42 years for mode 3, and 62 years for mode 4. All the results that follow are taken from the last year of integration for each mode.

The mean sea levels modeled in response to these wind forcings are presented in Fig. 7a (FSU), Fig. 8a (SAWIN), and Fig. 9a (FNOC). The sea level distributions are characterized by a system of zonally oriented troughs and ridges delineating major geostrophic currents in the model solutions. Between the sea level ridge at 20°N and the trough at 9°N flows a westward directed North Equatorial Current (NEC). An eastward flowing North Equatorial Countercurrent (NECC) is flanked by the NECC trough to the north (9°N) and a weak equatorial ridge to the south (2-4°N). This mean structure in the northern hemisphere is similar in all three solutions reflecting large-scale similarities in the mean wind stress curl off the equator. Notably absent in

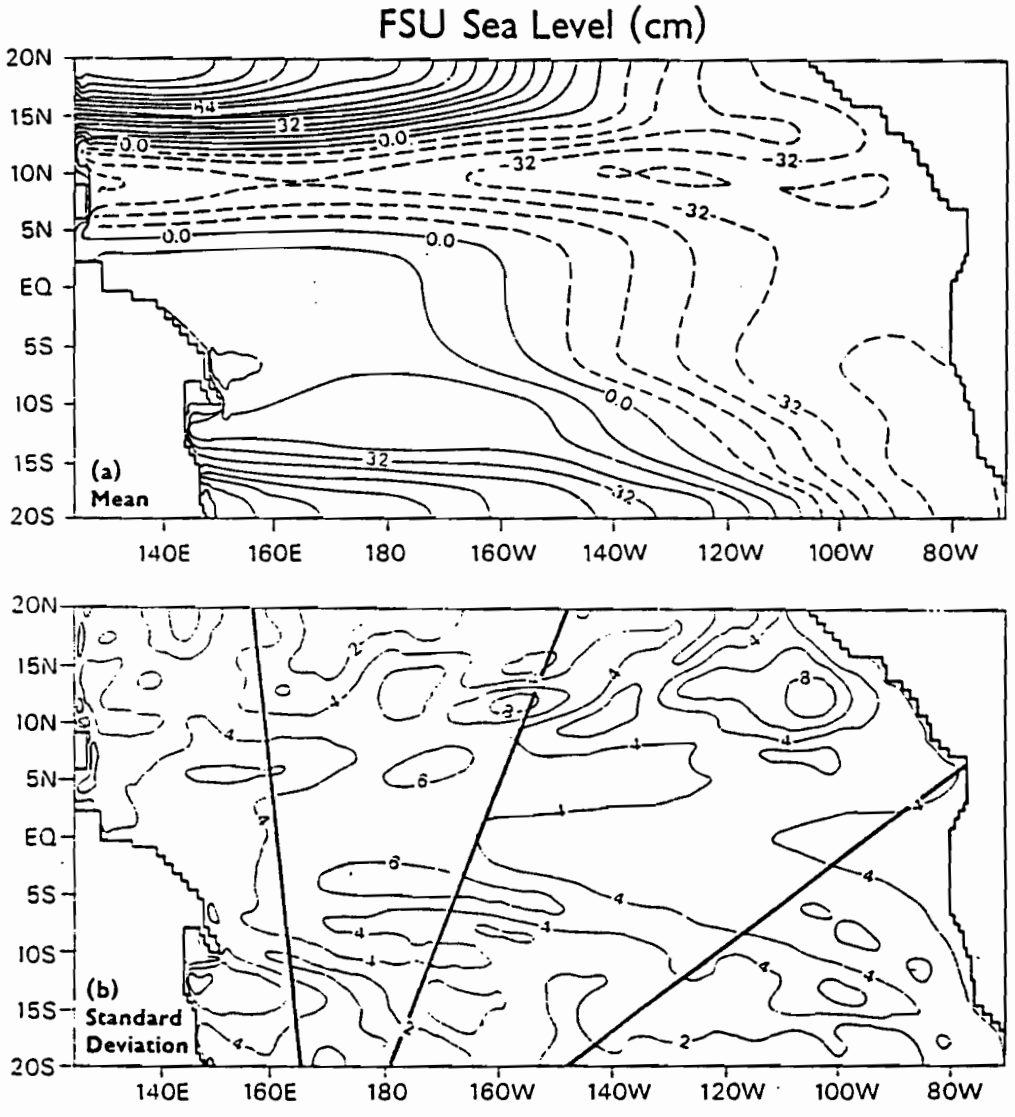

Fig. 7. Model sea level response to FSU wind forcing; a) mean and b) seasonal standard deviation (in cm). Heavy lines in (b) indicate the approximate mean position of XBT distributions in the eastern, central and western Pacific.

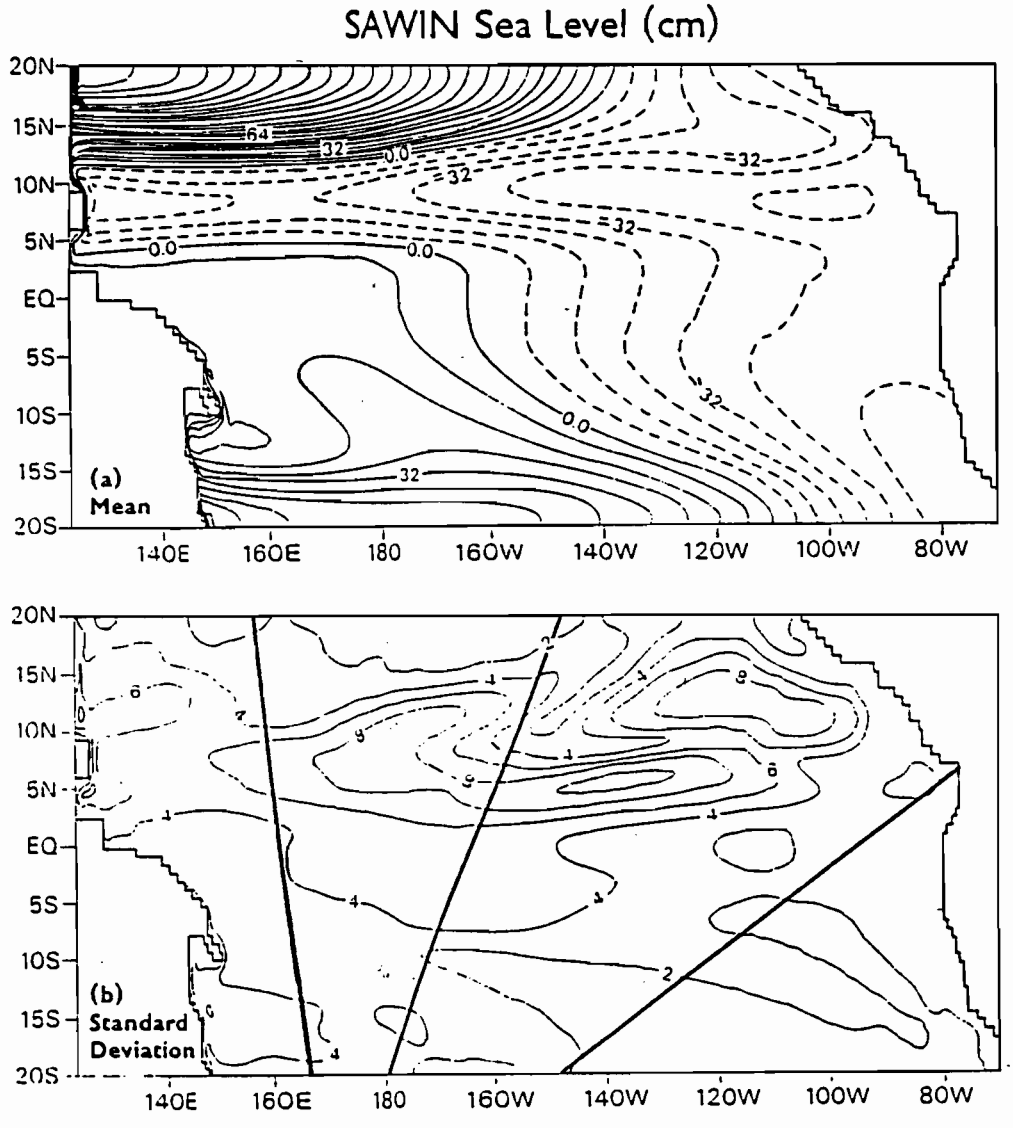

Fig. 8. Same as in Fig. 7, but for SAWIN wind forcing.

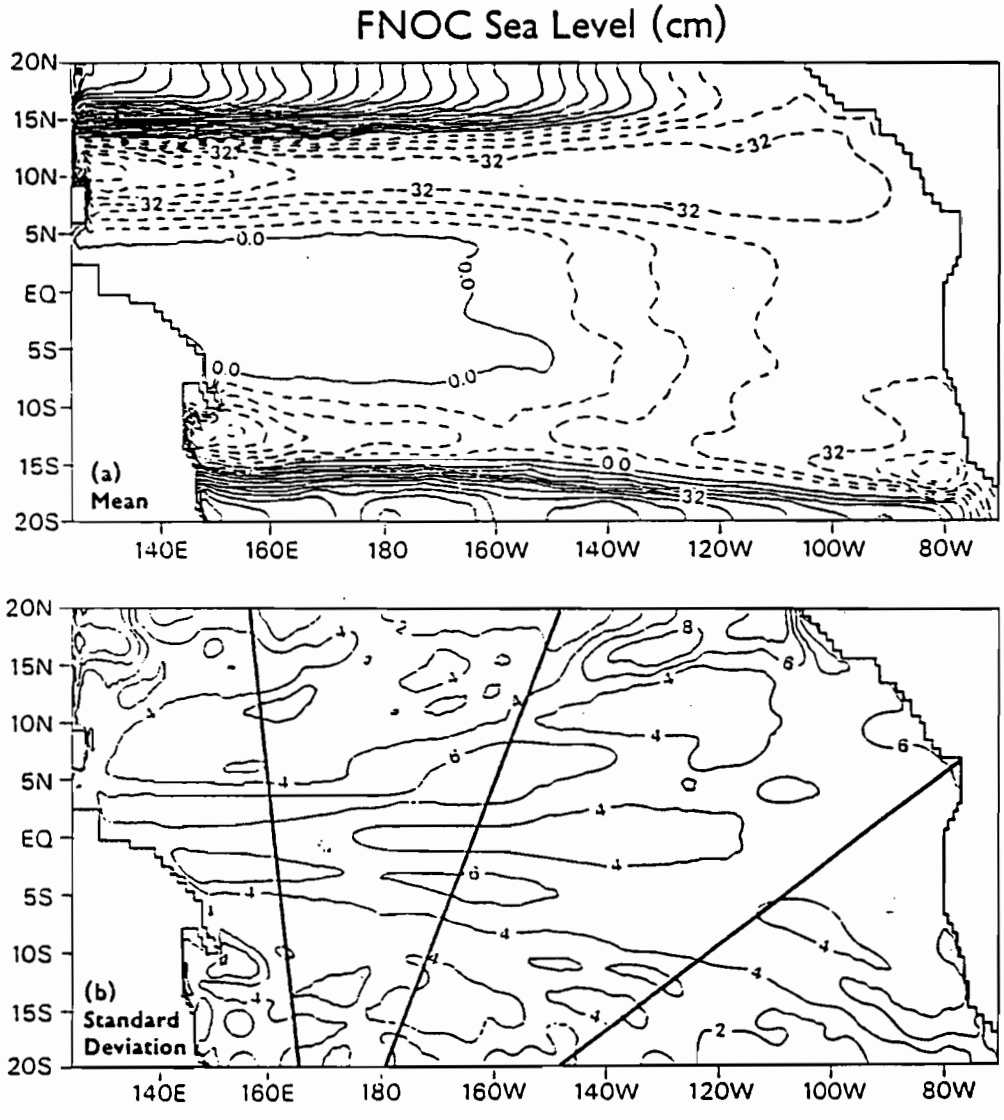

Fig. 9. Same as in Fig. 7, but for FNOC wind forcing.

the meridional topography of each solution is a clearly defined trough at the equator; furthermore, model equatorial ridges near 4°N are much less pronounced than observed (e.g. Wyrtki, 1975).

The mean topography in the FSU and SAWIN simulations is more structured in the northern hemisphere than in the southern hemisphere where a weak South Equatorial Current (SEC) is situated between 6-20°S. By contrast, the FNOC solution exhibits more hemispheric symmetry in that a well-defined South Equatorial Countercurrent (SECC) trough, analogous to the NECC trough, is centered between 12-15°S. This structure is the response to the more continuous band of negative wind stress curl in the southern hemisphere vis-a-vis the FSU and SAWIN fields (Figs. 6a, c, f). Though the mean FNOC stress fields contain a great deal of small-scale structure, the response of the model ocean is predominantly large scale because horizontal mixing eliminates the smallest scales. Moreover, the interior ocean in the model is in Sverdrup balance which involves a zonal integral of the winds from the eastern boundary. This tends to favor a large scale response by averaging out small scale wind fluctuations.

The variability about the mean sea level is summarized by standard deviations of the seasonal cycles (Figs. 7b, 8b, 9b). As in the winds 60-80% of the variance is associated with the annual harmonic. Geographically, the largest seasonal changes occur in the northeastern portion of the basin. Of the three solutions, the amplitude of the SAWIN response is the largest here with two maxima on either side of 8°N representing seasonal changes to the North Equatorial Current and Countercurrent system. These maxima tend to reflect the distribution of the variability in the wind stress curl and as a result, the SAWIN solution also has the largest zonal length scales. The sea level variability induced by the FSU winds is similar to the SAWIN case north

of 8°N, but exhibits a less well defined maximum between the equator and 8°N. This implies differences in current structures and in the zonal and meridional redistribution of mass in the two model simulations.

In contrast to the northern hemisphere, maxima in the southern hemisphere are smallest in the SAWIN case because of the weak SAWIN forcing south of the equator. The most distinctive southern hemispheric feature in the FSU and FNOC cases is a ridge of maximum variability extending SE-NW representing changes in the South Equatorial Current and South Equatorial Countercurrent. The FNOC induced sea level variability also appears more symmetric about the equator than either the FSU or SAWIN solutions.

5. Model/Data Intercomparison

In this section we compare model sea levels and dynamic heights with oceanic counterparts derived from tide gauge and SOP/XBT data. The SOP/XBT data are grouped along sections in the eastern, central and western Pacific as discussed in Section 2. For comparison with these data, we extract data from the mean seasonal model integrations along transects that closely approximate the mean position of XBT distributions in these regions. Model transects are represented as straight lines in latitude and longitude and are superimposed on the sea level standard deviation plots in Figs. 7b, 8b and 9b. For comparison with tide gauge data, we extract sea level data from the model at island locations in Fig. 3. Note that the largest oceanic signals occur in the northeastern quadrant of the basin and are not sampled by either the SOP/XBT network or the sea level network.

We will initially focus the discussion in this section on the central Pacific where there have been several observational studies of the seasonal cycle (e.g. Meyers, 1979; Taft, 1981; Kessler and Taft, 1987) in order to

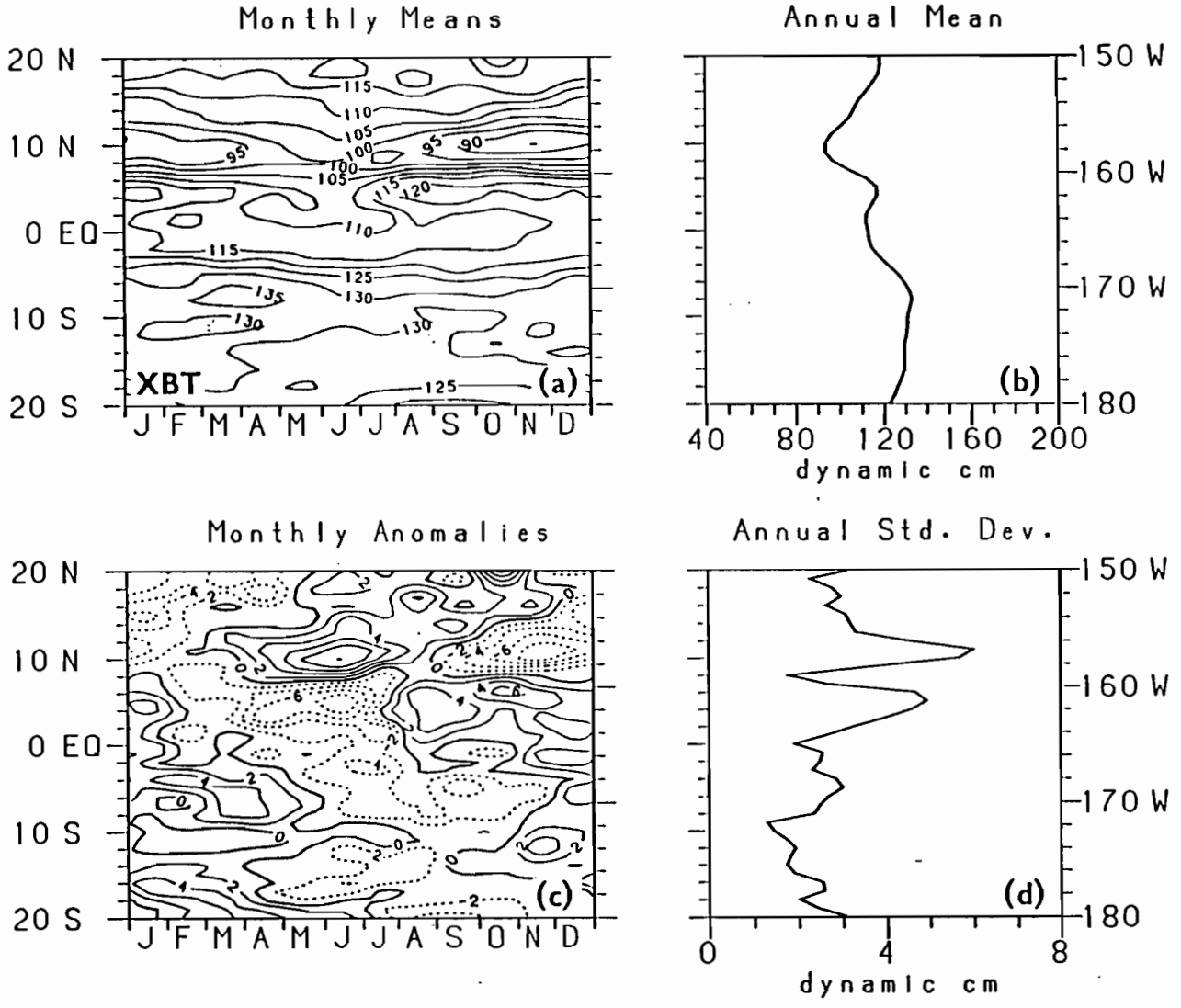

Fig. 10. XBT data processed to dynamic heights relative to 400 db from the central Pacific swath of data in Fig. 1b. a) monthly means, b) annual mean, c) monthly anomalies about the annual mean and d) annual standard deviation computed from monthly anomalies. Contour interval is 5 dynamic cm for monthly means and 2 dynamic cm for anomalies.

introduce the more basinwide analysis to follow. For consistency with XBT measurements, model dynamic heights are computed relative to 400 db using the mean density profile centered at 0°N, 179°W plus vertical density profiles associated with variations in each vertical mode. These dynamic heights are highly correlated with model sea level as are observed dynamic heights and sea level (e.g. Rebert *et al.*, 1985).

Figure 10 shows the mean seasonal cycle of surface dynamic height relative to 400 db calculated from XBT data in the central Pacific. We see that the NECC trough is located at 10°N, and is shallowest in boreal spring and deepest in boreal fall. There is an equatorial ridge at 5°N, and an equatorial trough centered on the equator. Variability in the vicinity of the equatorial ridge and trough is in phase, with low sea level in spring and early summer and high sea level in the fall and winter. An SECC ridge near 8°S is highest in the spring and lowest in the fall. Typical standard deviations of monthly means across 20°N to 20°S are 2-3 dynamic cm, with values of 5-6 dynamic cm in the vicinity of the NECC trough and equatorial ridge. Currents associated with this ridge/trough topography are the North Equatorial Current north of 10°N, the North Equatorial Countercurrent between 5°N and 10°N, the South Equatorial Current between 5°N and 8°S and the South Equatorial Countercurrent between 8°S and 12°S.

Seasonal variations in thermocline topography, which are highly coherent with dynamic height variations in the tropics, have been analyzed by Meyers (1979) and Kessler and Taft (1987) in the central equatorial Pacific. They find that Ekman pumping accounts for much of the variability in the vicinity of the NECC trough and that Rossby wave radiation makes a significant contribution to the variance near the equatorial ridge at 5°N. Kessler and Taft (1987) have also shown that Ekman pumping is important near 6°S and

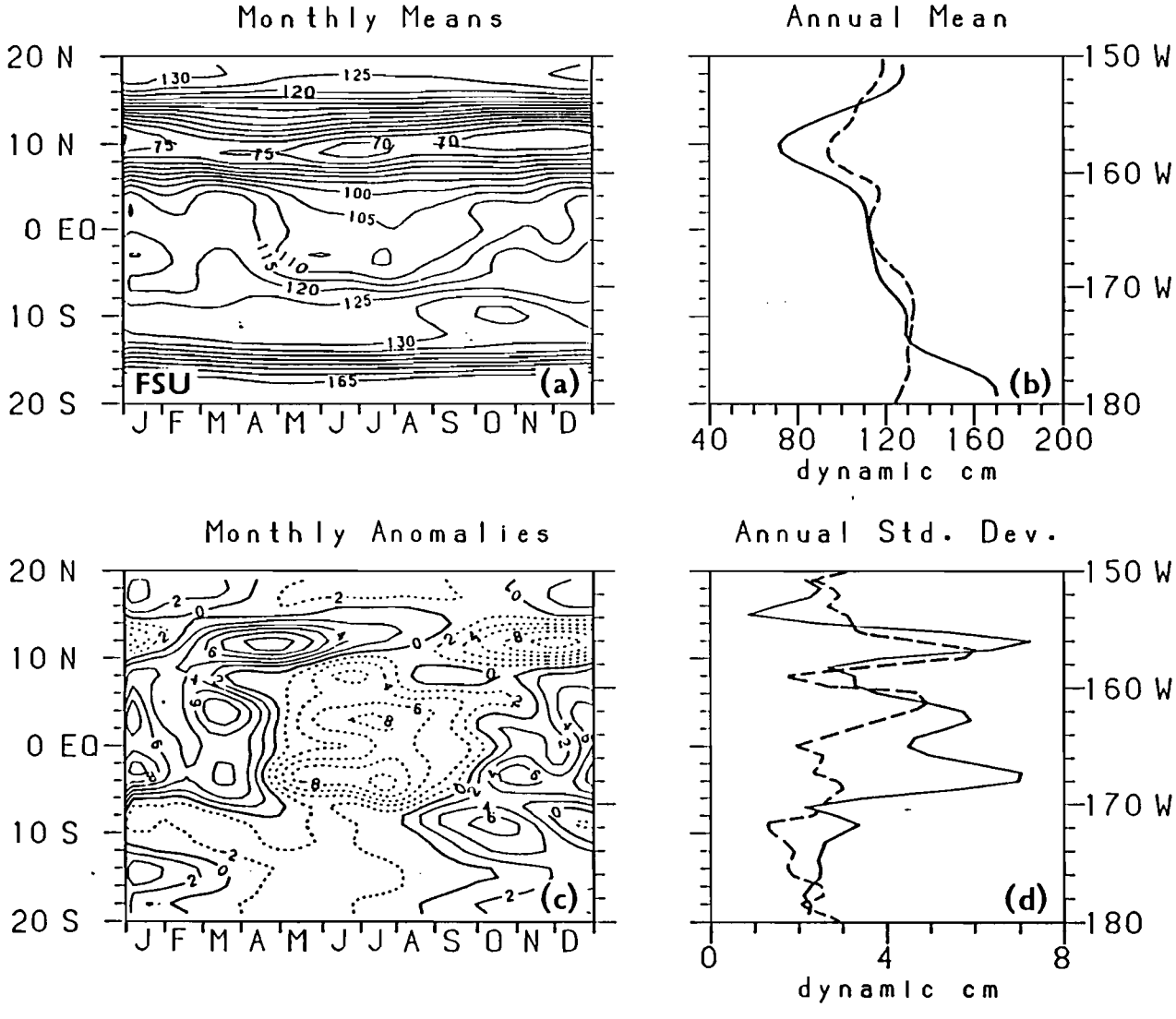

Fig. 11. Dynamic heights relative to 400 db as in Fig. 10, but for the central Pacific grid-point transect from the model forced by FSU winds. Dashed lines in (b) and (d) are the annual mean and standard deviation from XBT data.

between 12° and 18°S. These thermocline and height field variations are geostrophically balanced and lead to a strong NECC in the fall and a strong SEC and SECC in the spring.

Figure 11 shows the model transect taken from the central Pacific for the FSU simulation and processed to a mean seasonal cycle. We note that as in Figure 10, the NECC trough is located near 10°N, and is shallowest in boreal spring and deepest in boreal fall. Similarly, near the equator, dynamic height is low in spring and summer and high in fall and winter. In the southern hemisphere the pattern of highs and lows in Figure 11c is also similar to that observed in the data in Figure 10c. Model variations tend to be stronger than those in the XBT data, though as in the data an extremum in variability is found at 12°N near the NECC trough and another extremum is located near 3°-4°N (Figure 11d). The large amplitude variations in the model between 3-4°S are not seen in the data, however.

Analysis of the vorticity balance in the model indicates that dynamic height variance in the vicinity of the NECC trough results from a combination of local Ekman pumping and Rossby wave radiation. Evidence for Rossby wave radiation in both hemispheres is seen in the tilt of anomaly extrema with time poleward of about 10° (Fig. 11c; also see Figs. 12c and 13c). Rossby waves propagate faster to the west at lower latitudes than at higher latitudes so that a wave train generated in the eastern Pacific arrives in the central Pacific at progessively later times with increasing latitude. Ekman pumping is comparable to Rossby wave induced variability in the model at 10°S near a weakly defined SECC ridge and from 16°S to 20°S, consistent with Meyer's (1979) and Kessler and Taft's (1987) analyses of thermal variability discussed above. Equatorial Rossby waves contribute significantly to the high model variance at 3-4°N.

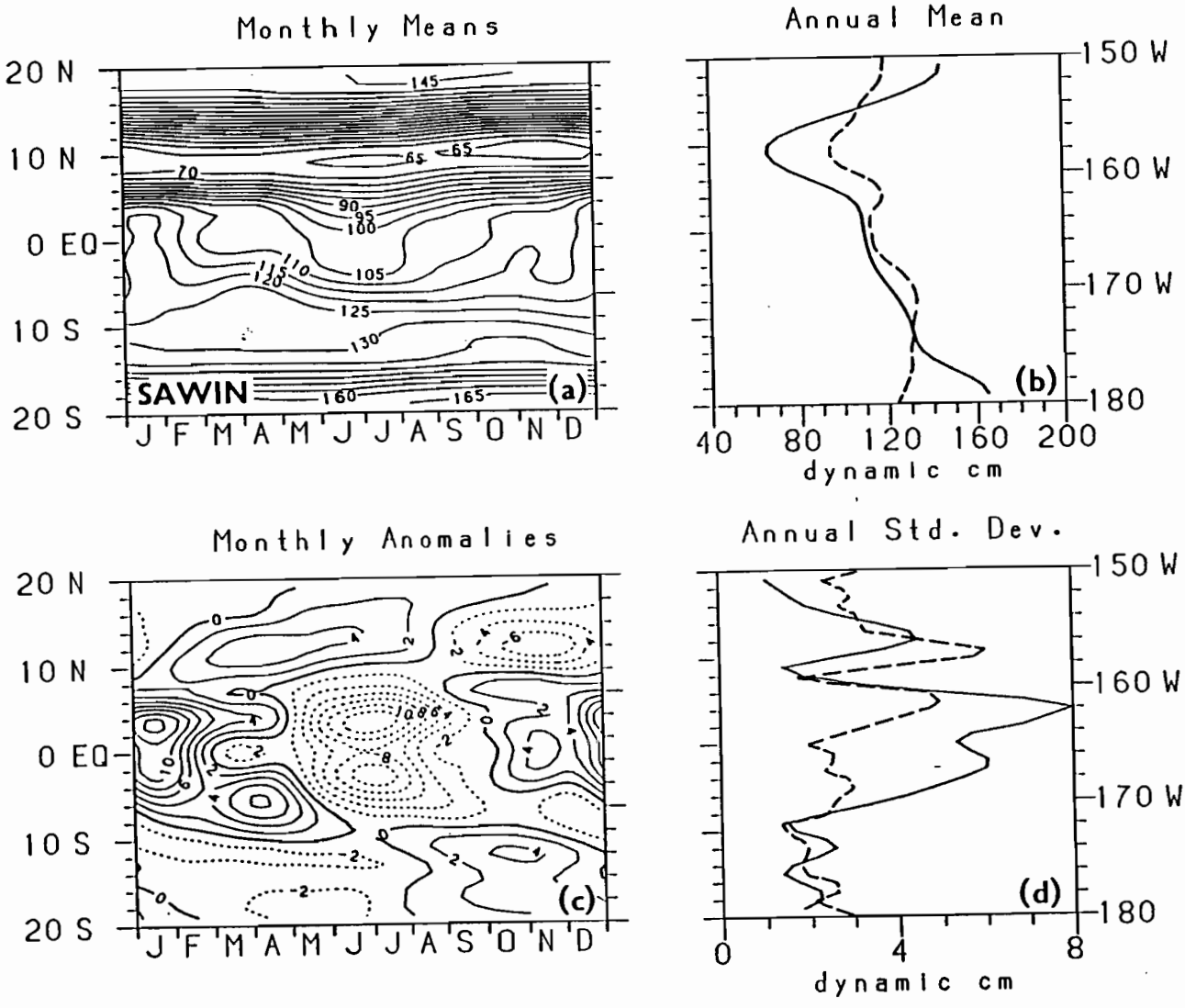

Fig. 12. Dynamic heights relative to 400 db as in Fig. 10, but for the central Pacific grid-point transect from the model forced by SAWIN winds. Dashed lines in (b) and (d) are the annual mean and standard deviation from XBT data.

There are a number of major differences between the XBT and the model transect, however, which are principally due to differences in the mean fields. The mean model surface topography (Fig. 11b) shows very high north and south equatorial ridges near 20°N and 20°S, a deeper than observed NECC trough at 10°N, a very weak equatorial ridge near 4°N and no equatorial trough. We suggest that the lack of a model equatorial trough is due to the absence of vertical mixing, nonlinearity and thermodynamics which allow for a mean Equatorial Undercurrent and associated cooling of the sea surface via equatorial upwelling. The lack of a pronounced equatorial ridge near 4°N is probably due in part to the linearity of the model. Philander and Pacanowski (1987) have shown in an OGCM that cross-equatorial advection of westward momentum from the southern to the northern hemisphere in response to Southeast Trade Wind forcing intensifies the SEC near 3°N. This implies a more pronounced equatorial ridge since the SEC is primarily a geostrophically balanced flow. Coarse 2° meridional resolution of the wind field could also contribute to a weaker than expected equatorial ridge since it may lead to underestimates of the wind stress curl amplitude. In the model, deformation of the thermocline and hence of the sea surface is proportional to $w_e = \frac{1}{f}\,\mathrm{curl}\,\tau - \frac{\beta}{f^2}\tau^{(x)}$ where w_e is Ekman pumping velocity, τ is wind stress, f is the Coriolis parameter and $\beta = \frac{\partial f}{\partial y}$. Weighting of the zonal stress term in this expression by $1/f^2$ compared to $1/f$ for the curl term means that near the equator, underestimation of the curl could bias w_e towards $-\frac{\beta}{f^2}\tau^{(x)}$. In the mean, the stress term is positive, i.e. upwelling favorable because $\tau^{(x)}$ is easterly nearly everywhere in the tropics (e.g. Figs. 4a, c, e). We see that east of 150°W near 4°N, the mean curl (e.g. Figs. 6a, c, e) tends to counteract the stress term, but not enough to create a sharp ridge in the eastern and central Pacific.

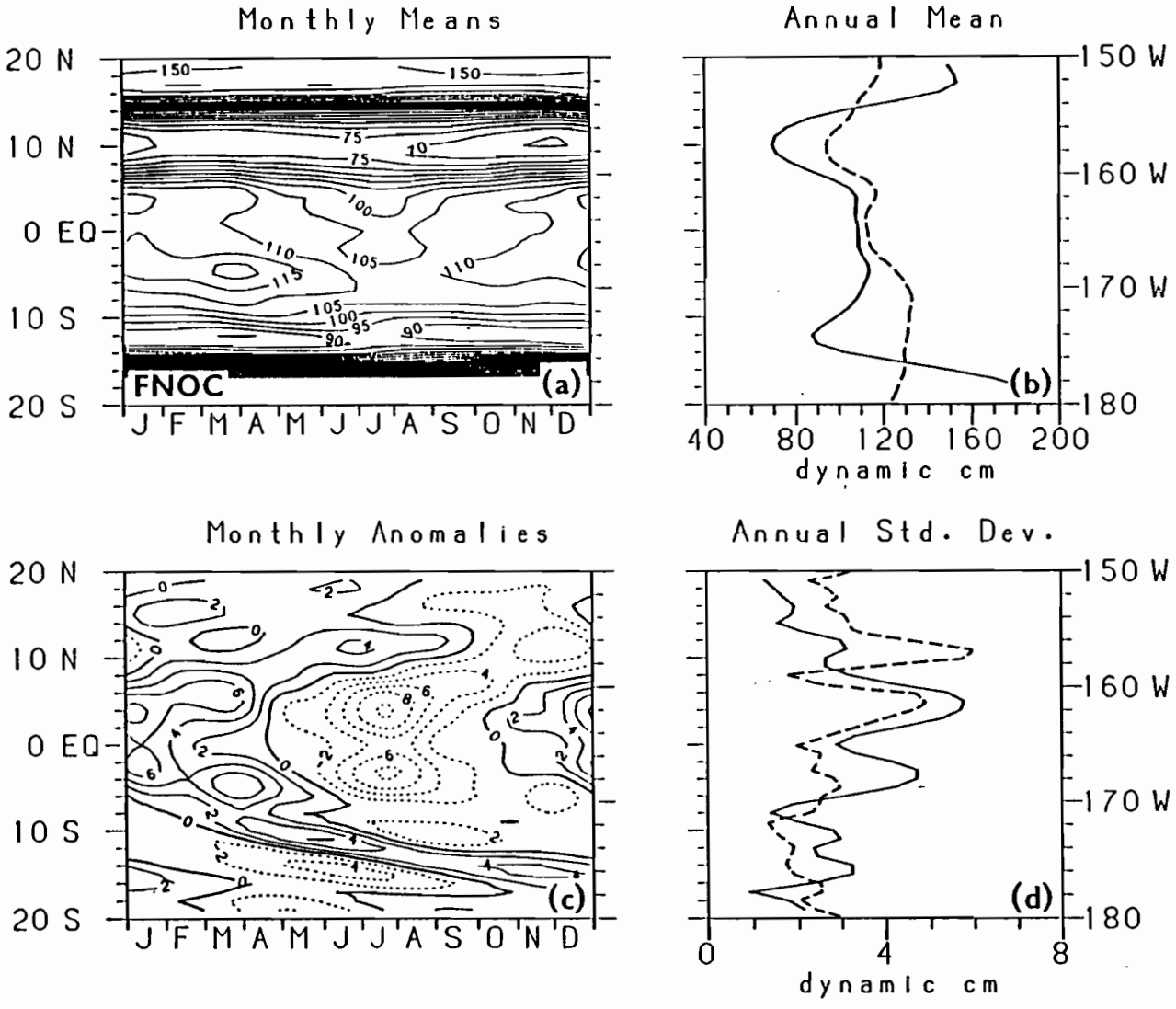

Fig. 13. Dynamic heights relative to 400 db as in Fig. 10, but for the central Pacific grid-point transect from the model forced by FNOC winds. Dashed lines in (b) and (d) are the annual mean and standard deviation from XBT data.

The high north and south equatorial ridges may result from the fact that the model phase speeds have been chosen from a Vaisala frequency profile typical of the central and western equatorial Pacific. The sharp thermocline there leads to an oceanic response which is weighted more towards the first and second vertical modes which have larger signatures in sea level than do higher vertical modes. Choosing a Vaisala frequency profile typical of the weaker stratification in the subtropical gyres would result in a relatively stronger model response in higher vertical modes which have a weaker sea level signature.

We note that choosing a drag coefficient of 1.2×10^{-3} for the winds (e.g. Large and Pond, 1981) would reduce the mean model topographic relief by 10-20%. This would diminish, but not eliminate, discrepancies between observed and modeled structures in Fig. 11b. Also, adding more vertical modes to the model will have little effect on the results. The winds project very weakly onto vertical modes higher than mode 1 and 2 which dominate the model sea level response (e.g. Cane, 1984). Moreover, by inspection of the linear, steady state equatorial β-plane equations which govern mean conditions in our system (q.v. Busalacchi and O'Brien, 1980), one can determine that the horizontal structure of the mean response in each vertical mode is identical. Thus, higher vertical modes can change the ridge/trough topography shown in Fig. 11b quantitatively but not qualitatively.

There are also major discrepancies between the observed and modeled time variability. We noted already the Rossby wave induced maximum in dynamic height near 4°S which is absent in the data (Fig. 11d). The model section also shows an SECC ridge which is best developed in boreal fall near 10°S as compared to near 8°S in boral spring in the data (cf. Figs. 10a and 11a). This leads to a model SECC that is strongest in the fall compared to an

observed SECC which is strongest in the spring. The difference in timing of the SECC appearance in the model is due to the large difference in the mean dynamic topography, however, upon which is superimposed only slightly different time/latitude variations.

Figure 12 shows the corresponding dynamic height transect for the SAWIN calculation. The mean ridge/trough structure is similar to that for the FSU calculation, but with higher amplitude relief in the northern hemisphere where the SAWIN curl tends to be stronger. Amplitude and phase of variations about this mean are likewise similar to the FSU calculation. For example, the NECC trough is shallow in the spring and deep in the fall and dynamic height is low between 5°N and 5°S in the spring and summer and high in fall and winter. Peaks in variance are located at 12°N, 4°N and 3°S with the 12°N peak weaker and the 4°N peak stronger than in the FSU calculation. The dynamics responsible for height variations in this model run are essentially the same as for the FSU run.

Fig. 13 shows dynamic height in the central Pacific for the FNOC simulation. Mean topography north of about 5°S resembles that in the FSU and SAWIN calculations in that an NECC trough is found at 10°N, a high north equatorial ridge is found near 17°N and there is no pronounced equatorial ridge/trough structure. Variations about the mean are usually lower in amplitude than for either the FSU or SAWIN calculation, although the phasing of fluctuations and latitudinal position of extrema is similar. The peak in variability which appears near 12°N in both the FSU and SAWIN calculations is present for example in the FNOC results, but is greatly diminished (Fig. 13d). The relative weakness of the response is due to weaker large scale wind variations in this product compared to the others (q.v. Fig. 4f, 5f, 6f). One of the most significant difference between this

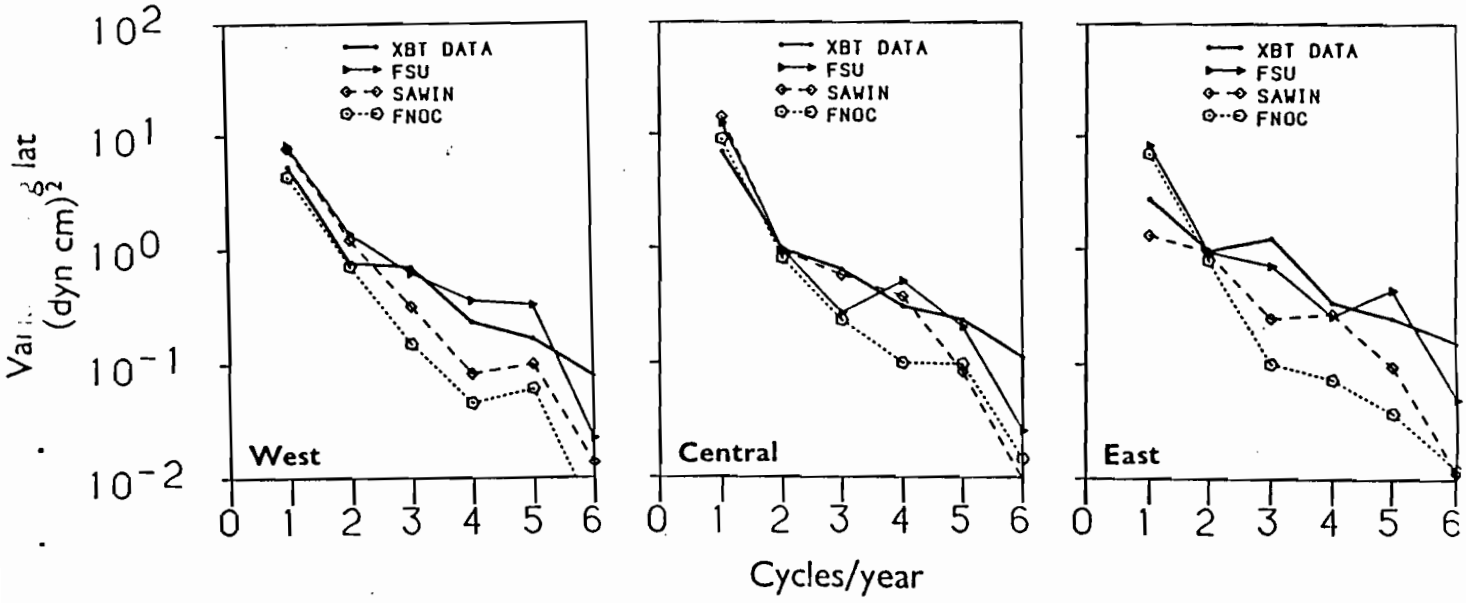

Fig. 14. Average variance per degree of latitude (in dynamic cm^2) as a function of frequency from the XBT data and model simulations in the eastern, central and western Pacific.

calculation and the others however is the presence a mean SECC trough at 12°S which is due to the greater zonal extent of the mean negative curl field in the southern hemisphere. This results in a SECC present at all times of the year between about 6°S and 12°S, though variations in this latitude band bear some resemblance to those observed in the XBT data (cf. Figs. 10c and 13c).

Figure 14 shows latitudinally averaged dynamic height variance as a function of frequency for the XBT data and each of the model simulations in the eastern, central and western Pacific. In each case the the spectra are red with most variance (75-90%) at 1 cpy. Western and central Pacific variance at 1 cpy is generally higher than in the east because the eastern transect is mostly confined to the southern hemisphere where wind forcing is weak. The FSU and SAWIN variances at 1 cpy are always higher than the XBT and FNOC variances, except in the eastern Pacific where SAWIN winds are the weakest of all three forcing functions and the model response is correspondingly low. The spread of values at 1 cpy is less than the difference between 1 cpy and 2 cpy variances in the western and central Pacific. Along all tracks the greatest differences are found at the higher frequencies.

To quantify the degree of correspondence between the model solutions and the XBT data, we computed coherence and phase as a function of frequency and latitude along each track. Results for 1 cpy dynamic heights averaged across all latitudes are presented in Table 2. Phase differences less than one month are probably not significant because we used monthly wind forcing in the model and because XBT data were binned into monthly averages. Approximate significance levels can be determined by assuming a meridional decorrelation scale of about 300 km for seasonal variations (White *et al.*, 1985). This leads to 90% confidence levels for coherence of 0.42 along the western and

	WEST		CENTRAL		EAST	
	Coh.	Pha.	Coh.	Pha.	Coh.	Pha.
XBT/FSU	0.73	-1.6	0.43	0.0	0.42	3.2
XBT/SAWIN	0.58	-1.0	0.53	0.4	0.29	4.8
XBT/FNOC	0.30	0.0	0.47	1.2	0.53	4.9

Table 2. Coherence and phase (in months) between dynamic heights relative to 400 db calculated from XBT data and from model simulations along three transects in the eastern, central and western Pacific. Coherences are significantly nonzero at the 90% confidence level if they exceed 0.42 in the central and western Pacific and 0.50 in the eastern Pacific. Positive (negative) phase means the XBT dynamic heights lead (lag) model simulated dynamic heights.

central tracks which span 39 degrees of latitude, and 0.50 along the eastern track which spans 27 degrees of latitude. Values falling below these levels are probably not different from zero.

The best model coherence with XBT data anywhere in the Pacific is for the FSU/XBT pair on the western track where coherence is 0.73, with the XBT data lagging by 1.6 months. The relatively high coherence is due to the fact that most XBT data are taken along a single transect during 1979-1981, that ship wind observations are relatively dense (about 30/month per 2° latitude by 10° longitude box) and that the seasonal variations in the winds are large (Fig. 4-6). Coherence of the SAWIN/XBT pair is also significant at 0.58 with a one month phase difference, whereas the FNOC/XBT coherence is below the 90% confidence level in the west. All coherences are above the 90% significance level in the central Pacific, with phase differences of about a month or less. The SAWIN/XBT pair shows the highest coherence in the central Pacific at 0.53, possibly due to the fact that ship wind observations are relatively sparse (about 3/month in some areas) whereas cloud motion vectors are plentiful in the central Pacific (e.g. Halpern and Harrison, 1982).

The eastern Pacific appears to be the most poorly modeled region of the basin. Only the FNOC/XBT coherence exceeds the 90% significance level; however, the phase between the 1 cpy harmonic from the model driven by the FNOC winds and the 1 cpy harmonic from the XBT data is almost 5 months. This poor coherence and phase in general is probably due to weak wind forcing and an equally weak response in the eastern Pacific. Contributing factors include poor ship wind data coverage in the southeastern Pacific (in the case of the FSU and FNOC products), and the use of a Vaisala frequency profile in the model representative of the western and central Pacific rather than the weaker stratification of the eastern Pacific. Phase speeds of vertical modes based

on Vaisala frequency profiles in the eastern Pacific are significantly lower than in the west (e.g. Eriksen *et al.*, 1983) so one would expect phases to be biased in our model simulations in the eastern Pacific. In addition, the very low coherence in the east between the the SAWIN model calculation and the XBT data may be due to errors in inferring surface winds from cloud motions near the equator where large climatological shears exist between cloud wind level and the surface (Sadler and Kilonsky, 1985). Noise in the XBT data due to track separation south of the equator (McPhaden *et al.*, 1987) is probably also a factor in the low coherences in the east between the model simulation and XBT data.

Figure 15 shows coherence and phase plots for each of the three model calculations with the XBT data at 1 cpy in three latitudinal ranges of 5°S-15°S, 5°S-5°N and 5°N-15°N. Coherence values are higher than in Table 1 because of the artificial coherence resulting from fewer degrees of freedom. Assuming every third degree of latitude is independent, the the 90% confidence limit for the null hypothesis is 0.76. Not all of the differences in coherence levels seen in Fig. 15 are statistically significant because of the limited numbers of degrees of freedom. However, the coherence patterns have a consistent physical interpretation which we elaborate on below.

Figure 15 shows a consistent pattern of high coherence (0.6-0.9) and phase differences less than 2 months (except in the east) in the equatorial band. This high coherence is due to the fact that variability in dynamic height along the equator is proportional to a zonal integral of the zonal winds which tends to average out the effects of small scale noise in the the wind products (e.g. Busalacchi and Cane, 1985). Coherence in general drops away from the equator with biggest decreases typically occurring in the FNOC/XBT coherences. Off equatorial coherences are lower because at higher

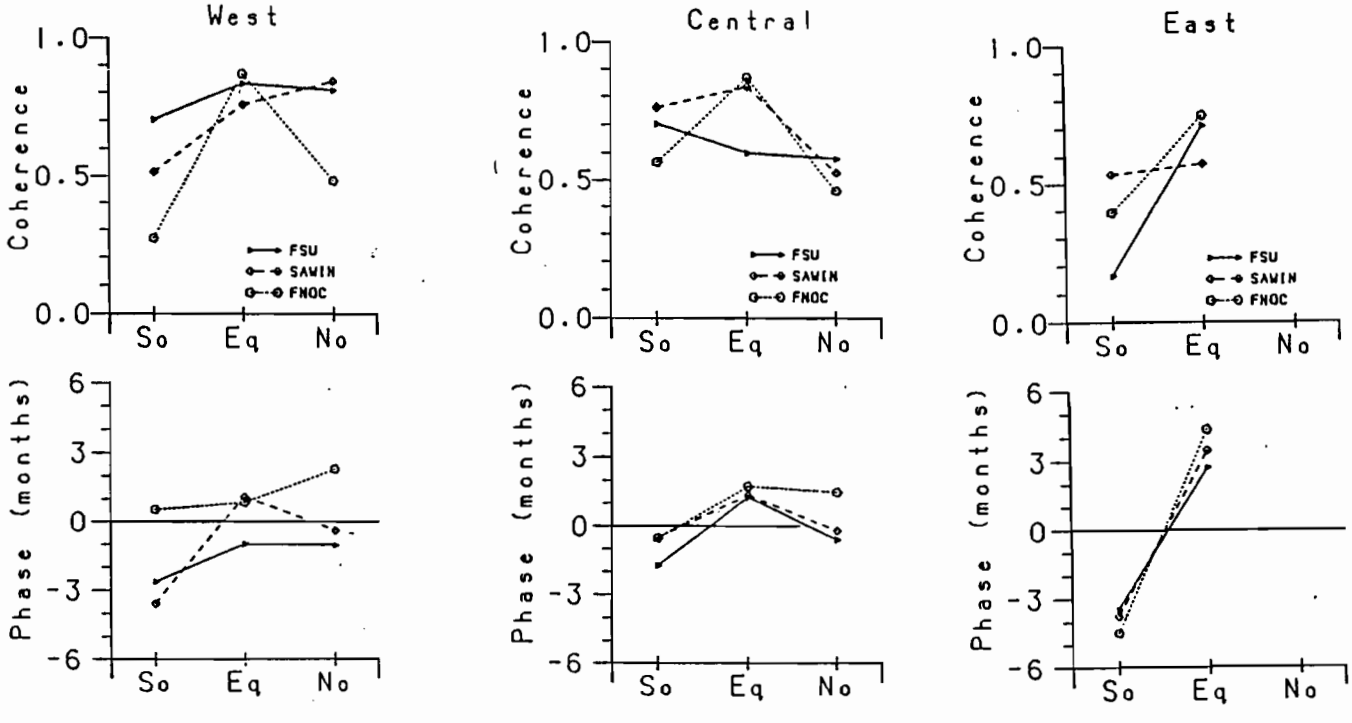

Fig. 15. Coherence and phase at one cycle per year between dynamic heights calculated from XBT data and from the model simulations forced with FSU, SAWIN and FNOC winds in the eastern, central and western Pacific. So = 5-15°S, Eq = 5°S-5°N, No = 5-15°N. Coherence is significantly nonzero at the 90% level of confidence if it exceeds 0.76. Positive (negative) phase means that dynamic heights calculated from XBT data lead (lag) model simulated dynamic heights.

latitudes, variability in dynamic height is proportional to wind stress curl which involves spatial derivatives of the wind field. Therefore noise in the wind field is amplified which degrades the accuracy of the simulation. There is a suggestion of hemispheric asymmetry to the coherence patterns in Figure 15, but differences are not statistically significant.

We have repeated these coherence calculations using model output sampled at the times and locations of actual XBT casts for a three-year simulation (1979-81) as opposed to the grid-point transects shown in Figures 7-9. Model XBT data were averaged in time to produce a mean seasonal cycle in the eastern, central and western Pacific areas outlined in Figure 1 as discussed in McPhaden *et al.* (1987). The coherences were generally lower than in Table 2 for this sampling scheme because of the additional noise introduced by aliasing of zonal variations. However, the differences were not significant because noise contamination is weak at 1 cpy. For example, coherences for the XBT/FSU pair in the east, central and west were 0.61, 0.38 and 0.49 for the XBT sampled model output compared to 0.73, 0.43 and 0.42 for the grid-point sampled output.

We have also repeated these coherence calculations for frequencies higher than 1 cpy and found that they are generally lower and less consistent than at 1 cpy because of the weaker signals at higher frequency (e.g. Fig. 14). Similarly, we have computed coherences for geostrophic transport per unit width (i.e. depth integrated geostrophic velocity) orthogonal to the transects poleward of 2° latitude. Transport is a spatial derivative, i.e. high-pass filtered version, of the dynamic height field in which high wavenumber variability is amplified. This makes transport estimates more susceptible to contamination by small scale noise so that in general transport coherences were smaller than for dynamic height.

As a complementary calculation we computed coherence and phase for model simulations with data from the island sea level network in Fig. 3. Table 3 summarizes the results at 1 cpy along with ensemble averaged amplitudes of the annual harmonic for each sea level data set. We find that the annual harmonic amplitude ranges between a low value of 3.7 cm for FNOC simulation and 5.6 cm for the SAWIN simulation. The range of percent variance explained by this harmonic is 69% for the island data and 81% for the SAWIN simulation. Coherences are about 0.6 with phase differences less than one month. These results are generally consistent with the coherence relationships along the western and central SOP transects since most of the islands are in the western and central Pacific. However, phase agreement is better between the FSU and SAWIN simulations and sea level, which may be due to better temporal resolution of the sea level data and to the lack of spatial scatter as occurs in the XBT data. Reduction of temporal and/or spatial aliasing in the sea level data may also explain the higher FNOC/sea level coherence (0.62) relative to the FNOC/XBT coherences (0.30 in the west and 0.47 in the central Pacific).

6. Summary and Conclusions

In the foregoing sections we have examined simulations of the mean seasonal cycle in the tropical Pacific using a multi-vertical mode version of the Busalacchi and O'Brien (1980) linear model. The model was forced with FSU, SAWIN and FNOC surface wind stress analyses for the period 1979-1981 and was run to equilibrium for each of four vertical modes. The mean seasonal cycle of dynamic height relative to 400 db was computed and compared to identical calculations based on XBT data for the 1979-1981 period. The XBT data set we used is an augmented version of the ORSTOM/SIO SOP data set in

	Amp.	%	Coh.	Pha.
Islands	4.8	69	--	--
FSU	4.6	74	0.64	0.0
SAWIN	5.6	81	0.57	0.0
FNOC	3.7	78	0.62	0.9

Table 3. Amplitude (in cm) and percent variance of monthly means (%) represented by the one cycle per year harmonic ensemble averaged over the 29 sea level station shown in Fig. 3 for tide gauge measurements and for model simulations. Also shown is is the coherence and phase between observed sea level and model simulated sea level. Assuming only one in three sea level stations is independent, coherence is significantly nonzero at the 90% confidence level if it exceeds 0.48. Positive (negative) phase means that tide gauge sea level leads (lags) simulated sea level.

which the number of data was more than quadrupled. We also computed model sea level and compared it with tide gauge data from 29 island stations for 1979-1981.

The wind data sets were compared noting features in the mean and seasonal standard deviations that had an impact on the model results. All wind fields showed the basic large scale features of the Pacific Trade Wind system, though the SAWIN winds were the smoothest and the strongest and the FNOC winds were generally the weakest and exhibited the most small scale structure. FSU winds were intermediate between these two in both smoothness and amplitude. The ITCZ was several degrees closer to the equator in the eastern Pacific in the FNOC product as compared to the SAWIN and FSU products.

In response to these wind forcing functions, model simulated mean dynamic topographies showed some features in common with the observed topography, e.g. the position of the NECC trough and NEC ridge. However, north and south equatorial ridges were much higher than observed, north equatorial countercurrent troughs that were too deep, equatorial ridges near 4°N were too weak and no significant equatorial troughs were generated. The high north and south equatorial ridges were attributed to the specification of the model background Vaisala frequency profile which is representative of the central and western equatorial Pacific but not the higher latitudes. Weak equatorial ridges were interpreted in terms of omitted nonlinearity and coarse wind resolution. The absence of equatorial troughs was interpreted in terms of the lack of vertical mixing, nonlinearity and thermodynamics which allows for surface cooling via equatorial upwelling. One of the most notable distinctions between simulations was the presence of a pronounced mean South Equatorial Countercurrent ridge/trough structure in the FNOC simulation compared to the FSU and SAWIN calculations due to a relatively unbroken zonal band of negative curl in the southern hemisphere in the FNOC product.

Observed and simulated mean seasonal height variations were on the order of a few centimeters and patterns of variability, e.g. near the equator and in the vicinity of the NECC trough, were often similar. To quantify the level of agreement between the observations and the model runs, we computed coherence and phase estimates for the 1 cycle per year harmonic which dominates the annual cycle over most of the tropical Pacific. Significant coherence levels of 0.5-0.7 were found which suggest that roughly 25-50% of the variance of the mean seasonal cycle in dynamic height can be accounted for by linear dynamics. Typically the phase difference between the model simulations and observations was about one month, which is probably not significant because this is the resolution of the wind forcing functions and oceanic data sets used in the study. Frequencies higher than 1 cpy were generally not as coherent because of the lower signal amplitudes in both the XBT data and model simulations. Also, coherence between modeled and observed geostrophic transport per unit width was lower than for dynamic height because of lower transport signal-to-noise ratios.

A similar set of calculations was performed using sea level data from the island tide gauge network. Results were comparable to those found with the XBT data, though coherence and phase estimates were slightly better at 1 cpy. This may have been due to the finer temporal resolution and lack of spatial aliasing in the tide gauge data.

We found significant regional variations in the coherence and phase calculations for dynamic height at 1 cpy. Latitudinally, equatorial (i.e. 5°N to 5°S) coherence levels were usually higher than either to the north or to the south because of the ocean responds to the zonal integral of wind stress along the equator vis-a-vis spatial gradient of the wind stress at higher latitudes. The former diminishes the effects of random noise in the wind

field whereas the latter amplifies noise. Coherences with the FNOC wind forced solutions generally showed the most rapid falloff with latitude consistent with the high degree of small scale incoherent structure in this product vis-a-vis the SAWIN and FSU products.

Longitudinally, the eastern Pacific was the most poorly modeled region with low coherences and phase lags of several months. The low coherence is most likely due to weak wind stress forcing and resultant weak oceanic signals. The SAWIN product performed worst of the three wind products in the eastern Pacific where strong wind shears are found between the surface and the cloud motion level. Poor shipwind data coverage, model phase speeds tuned to the central and western Pacific and noise in the XBT data due to divergence of the SOP ship tracks may also be imporant in reducing coherence in this region.

In summary, we have shown for the tropical Pacific that there is coherence between the observed and simulated annual (i.e. 1 cpy) harmonic in surface height for the period 1979-81. Simulations were based on a linear model driven by three different realizations of the surface stress. In both the observations and the simulations, the annual harmonic was the most energetic frequency component of mean seasonal cycle. However, because confidence limits on our coherence calculations are wide, it is not possible to determine unambiguously that one wind stress product is superior to the others for simulating the mean seasonal cycle. Indeed, we found that the simulations were more coherent at 1 cpy among themselves (by about 0.1 to 0.2) than they were with the XBT and sea level data. This is because as noted in Section 3, the large scale structures in all three products are very similar, even though the small scale structures are quite different. More obvious distinctions between the three products may be apparent in a follow-up study

of the 1982-83 El Niño event in which both the forcing and the ocean response are much larger than for the mean seasonal cycle.

In closing, we note that model sea level signals in all three simulations are largest in the northeastern tropical Pacific (Figs. 7b, 8b and 9b) and are associated with seasonal movements of the ITCZ (Figs. 6b, d and f). However, neither the SOP/XBT program nor the sea level network provide data from this region. Given the large amplitude of the wind forcing and of the ocean's dynamical response, a high priority should be given to monitoring this region of the tropics during the TOGA decade. Strong seasonal variations in sea level imply large changes in the meridional redistribution of heat and in the zonal transports of the NECC and NEC. Perturbation of this large seasonal cycle may be important in the evolution of El Niño/Southern Oscillation events by affecting air-sea interaction in the climatically sensitive region of the ITCZ.

Acknowledgments

The authors would like to thank J. O'Brien of Florida State University for providing the FSU wind analysis, J. Sadler of the University of Hawaii for providing the SAWIN wind analysis and J. Kindle of Naval Oceanographic Reseach and Development Activity for the FNOC wind analysis. We would also like to thank K. Wyrtki of the University of Hawaii for making data from the Pacific island sea level network available to us. D. Moore provided partial support for the authors to visit the Joint Institute for Marine and Atmospheric Research of the University of Hawaii where several of the ideas in this manuscript were developed and elaborated on. G. Raymond, D. Allison and V. Fabre provided programming and technical assistance. Financial support was made available by NOAA's U.S. TOGA Project Office and EPOCS program (MJM), by NASA RTOP 161-20-31 (AJB) and by ORSTOM and PNEDC (JP).

References

Busalacchi, A.J. and J.J. O'Brien, 1980: The seasonal variability in a model of the tropical Pacific. *J. Phys. Oceanogr., 10*, 1929-1951.

Busalacchi, A.J. and J.J. O'Brien, 1981: Interannual variability of the equatorial Pacific in the 1960's. *J. Geophys. Res., 86*, 10,901-10,907.

Busalacchi, A.J., K. Takeuchi and J.J. O'Brien, 1983: Interannal variability in the equatorial Pacific-revisited. *J. Geophys. Res., 88*, 7551-7562.

Busalacchi, A.J. and M.A. Cane, 1985: Hindcasts of sea level variations during the 1982-83 El Niño. *J. Phys. Oceanogr., 15*, 213-221.

Cane, M.A., 1984: Modeling sea level during El Niño. *J. Phys. Oceanogr., 14*, 1864-1874.

Cressman, G.P. 1959: An operational objective analysis system. *Mon. Wea. Rev., 87*, 367-374.

Delcroix, T., G. Eldin and C. Henin, 1987: Water masses and transport variability at 165E in the tropical Pacific Ocean. *J. Phys. Oceanogr.*, submitted.

Donguy, J.R. and G. Meyers, 1987: Observed and modelled topography of the 20° isotherm in the tropical Pacific. *Oceanol. Acta, 10*, 41-48.

Eriksen, C.C., M.B. Blumenthal, S.P. Hayes and P. Ripa, 1983: Wind-generated equatorial Kelvin waves across the Pacific Ocean. *J. Phys. Oceanogr., 13*, 1622-1640.

Gent, P.R., 1985: On the annual cycle in the central equatorial Pacific Ocean. *J. Mar. Res., 43*, 743-745.

Goldenberg, S.B. and J.J. O'Brien, 1981: Time and space variability of tropical Pacific wind stress. *Mon. Wea. Rev., 109*, 1190-1207.

Halpern, D. and D.E. Harrison, 1982: Intercomparison of tropical Pacific mean November 1979 surface wind fields. MIT Dept. of Meteorology and Physical Oceanography Tech. Rept. 82-1, 40pp.

Harrison, D.E., editor, 1984: Report of the Ad-Hoc Committee on surface wind and wind stress fields. Technical Rept., USTOGA2. University Corporation for Atmospheric Research.

Hayes, S.P., 1982: A comparison of geostrophic and measured velocities in the Equatorial Undercurrent. *J. Mar Res., 40* (Supplement), 219-229.

Hayes, S.P. and M.J. McPhaden, 1987: Temporal sampling requirements for low frequency temperature variability in the eastern equatorial Pacific Ocean. Manuscript in preparation.

Kessler, W.S. and B.A. Taft, 1987: Dynamic heights and zonal geostrophic transports in the central tropical Pacific during 1979-1984. *J. Phys. Oceanogr., 17*, 97-122.

Large, W.G. and S. Pond, 1981: Open ocean momentum flux measurements in moderate to strong winds. *J. Phys. Oceanogr., 11*, 324-336.

Levitus, S. 1982: Climatological Atlas of the World Ocean. NOAA Prof. Pap. 13, U. S. Govt. Printing Office, 173pp.

McPhaden, M.J., A.J. Busalacchi, J. Picaut and G. Raymond, 1987: Aliasing of zonal variability in the tropical Pacific Ship-of-Opportunity XBT program. *J. Geophys. Res.*, submitted.

Meyers, G., 1979: The annual Rossby wave in the tropical North Pacific. *J. Phys. Oceanogr., 9*, 663-674.

Philander, S.G.H. and A.D. Seigel, 1985: Simulation of El Niño of 1982-83. In Coupled Ocean-Atmosphere Models, J.C.J. Nihoul, editor, Elsevier Oceanography Series, 40, Elsevier Amsterdam, 517-540.

Philander, S.G.H., W.J. Hurlin and A.D. Seigel, 1987: Simulation of the seasonal cycle of the tropical Pacific Ocean. Manuscript in preparation.

Philander, S.G.H. and R.C. Pacanowski, 1987: Nonlinear effects in the seasonal cycle of the tropical Atlantic Ocean. *Deep-Sea Res., 34*, 123-137.

Picaut, J., R. Tournier and V. Fabre, 1987: Champs mensuel 1979-1985 de temperature, hauteurs dynamiques et courants geostrophiques, deduits de mesures XBT 0-400m le long des trois rails moyens de navigation dans le Pacifique tropical. Manuscript in preparation.

Rasmussen, E.M. and T.H. Carpenter, 1982: Variations in tropical sea surface temperature and surface wind fields associated with the Southern Oscillation/El Niño. *Mon. Wea. Rev., 111*, 353-384.

Rebert, J.P., J.R. Donguy, G. Eldin and K. Wyrtki, 1985: Relations between sea level, thermocline depth, heat content and dynamic height in the tropical Pacific Ocean. *J. Geophys. Res.*, 11719-11725.

Roed, L.P. and O.M. Smedstad, 1984: Open boundary conditions for forced waves in a rotating fluid. *SIAM J. Sci. Stat. Comput., 5*, 414-426.

Sadler, J.C. and B.J. Kilonsky, 1985: Deriving surface winds from satellite observations of low-level cloud motions. *J. Clim. Appl. Met., 24*, 758-769.

Taft, B.A., 1981: Geostrophic flow and surface water masses in the central Pacific. In Recent Progress in Equatorial Oceanography, J.P. McCreary, Jr., D.W. Moore and J.M. Witte, editors, Nova University Press, 141-150.

White, W.B., Meyers, G.A., J.R. Donguy and S.E. Pazan, 1985: Short-term climatic variability in the thermal structure of the Pacific Ocean during 1979-1983. *J. Phys. Oceanogr., 15*, 917-935.

Wyrtki, K., 1975: Fluctuations of the dynamic topography in the Pacific Ocean. *J. Phys. Oceanogr., 5*, 450-459.

Wyrtki, K., 1985: Water displacements in the Pacific and the genesis of El Niño. *J. Geophys. Res.*, *90*, 7129-7132.

II. A Model Study of Aliased Zonal Variability in Tropical Pacific XBT Data

by

Michael J. McPhaden
NOAA/Pacific Marine Environmental Laboratory
Seattle, WA 98115

Antonio J. Busalacchi
Laboratory for Oceans
NASA/Goddard Space Flight Center
Greenbelt, MD 20771

Joel Picaut
Institut Francais de Recherche Scientifique pour
le Developpement en Cooperation (ORSTOM)
Noumea, New Caledonia

Gary Raymond
School of Oceanography WB-10
University of Washington
Seattle, WA 98195

September 1987

For submission to *J. Geophys. Res.*

Contribution No. 963 from NOAA/Pacific Marine Environmental Laboratory

Abstract

We describe a series of sampling sensitivity experiments to examine the effects of aliased zonal variability in estimates of mean seasonal and interannual variations along XBT transects in the tropical Pacific. We use a linear, multi-vertical mode model forced with three different monthly mean wind stress sets for the period 1979-1983. The model is sampled along approximately straight lines of grid points corresponding to the mean positions of XBT tracks in the eastern, central and western Pacific and then sampled again at the dates and locations of actual XBT casts for 1979-1983. Model data are processed to dynamic height for computation of a monthly mean seasonal cycle and anomalies associated with the 1982-83 El Niño. Comparing results for the two methods of sampling the model indicates that zonal aliasing in general can lead to about a 2 dynamic cm error in dynamic height (equivalent to a 10 m error in model pycnocline displacement). This magnitude of error generally does not obscure anomalies associated with the 1982-83 El Niño or the annual and semi-annual harmonics of the mean seasonal cycle in the model, though frequencies higher than the semiannual can be adversely affected. Errors larger than 2 dynamic cm occur in regions where XBT sample spacing in the zonal direction is insufficient to resolve Rossby wave variations in the model, e.g. from 16°N to 20°N in the central Pacific and from 8°S to 20°S in the eastern Pacific. Smoothing in latitude and/or time can reduce noise levels slightly, but cannot eliminate the effects of unresolved zonal variations in estimates of dynamic height. These conclusions are insensitive to the choice of monthly mean wind stress used to force the model.

1. Introduction

TOGA (Tropical Ocean-Global Atmosphere) is a 10-year multi-national program to measure, understand, model and predict variability in the coupled ocean-atmosphere system on time scales of months to years, with particular emphasis on the El Niño/Southern Oscillation phenomenon. A central oceanographic objective is to develop an observational array with sufficient accuracy and resolution to determine the time dependent variability of upper ocean thermal and current structures. Data from the tropical Pacific Ship-of-Opportunity (SOP) XBT Program (National Academy of Sciences, 1986), together with complementary CTD data, hydrocast data and XBT data from research and naval vessels, are an important component of this observational effort in that they provide basin scale temperature information in the upper 450 m. Present and anticipated uses of these thermal data include description of short-term climate variations in sea surface temperature, heat content, dynamic height and geostrophic transport; diagnosis of processes responsible for climate scale variability; and initialization, assimilation, and verification studies of model simulated variability in tropical oceans. Thus, it is important to understand the strengths and limitations of the present thermal sampling program and how these impact overall TOGA objectives.

A number of recent studies have dealt with tropical Pacific XBT sampling issues of relevance to TOGA. For example, White *et al.* (1982) estimated time and space scales and signal-to-noise ratios of climate scale variability from pre-1979 hydrographic data in the western Pacific. This study provided a rationale for the original design of the SOP network. More recently, Kessler *et al.* (1985) have addressed issues of oversampling in the central Pacific, of the shallow 450 m reference level and of data loss with increasing depth. Kessler and Taft (1987) examined the implications of using a climatological

T/S relationship for estimating dynamic height from temperature alone in the central Pacific. Firing and Lukas (1985) and Hayes and McPhaden (1987) investigated the effects of aliased high frequencies on central and eastern equatorial Pacific temperature data sparsely sampled in time. These and other efforts to define errors inherent in thermal field sampling strategies have made an important contribution to quantitative analyses of existing XBT data.

XBT data are commonly processed for analysis in two ways. One is to grid the data on horizontal planes for mapping (e.g. White *et al.*, 1985) and another is to group data scattered zonally about major shipping lanes into two-dimensional vertical sections (e.g. Kessler and Taft, 1987). The error associated with aliased zonal variability when grouping data into vertical sections has not yet been evaluated because of limitations in the observational data base. An error analysis using field data would require large numbers of simultaneous casts separated zonally in such a way that temporal aliasing could be ruled out as a source of error. Data separated in time by even a few hours would not satisfy this requirement because of internal wave noise.

The purpose of this study is therefore to examine the possible effects of aliased zonal variability in grouping the data into vertical sections using a linear, multi-vertical mode model. Similar versions of the model have been used successfully to study the 1982-83 El Niño (e.g. Busalacchi and Cane, 1985; Inoue *et al.*, 1987) and the mean seasonal cycle for the period 1979-81 (McPhaden *et al.*, 1987). In each case, quantitative agreement was found between observed and modeled sea level, dynamic height and/or thermocline depth variability so that the model can be used with some confidence in this sampling study. We examine the period 1979-1983 because there are several

contemporaneous monthly wind products that can be used to force the model and extensive XBT data coverage (Fig. 1). The procedure is to sample model integrations at a series of grid points closely approximating straight lines which correspond to the mean positions of XBT transects in the eastern, central and western Pacific; then for comparison, to sample at the dates and locations of actual XBT casts in each of the three regions defined in Figure 1. Model results are processed to a mean seasonal cycle and 1982-83 El Niño anomalies in dynamic height. Differences in the two methods of sampling provide a measure of the potential for error due to unresolved zonal variations.

This paper is outlined as follows. The XBT data distribution and sampling patterns are described in Section 2, followed by a discussion in Section 3 of the numerical model and wind forcing used for the sampling experiments. Results of the simulation experiments are presented in Section 4 and a summary of major conclusions is presented in Section 5. The principal results of this work are that zonal aliasing may introduce a 2 dynamic cm error in dynamic heights (equivalent to 10 m pycnocline or thermocline displacements) in composite sections of XBT data (though larger errors may occur in regions where ship tracks are separated by 10 degrees of longitude or more). This 2 dynamic cm error, which is comparable to other observational errors (e.g. due to use of a mean temperature/salinity relationship or to the aliasing of internal waves) should not obscure detection of El Niño anomalies or of annual and semi-annual harmonics in the mean seasonal cycle. Frequencies higher than the semi-annual, however, may be adversely affected.

2. XBT Data

Figure 1 shows the distribution of nonredundant, research quality thermal data available to the TOGA community in the tropical Pacific for the period 1979-1983. The total number of casts is close to 35,000, which includes the SOP XBT data, additional XBT data from national hydrographic offices and navies, and some CTD and hydrocast data (Picaut *et al.*, 1987). Many of these data are concentrated along well-traveled shipping lanes in the eastern Pacific, central Pacific and western Pacific. For the period 1979-1983, the regions outlined in Figure 1 contain a total of 18,565 XBT casts of which 4550 are in the east, 8229 in the central and 5786 in the west Pacific. Data have been grouped without regard to longitude in these regions producing data densities of 2.8, 3.3 and 2.4 XBT/month/degree latitude, respectively. These regions have been defined subjectively for other studies (e.g. McPhaden *et al.*, 1987; Picaut *et al.*, 1987) so that they contain at least one XBT per month per degree of latitude, though other groupings are possible (e.g. Kessler and Taft, 1987). Within each region there is a spread of data in the longitudinal direction, however. Most of the data in the western Pacific tend to be concentrated along a single track between Noumea and Japan for the 1979-1983 period covered in this study. Data in the central Pacific are spread across two broad swaths which intersect around 10°S, 175°W, but which are separated by more than 20 degrees of longitude at 20°N. In the eastern Pacific, two heavily traveled tracks diverge south of the equator and are separated by more than 10 degrees of longitude by 10°S.

Figure 2 shows surface dynamic height relative to 400 db calculated by grouping all the data from 1979-1983 along the central Pacific track into one degree latitude and one month bins. Dynamic height has been calculated using XBT temperatures and a mean T/S from Levitus (1982). We present these data

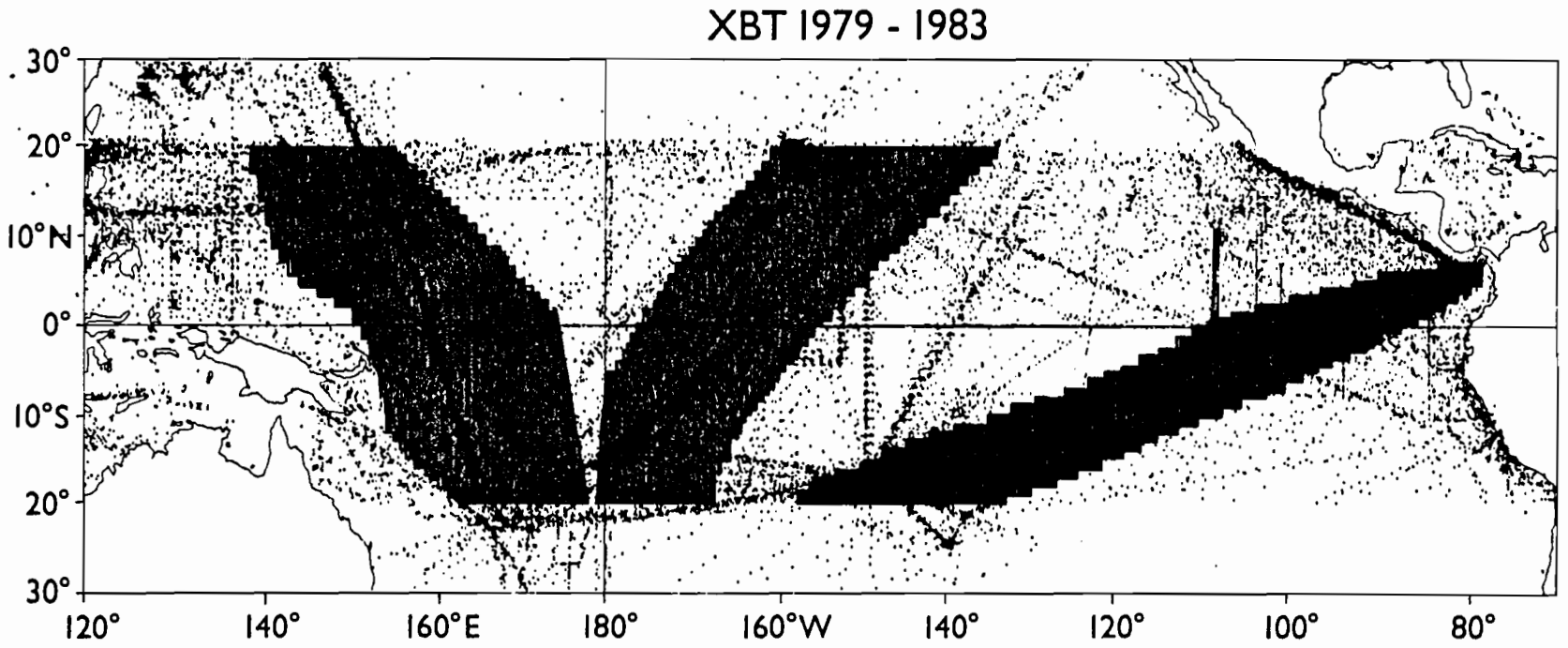

Figure 1. Distribution of XBT data in the tropical Pacific for the period 1979-1983. Outlined areas indicate groupings of XBT data in the eastern, central and western Pacific.

for a brief comparison with model simulated dynamic height in Section 4. More extensive discussion of the data can be found in McPhaden *et al.* (1987).

Figures 2a-d show respectively the mean seasonal cycle for 1979-81, the annual mean for 1979-81, seasonal variations about the annual mean, and the standard deviation of mean seasonal cycle. In the central Pacific, the North Equatorial Countercurrent (NECC) trough is located on average at 10°N (Figure 2b), and is shallowest in boreal spring and deepest in boreal fall (Figure 2a). There is an equatorial ridge at 5°N, and an equatorial trough centered on the equator. Variability in the vicinity of the equatorial ridge and trough is in phase, with low sea level in spring and early summer and high sea level in the fall (Figure 2c). A South Equatorial Countercurrent (SECC) ridge near 8°S is highest in the spring and lowest in the fall. Typical standard deviations of monthly means across 20°N to 20°S is 3 dynamic cm, with values of 5-6 dynamic cm in the vicinity of the NECC trough and equatorial ridge (Figure 2d). Currents associated with this ridge/trough topography are the North Equatorial Current (NEC) north of 10°N, the NECC between 5°N and 10°N, the South Equatorial Current (SEC) between 5°N and 8°S and the South Equatorial Countercurrent (SECC) between 8°S and 12°S in boreal spring.

Figure 2e shows July 1982-June 1983 El Niño anomalies from the 1979-81 mean seasonal cycle and Figure 2f shows their standard deviation. For our purposes it is important to note that El Niño anomalies, which often exceed 10 dynamic cm, are larger in general than variations in the mean seasonal cycle, particularly between 5-10°S. Kessler and Taft (1987) find similar variations in dynamic topography in the central Pacific using an XBT data set similar to ours, but with about 35% fewer data during 1979-83.

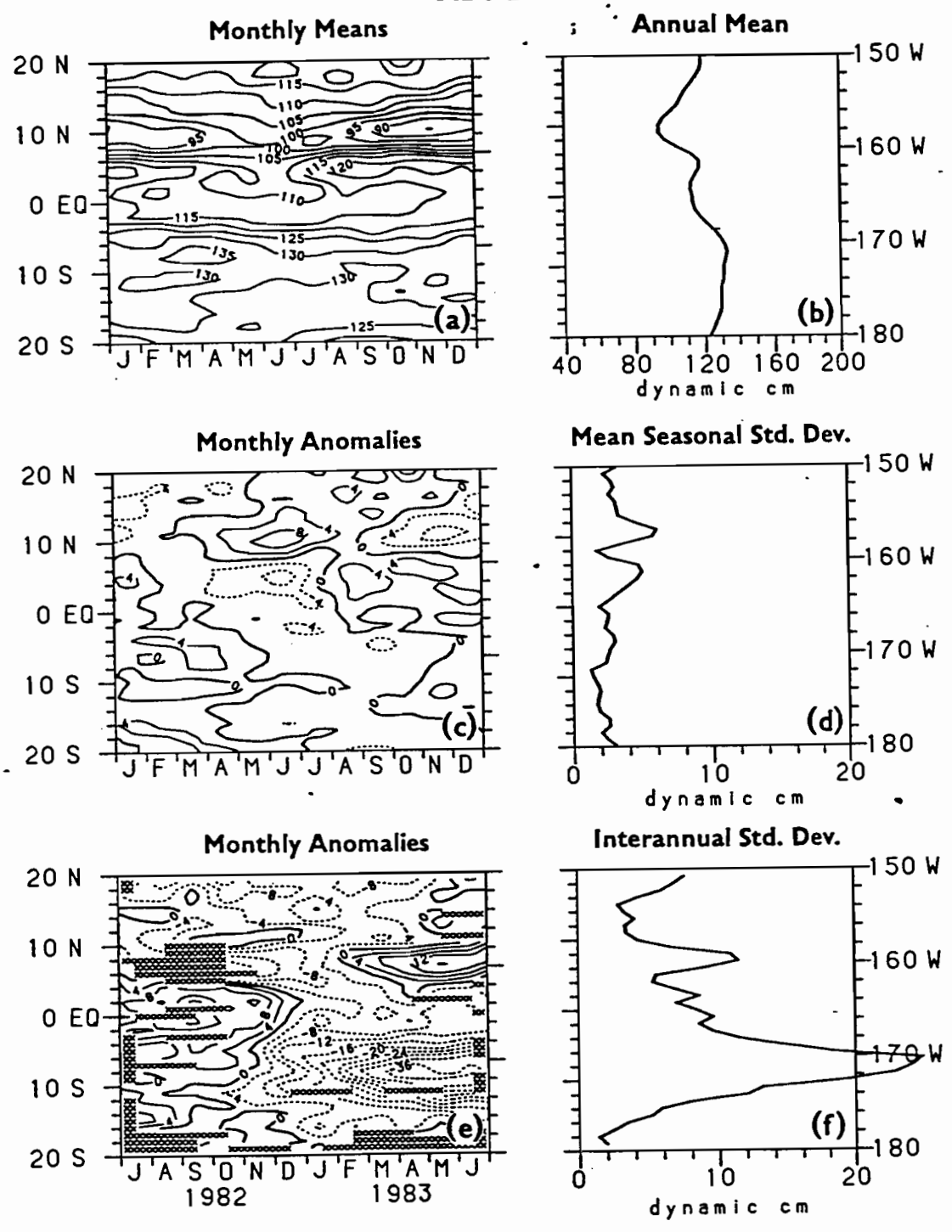

Figure 2. XBT data processed to dynamic heights relative to 400 db as a function of latitude and longitude from the central Pacific swath of data in Figure 1 for the period 1979-1983; (a) Monthly means, (b) annual mean (c) monthly anomalies computed as the difference of the annual mean from the monthly mean, (d) mean seasonal standard deviation computed from monthly anomalies, (e) July 1982-June 1983 anomalies from the mean seasonal cycle and (f) standard deviation of the El Niño anomalies. Contour interval is 5 dynamic cm in (a) and 4 dynamic cm in (c) and (e). Hatching in (e) indicates no XBT data were available.

3. Model and wind forcings

The model used in this study is similar to that employed by Busalacchi and O'Brien (1980). A linear, numerical treatment of the shallow water wave equations is used here to address sampling questions with respect to the wind-driven dynamic response of the tropical Pacific Ocean. Changes to the previous version of the model include increased horizontal resolution of 40 km between like variables and a horizontal Laplacian friction of 10^7 cm^2 s^{-1}. The model basin extends from 20°N to 20°S and 126°E to 70°W. A no-slip condition is imposed along the idealized coastal boundaries and an open boundary condition (Roed and Smedstad, 1984) is applied at the northern and southern boundaries. The open boundary condition has little effect on the solution except within the local internal radius of deformation from the boundary (i.e., poleward of about 19°). Model height field solutions are generated for the four gravest baroclinic modes of a specific Brunt-Väisälä profile. A final solution is found by summing the individual contributions of all four modes. The modal decomposition, based on stratification data between 1.5°N and 1.5°S at 179°W as presented by Eriksen *et al.* (1983), is also the same as in Cane (1984) and Busalacchi and Cane (1985). These data were chosen because they were obtained within the equatorial wave guide in a region with significant wind stress fluctuations on seasonal and interannual time scales. The internal wave speeds for the four vertical modes are c1 = 2.90 m s^{-1}, c2 = 1.77 m s^{-1}, c3 = 1.13 m s^{-1}, c4 = 0.84 m s^{-1}.

Due to the range of the four wave speeds the time step of the model is mode dependent. All mode 1 calculations have a 1-hour time step whereas the slower speeds of modes 2-4 permit a 2-hour time step without compromising numerical stability. Similarly, the time required for initial transients to die out during spin-up is mode dependent. Beginning from a state of no motion

and in response to a mean seasonal wind stress for 1979-1981, an exact repeating seasonal cycle is obtained basin-wide after a spin-up of 12 years for mode 1, 22 years for mode 2, 42 years for mode 3, and 62 years for mode 4. After the seasonal cycle has spun up, the u, v, and h fields at the end of the mean seasonal year are used as the initial conditions for a three year integration forced by individual monthly mean wind stresses for 1979 through 1983.

The model integrations are performed using three distinct wind stress products for which monthly means are currently available for January, 1979 through December, 1983. Two of these data sets are derived from subjective analyses and the third from an operational objective analysis. One of the subjective analyses is the Florida State University (FSU) analysis of ship wind observations provided by James J. O'Brien. The analysis procedure of transforming individual ship-board observations into monthly mean wind stress fields on a 2° × 2° grid is described by Goldenberg and O'Brien (1981). The other subjective analysis is a combination of satellite-observed, low-level cloud motions, ship wind observations, island wind observations, and buoy wind observations performed by James Sadler at the University of Hawaii. This derivation of monthly mean surface winds on a 2.5° × 2.5° grid from satellite observations of low-level cloud drift (referred to hereafter as SAWIN) is described in Sadler and Kilonsky (1985). The third data set we use is an objectively analyzed, operational product from the Global Band Analyses of the United States Navy's Fleet Numerical Oceanography Center (FNOC). An objective analysis based on Cressman (1959) is used on all reports (ship, island, buoy, etc.) in an operational data base for six hour intervals on a 2.5° × 2.5° grid. The six hourly data have been averaged to form the monthly means used here. In the present study a constant drag coefficient of 1.5×10^{-3} is used to convert from wind to wind stress for each of the three wind data sets.

The 1979-81 mean zonal wind stress from the FSU analysis is shown in Figure 3a. The easterly component of the northeast and southeast trade winds is predominant over most of the basin. Quite evident are the core regions (>0.8 dyne cm^{-2}) of the trades poleward of 10°. Weak mean westerlies are present at low-latitudes at the extreme ends of the basin. In general, similar mean features are present in the SAWIN and FNOC fields. The standard deviation of the mean seasonal cycle for 1979-1981 is shown in Figure 3b. Zonal wind stress fluctuations over this three year period are smallest in those regions where the mean wind is weakest, i.e. 5° from the equator. The largest fluctuations (>0.4 dyne cm^{-2}) occur off the equator where gradients in the mean zonal wind stress are largest and also within the monsoon regimes of both hemispheres in the west. Basin wide, sixty to eighty percent of this mean seasonal variability is due to the annual harmonic. The standard deviation of zonal wind stress anomalies about the mean seasonal cycle is shown in Figure 3c. Variations are dominated by the extreme variations associated with the 1982-83 El Niño. The largest variability occurs near and south of the equator in the central Pacific in regions where the mean seasonal fluctuations are generally small (cf. Figure 3b). Similar large scale features of the variability are present in the SAWIN and FNOC analyses as well.

The mean 1979-81 sea level modeled in response to this wind forcing is presented in Figure 4a. The sea level distribution is characterized by a system of zonally oriented troughs and ridges delineating the major geostrophic currents of the model solution. Between the sea level ridge at 20°N and the trough at 9°N flows a westward directed North Equatorial Current. An eastward flowing North Equatorial Countercurrent is flanked by the North Equatorial Countercurrent Trough to the north (9°N) and an

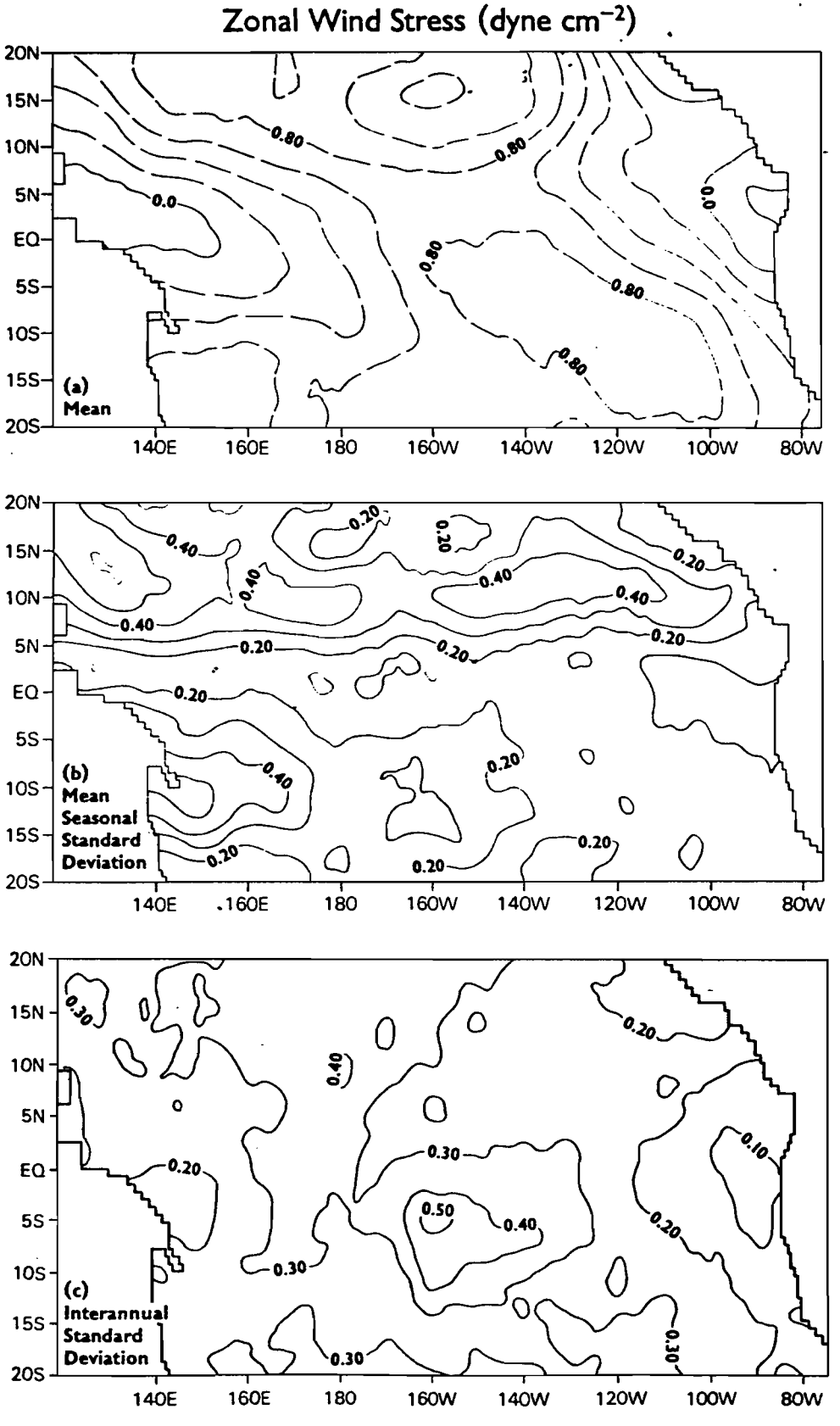

Figure 3. FSU zonal wind stress (in dyne cm^{-2}); (a) mean for 1979-81, (b) standard deviation of mean seasonal cycle for 1979-81 and (c) standard deviation of 1979-83 anomalies about the mean seasonal cycle.

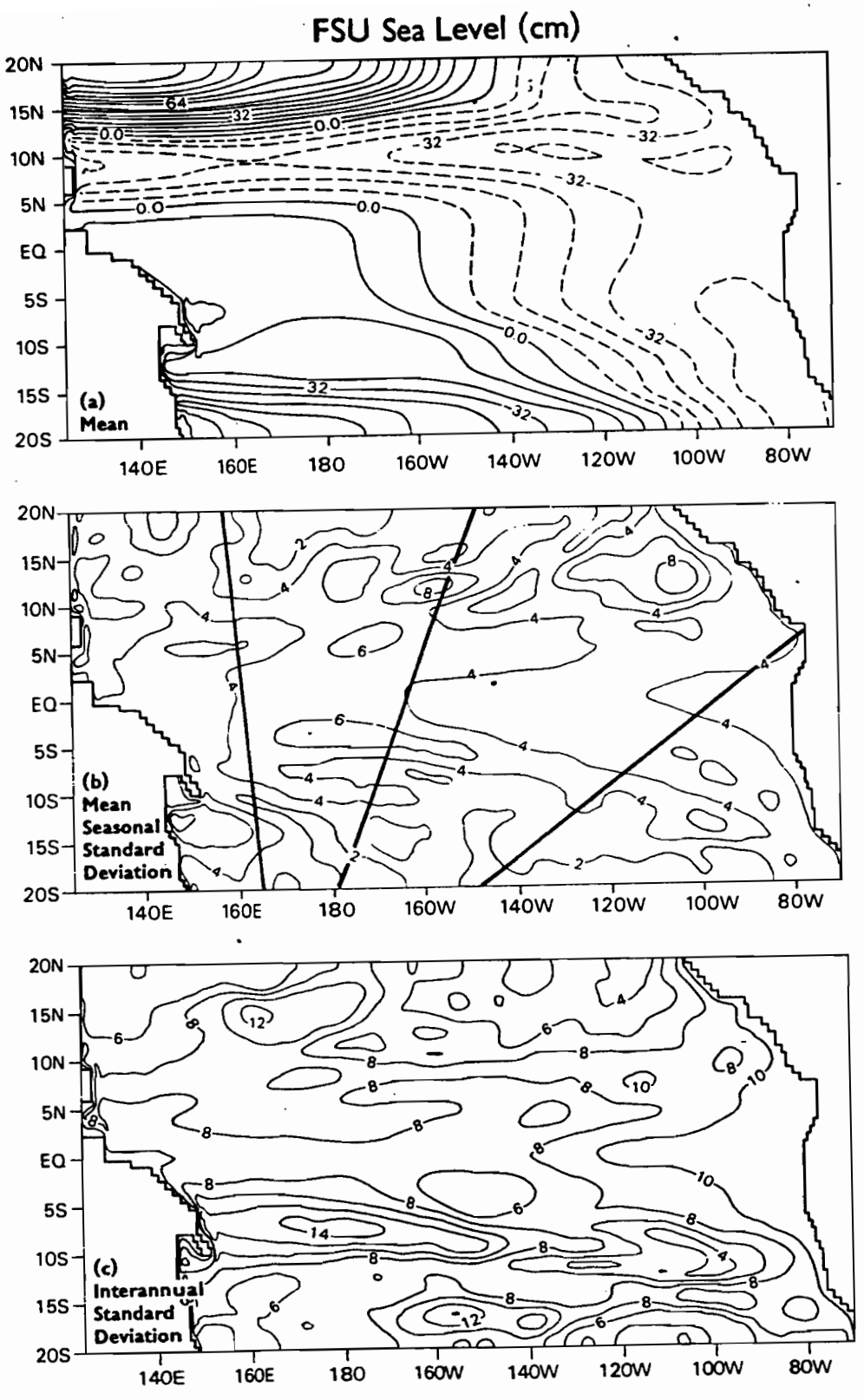

Figure 4. Model sea level response to FSU wind forcing (in cm); (a) mean for 1979-81, (b) standard deviation of mean seasonal cycle for 1979-81 and (c) standard deviation of 1979-83 anomalies about the mean seasonal cycle. Heavy lines in (b) indicate the approximate mean position of XBT distributions in the eastern, central and western Pacific.

Equatorial Ridge to the south (2-4°N). Considerably less structure is found in the southern hemisphere where a weak South Equatorial Current is found between 6-20°S. Mean seasonal fluctuation are summarized by a standard deviation of the variability for 1979-1981 (Figure 4b). As in the winds, 60-80% of the variance is associated with the annual harmonic. The largest seasonal changes ($\geq$8 cm) occur in the northeastern corner of the basin in a region known as the Costa Rica Dome. Further to the west most of the dominant variability is found within the same latitudinal band of 10-15°N, resulting in seasonal changes to the North Equatorial Current and Countercurrent system. Maxima in the southern hemisphere are representative of seasonal changes to the South Equatorial Current and the reversal and intensification of a South Equatorial Countercurrent. The pattern of interannual fluctuations about the mean seasonal cycle, which is dominated by the 1982-83 El Niño, is shown in Figure 4c. The variations are stronger in general than for the mean seasonal cycle and have a somewhat different pattern. Variations in excess of 10 cm rms occur east of 120°W between 10°N and 10°S, and west of 160°W between 10-15°N and 5-10°S.

4. Results of Sampling Experiments

The results presented in this section are derived from sampling the model in two different ways. The first is to extract data from the model along "grid-point transects" i.e. from approximately straight lines of grid points in the model that correspond to the mean position of XBT tracks in the eastern, central and western Pacific. Grid-point transects are superimposed on the sea level standard deviation plot in Figure 4b. A mean seasonal cycle for 1979-81, as well as July 1982-June 1983 anomalies from this seasonal cycle, are then computed at each degree of latitude. The second method of

extracting data from the model is to sample at the exact dates and latitude/longitude positions of actual XBT casts during 1979-1983. Data are then binned by month and by degree of latitude in each of the three regions outlined in Figure 1 for computation of a mean seasonal cycle and El Niño anomalies. Data density in time (2.8-3.3 XBT/month/degree latitude) is sufficient to resolve the highest model frequency of 1 cycle per 2 months, so that any differences between these "XBT transects" and the corresponding grid-point transects result from aliasing of zonal variations in the model. For consistency with XBT measurements, model dynamic heights are computed relative to 400 db, though the correlation between model sea level and dynamic heights is high as is the correlation between observed sea level and dynamic heights in the tropics (e.g. Rebert *et al.*, 1985).

Figure 5 shows variations along the grid-point transect taken from the central Pacific in the model. We note that as in the observations (Figure 2), the NECC trough is located near 10°N (Figure 5b), and is shallowest in boreal spring and deepest in boreal fall (Figure 5a). Similarly, near the equator dynamic height is low in spring and summer and high in winter. Variations are comparable in magnitude to those in the XBT data shown in Figure 2, with a maximum just north of the NECC trough of 7 dynamic cm and another maximum near 3°N (two degrees latitude south of the corresponding maximum in the data) of 5 dynamic cm. Anomalies in 1982-83 (Figure 5e and 5f) are generally stronger than variations in the mean seasonal cycle, especially between 5-10°S in the first part of 1983 when there is a very large 20-30 dynamic cm depression in surface elevation similar to that seen in Figure 2e. There are significant differences between the data sets however, which are elaborated on in McPhaden *et al.* (1987). The model has very high north and south equatorial ridges at 20°N and 20°S and no mean equatorial trough. Also, the model section contains

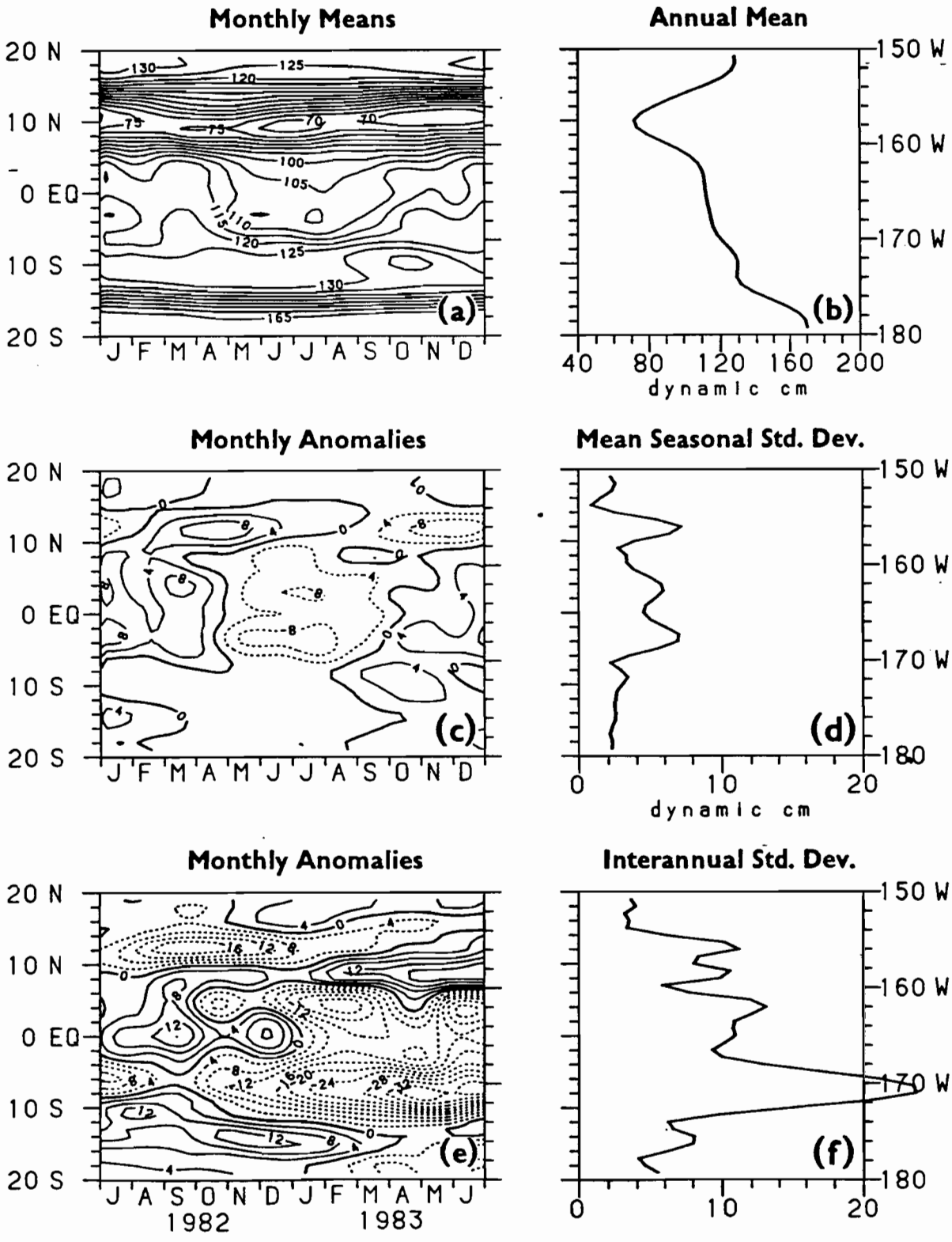

Figure 5. Dynamic heights relative to 400 db as in Figure 2, but for the central Pacific grid-point transect from the model forced by FSU winds for the period 1979-1983.

a maximum in dynamic height variability near 4°S which is absent in the data. Finally, the SECC ridge is best developed in boreal fall near 10°S in the model as compared to near 8°S in boreal spring in the data. Thus, as expected, the model is an imperfect analogue of the real ocean, though the model variability has many features in common with that inferred from XBT data. We proceed with a sampling sensitivity study with these limitations in mind.

Figure 6 shows the effect of sampling the model at XBT times and locations. Most of the major features evident in the grid-point transect are evident in the XBT transect, e.g. the seasonal variations in the NECC trough and along the equator. However, there is a significant amount of small scale noise introduced into the analysis which is most pronounced in the monthly anomalies and standard deviation. The most noticeable effects of this noise are a reduction in amplitude of mean seasonal variations near 12°N and very large amplitude fluctuations between 16°N and 20°N. This noise due to sampling error, defined as the difference between the XBT transect minus the grid-point transect time series, is shown in Figure 7. (The difference during 1982-83 is the difference of the total dynamic height time series, not the anomaly time series, since differences of the latter include differences of the mean seasonal cycle). The error on average is about 2 dynamic cm for both the mean seasonal cycle and the El Niño period, except between 16°N and 20°N where in both cases it rises well above 4 dynamic cm. The reason for this large error in the northernmost portion of the XBT transect is that the data are collected along two broad swaths separated by more than 20 degrees of longitude. At this separation, first vertical mode Rossby waves at the annual period, which are an important source of variability at these latitudes in the model, are badly aliased because their zonal wavelengths are only about 17 degrees of longitude.

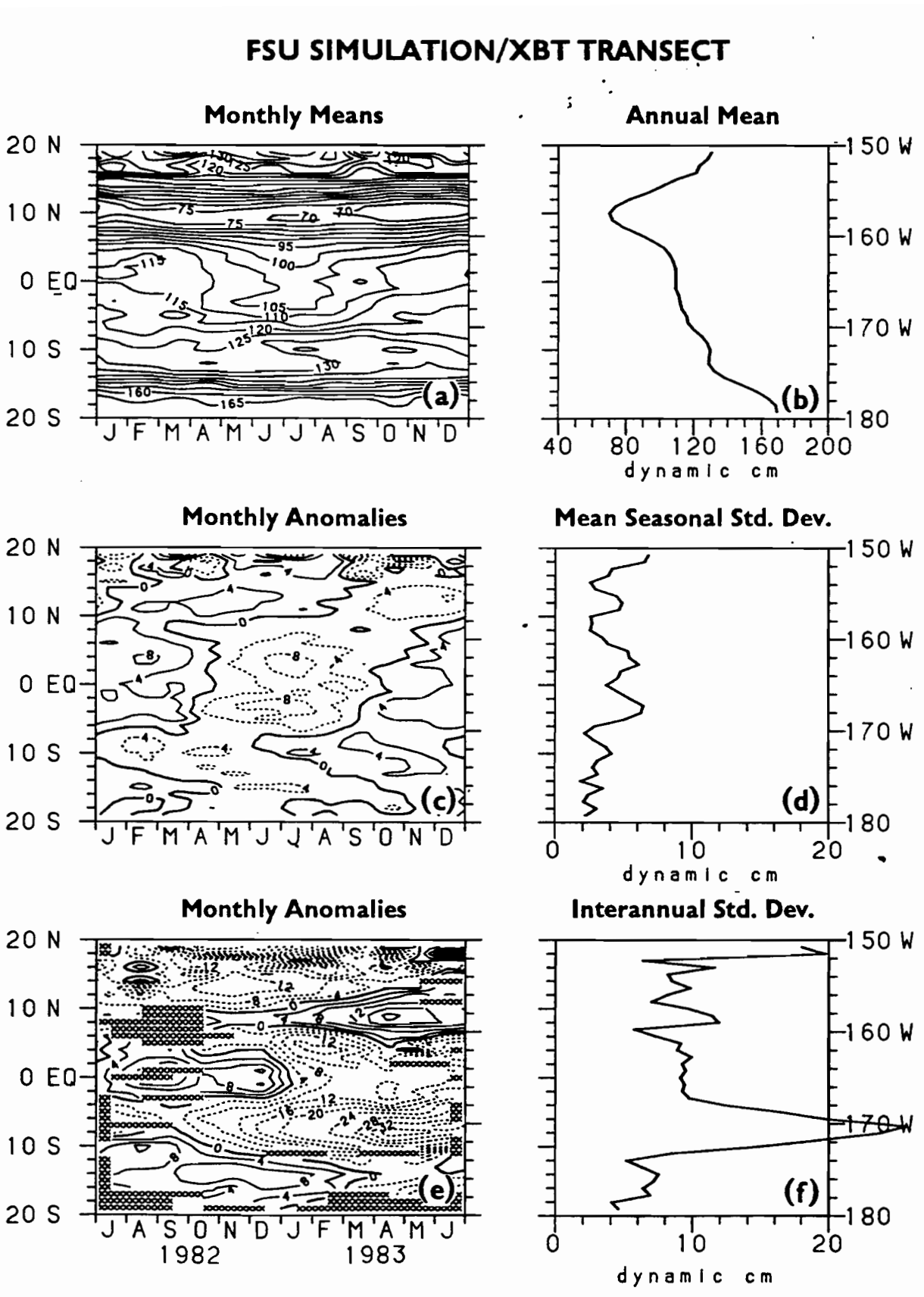

Figure 6. Dynamic heights relative to 400 db as in Figure 5, but for the central Pacific model XBT transect.

Noise levels in the XBT transect can be reduced slightly by averaging in latitude and/or time. Figure 8 for example shows the effects of passing a 1-2-1 filter over the mean seasonal data in the latitudinal direction at one degree intervals. Variations in dynamic topography are smoother than in the XBT transect in Figure 6c and 6d and features corresponding to the grid-point transect in Figure 5 are better defined. However, noise levels are still about 2 dynamic cm in amplitude. Moreover, smoothing does not recover the signal amplitude at 12°N, nor does it eliminate the noise variance between 16°N and 20°N.

Comparison of Figures 5 and 7 suggest that aliasing of zonal variability is more of a problem for detection of typical seasonal variations than for El Niño anomalies. Mean seasonal variations are of smaller amplitude than El Niño variations, but noise levels are comparable for both (except between 16°N and 20°N). We thus examine the limits of detectability in greater detail for seasonal variations. Figure 9 shows model frequency spectra of mean seasonal dynamic height variance averaged over all latitudes in the central Pacific. Figure 9a shows the total variance for the grid-point transect, the XBT transect, the XBT transect smoothed in latitude with a 1-2-1 filter and the XBT transect smoothed in time with a monthly 1-2-1 filter. The spectra are red with most variance at one cycle per year (1 cpy) in each case. Energy levels in the XBT transect are higher at all frequencies compared with the grid-point transect due to small scale noise. Smoothing in latitude and/or time reduces variance levels at the higher frequencies where this noise is most prominent. Figures 9b and 9c separate the signal and noise components of the total spectra in Figure 9a. Smoothing in latitude does not remove much signal variance, whereas noise levels are reduced uniformly in frequency. Conversely, smoothing in time eliminates the highest frequencies in both the signal and noise spectra.

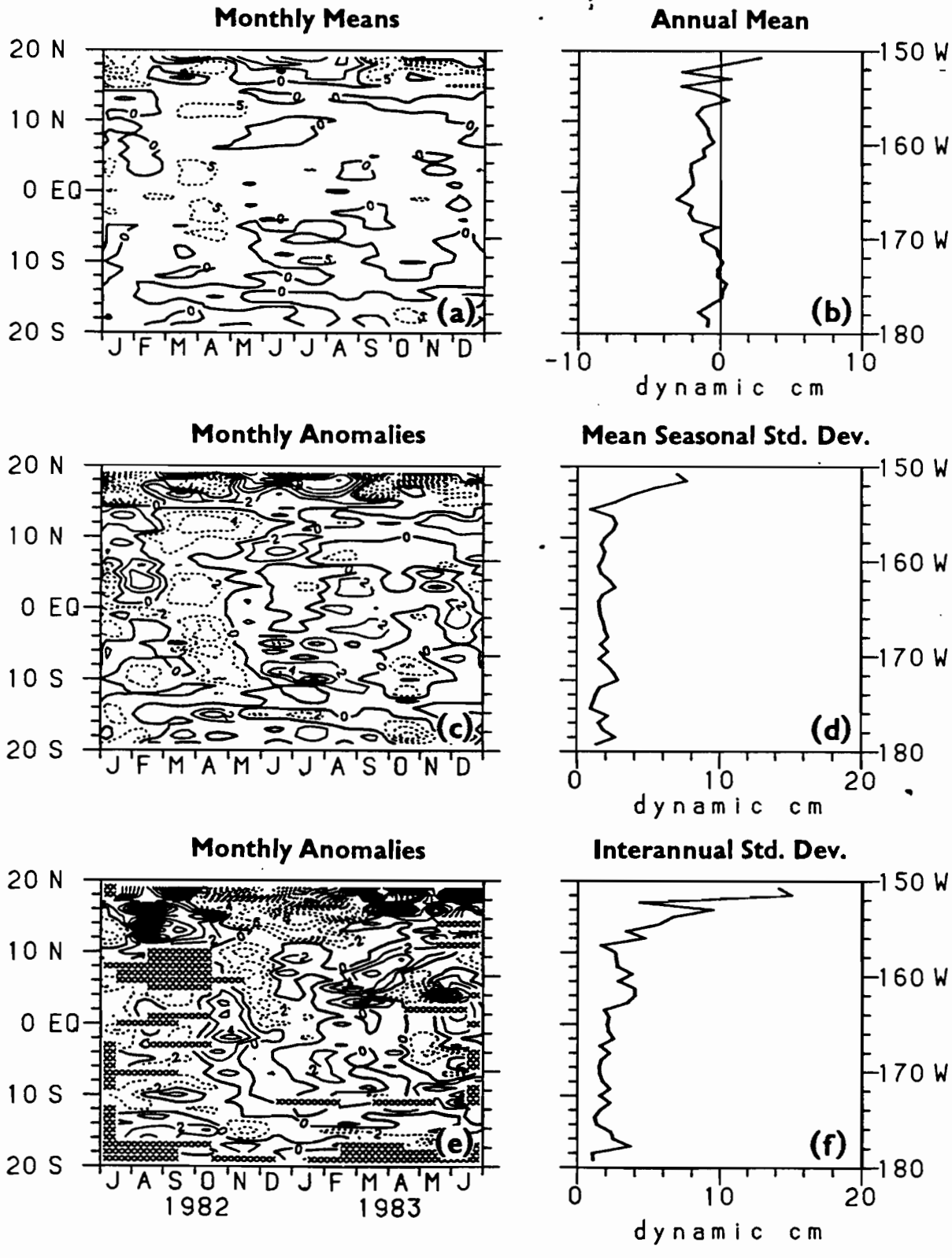

Figure 7. The dynamic height difference field obtained by subtracting the grid-point transect from the XBT transect. Contour interval in (a) is 5 dynamic cm and in (c) and (e) is 2 dynamic cm.

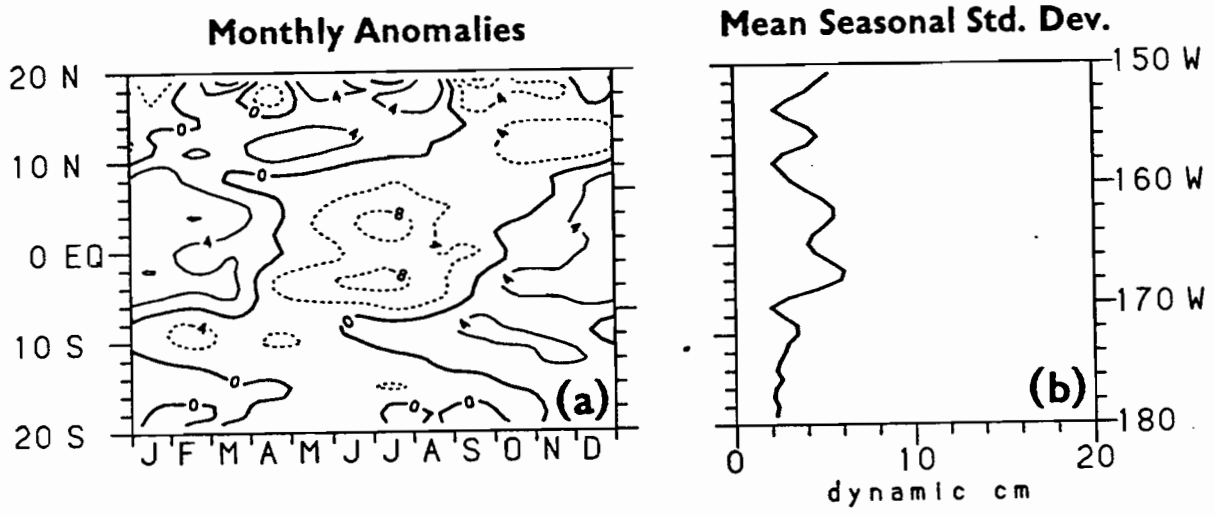

Figure 8. Mean seasonal variations from the model XBT transect in Figure 6 smoothed with a 1-2-1 latitudinal filter: a) deviations from annual mean and b) mean seasonal standard deviation.

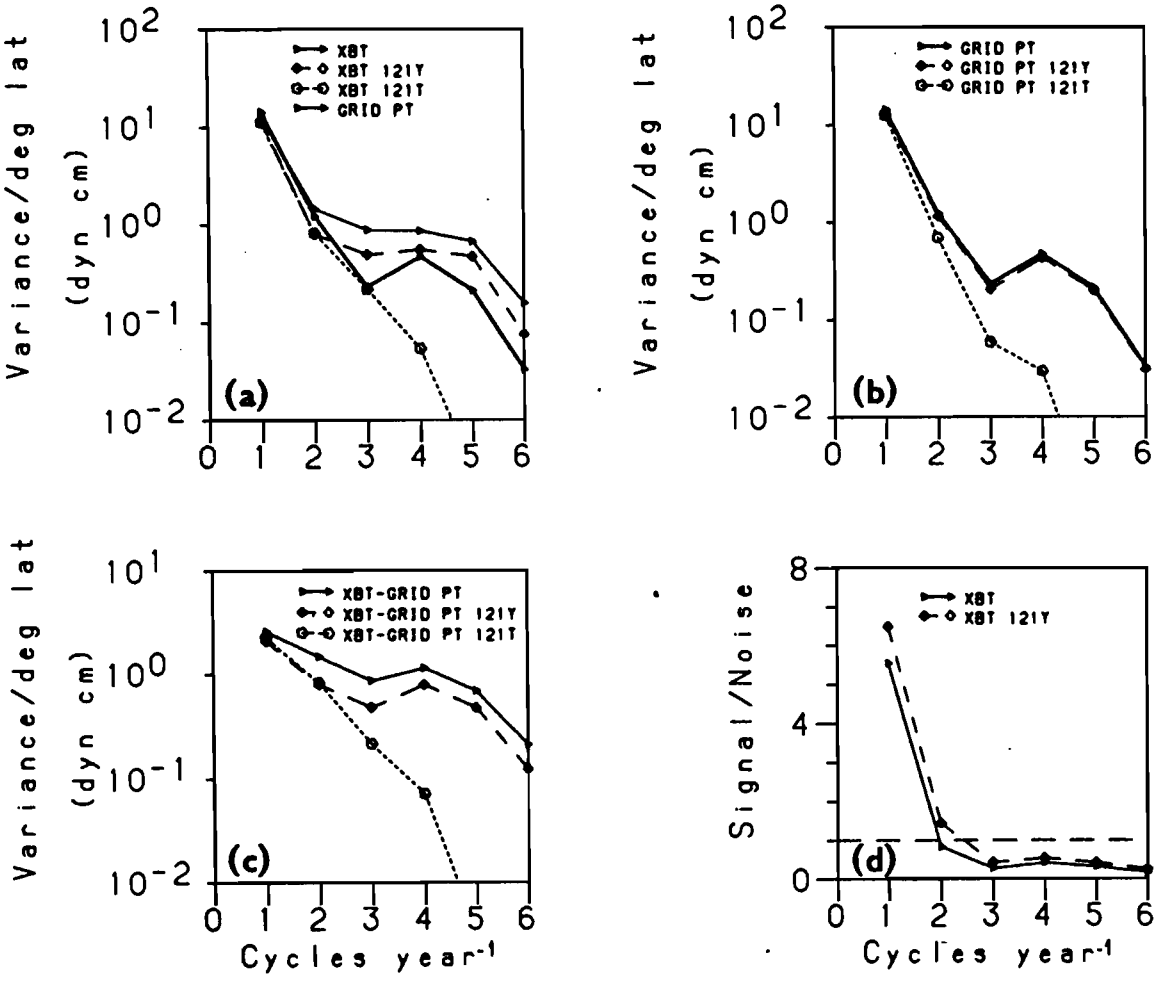

Figure 9. (a) Latitudinally averaged dynamic height variance relative to 400 db (in dynamic cm^2) as a function of frequency for the grid-point transect, the XBT transect, the XBT transect smoothed in latitude with a 1-2-1 filter (i.e. 121Y) and the XBT transect smoothed in time with a 1-2-1 monthly filter (i.e. 121T); (a) total variance, (b) signal variance and (c) noise variance due to zonal aliasing; (d) is a signal-to-noise spectrum computed as a ratio of spectral coefficients in (b) to those in (c).

Signal-to-noise variance ratios for the XBT transect and the XBT transect smoothed in latitude are shown in Figure 9d. Signal-to-noise for the XBT transect smoothed in time is identical to that for the unsmoothed XBT transect because both signal and noise are reduced in proportion to one another. Signal-to-noise variance ratios at 1 cpy are 5.6 for the XBT transect and 6.7 for the latitudinally smoothed version of the XBT transect. This ratio drops to near unity at 2 cpy and is less than 0.5 for all higher frequencies.

Thus, we can conclude from Figure 9 that zonal aliasing affects all frequencies in monthly mean time series and that it most severely impacts frequencies higher than 1 cpy. Signal-to-noise variance drops below unity at 2 cpy which marks the probable limits of accurate frequency resolution. Smoothing in time leads to lower overall noise levels than smoothing in latitude, while the latter leads to higher signal-to-noise ratios at low frequencies which contain most of the signal variance.

Figure 10 presents plots of the annual mean and standard deviation of model dynamic height along transects in the eastern, central and western Pacific. Both signal amplitudes and noise amplitudes due to zonal aliasing are presented for comparison. We see that like the central Pacific, zonal aliasing in general introduces about a 2 dynamic cm error in the eastern and western Pacific. Estimates of mean dynamic topography are relatively unaffected and signal amplitude for the mean seasonal cycle is generally greater than noise amplitude by a factor of 2. Areas where the noise amplitude rises significantly above 4 dynamic cm are found between 16°N and 20°N in the central Pacific as noted above, and in the eastern Pacific between 8°S and 16°S. Noise amplitude is also consistently higher than the signal amplitude in both these regions (extending to 20°S in the east) where data from SOP program are collected along shipping lanes separated by about 10

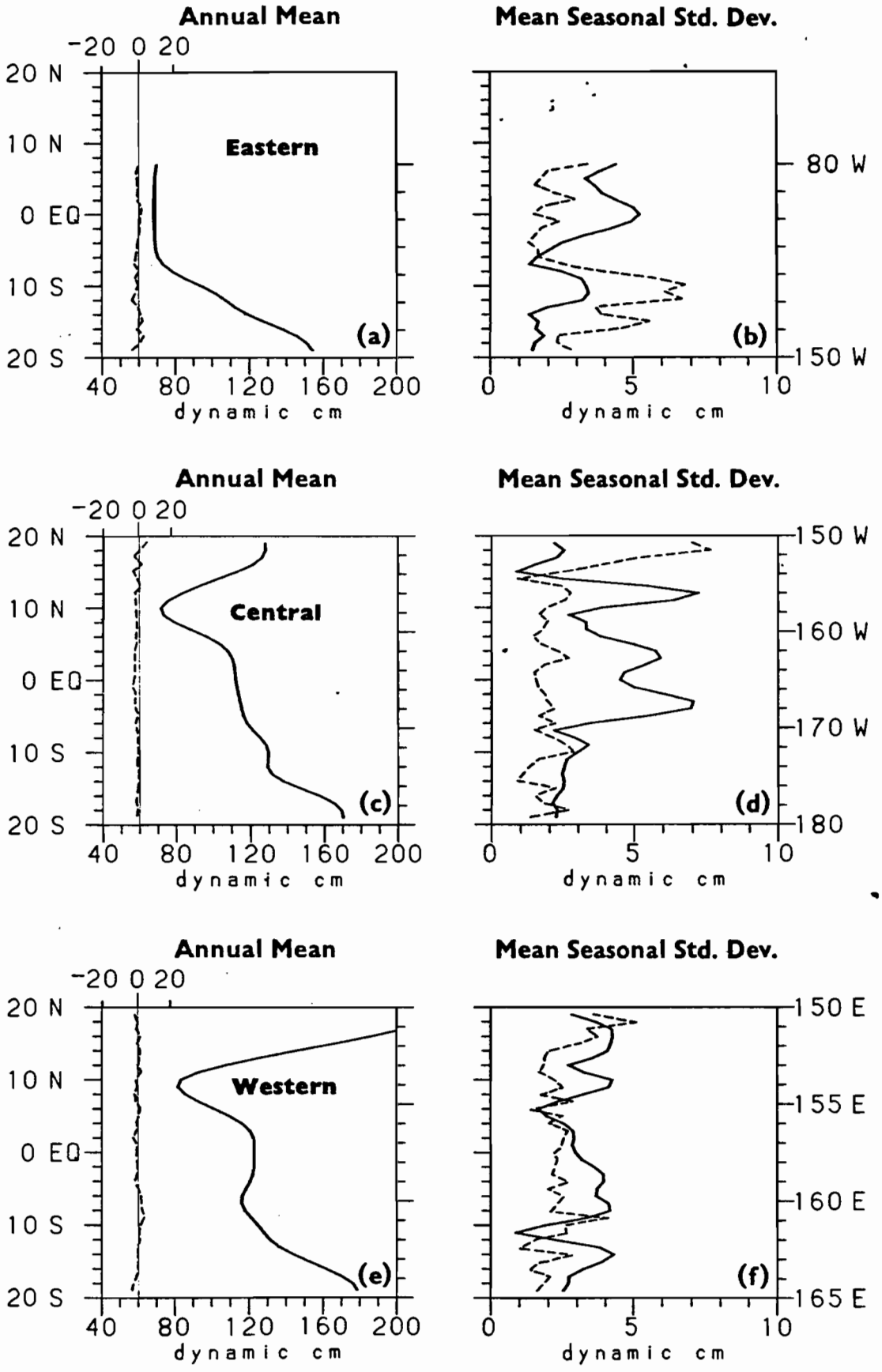

Figure 10. Dynamic height annual means and standard deviations relative to 400 db (in dynamic cm) from grid-point transects in the eastern, central and western Pacific (solid lines) superimposed on noise due to zonal aliasing in XBT transects (dashed lines).

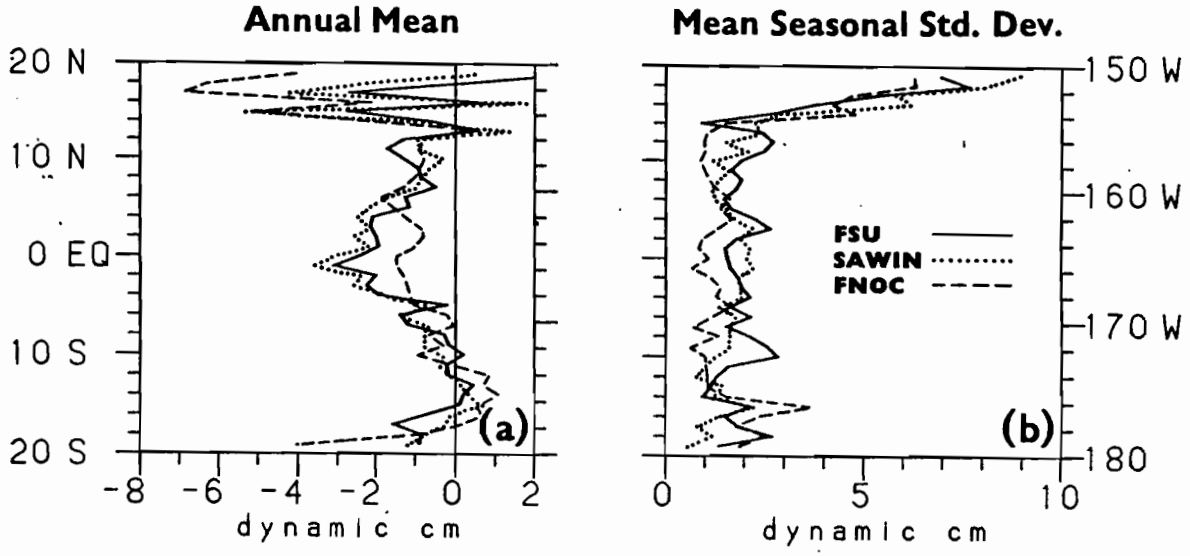

Figure 11. Noise in dynamic height relative to 400 db due to zonal aliasing in the central Pacific for the model driven by FSU (—), SAWIN (···), and FNOC (---) wind fields.

degrees of longitude or more (Figure 1). In the model, those regions are strongly affected by Rossby wave radiation at 1 cpy which is badly aliased by the sampling distribution of XBT data.

The sampling sensitivity studies discussed above were repeated for the model driven by the SAWIN and FNOC wind products. Figure 11 shows the noise levels in dynamic height for the mean seasonal cycle in the central Pacific. All three model results show a 1-3 dynamic cm mean and standard deviation noise level except between 16°N and 20°N where errors can be 4 dynamic cm or more. The FNOC calculation tends to show slightly lower noise levels along this transect between 15°N and 15°S, though this is not true in general in the eastern and western Pacific. Thus, our basic results are insensitive to which wind set is used to force the model.

5. Summary and Conclusions

In the preceding sections we have described a series of sampling sensitivity experiments to examine the effects of zonal aliasing in estimates of mean seasonal and El Niño dynamic height variations along XBT transects in the tropical Pacific Ocean. We have used a linear, multi-vertical mode model forced with three different monthly mean wind stress sets for the period 1979-1983. The model is sampled at approximately straight lines of grid points corresponding to the mean positions of XBT tracks in the eastern, central and western Pacific and then sampled again at the dates and locations of actual XBT casts for 1979-1983. Model data are processed to a mean seasonal cycle and El Niño anomalies in dynamic height with a resolution of one degree in latitude and one month in time. Comparing results for the two methods of sampling the model indicates that zonal aliasing in general may lead to about a 2 dynamic cm error in dynamic height. The error in dynamic

height translates into about a 10 m pycnocline displacement in the model. In general, salinity has a secondary effect on density stratification in the tropics, so that these pycnocline displacements would be mirrored in thermocline displacements.

The 2 dynamic cm error is comparable to the error that results in the ocean from unresolved internal gravity waves (Hayes, 1982), as is the equivalent 10 m error in thermocline displacement (e.g. Munk, 1981). This error is also comparable to the 1-2 dynamic cm error expected from using a mean T/S relationship to estimate dynamic heights from XBT data (Kessler and Taft, 1987). This magnitude of error generally does not obscure detection of the 1982-83 El Niño signal or of the weaker mean seasonal cycle in the model. Exceptions to this generalization occur in regions where XBT sample spacing in the zonal direction is insufficient to resolve Rossby wave variations in the model. Specific sites of severe aliasing are 16°N to 20°N in the central Pacific and 8°S to 20°S in the eastern Pacific. Smoothing in latitude and/or time can reduce noise levels slightly, but cannot eliminate the effects of unresolved zonal variations. In the model we also found that detection of the mean seasonal cycle was limited to 1 and 2 cpy variations since at higher frequencies signal-to-noise ratios dropped below unity. Thus caution should be exercised in drawing conclusions at frequencies higher than 2 cpy from XBT data grouped along transects as in Figure 1. These results are insensitive to the choice of wind forcing used in the model, since comparable noise levels and patterns appear in simulations forced by the FSU, SAWIN and FNOC winds.

We performed a similar set of calculations for geostrophic transport per unit width over 0 to 400 m. Transports were calculated orthogonal to each transect for latitudes poleward of 2°N and 2°S. In the mean, the largest

transport errors occurred equatorward of 10° where the geostrophic calculation is most sensitive to small amplitude fluctuations. Both here and at higher latitudes, however, mean errors were relatively small and would not obscure the main features of the mean circulation. Errors in time varying transport were about 10 m^2 sec^{-1} (equivalent to 5 cm sec^{-1} over 200 m), with larger values near the equator and smaller values at higher latitudes. The signal-to-noise amplitude ratio was typically closer to unity, which is lower than for dynamic height. This is consistent with the fact the transport is a spatial derivative and therefore a high-pass filtered version of dynamic height. Dynamic height variations tend to be most energetic on large space scales whereas noise variations tend to be white in wavenumber space. Hence, signal-to-noise is less favorable on the smaller scales on which transport variations occur.

The fact that the model used in this study is linear and forced by monthly winds means that it can only simulate frequencies lower than 6 cpy. It is known that there is significant energy at higher frequencies in the tropics (e.g. Hayes and McPhaden, 1987) due to instabilities of the large scale current system (e.g. Legeckis *et al.*, 1983), wind forcing (e.g. Wunsch and Gill, 1976) and tidal forcing (e.g. Weisberg *et al.*, 1987). To the extent that these higher frequencies can have zonal scales comparable to or smaller than the XBT sample spacing, as is the case for instability waves with O(100 km) zonal scales, our results probably underestimate the effects of zonal aliasing.

Acknowledgments

The authors would like to thank J.J. O'Brien for providing the FSU wind product, J. Sadler for providing the SAWIN product and J.C. Kindle for

providing the FNOC wind product for this study. Support for this work was provided by NOAA's U.S. TOGA Project Office and EPOCS Program (MJM and GR), by NASA RTOP 161-20-31 (AJB) and by ORSTOM and PNEDC (JP). We also thank D. Allison, R. Rosario and V. Fabre for technical assistance.

References

Busalacchi, A.J. and J.J. O'Brien, The seasonal variability in a model of the tropical Pacific, *J. Phys. Oceanogr., 10*, 1929-1951, 1980.

Busalacchi, A.J. and M.A. Cane, Hindcasts of sea level variations during the 1982-83 El Niño, *J. Phys. Oceanogr., 15*, 213-221, 1985.

Cane, M.A., Modeling sea level during El Niño, *J. Phys. Oceanogr., 14*, 1864-1874, 1985.

Cressman, G.P., An operational objective analysis system, *Mon. Wea. Rev., 87*, 367-374, 1959.

Eriksen, C.C., M.B. Blumenthal, S.P. Hayes and P. Ripa, Wind-generated equatorial Kelvin waves across the Pacific Ocean, *J. Phys. Oceanogr., 13*, 1622-1640, 1983.

Firing, E. and R. Lukas, Sampling and aliasing during the NORPAX Hawaii-to-Tahiti Shuttle Experiment, *J. Geophys. Res., 90*, 11709-11718, 1985.

Goldenberg, S.B. and J.J. O'Brien, Time and space variability of tropical Pacific wind stress, *Mon. Wea. Rev., 109*, 1190-1207, 1980.

Hayes, S.P., A comparison of geostrophic and measured velocities in the Equatorial Undercurrent, *J. Mar Res., 40 (Supplement)*, 219-229, 1982.

Hayes, S.P. and M.J. McPhaden, Temporal sampling requirements for low frequency temperature variability in the eastern equatorial Pacific Ocean, Manuscript in preparation.

Inoue, M., J.J. O'Brien, W.B. White and S.E. Pazan, 1987: Interannual variability in the tropical Pacific Ocean for the period 1979-1982. *J. Geophys. Res.*, in press.

Kessler, W.S., B.A. Taft and M.J. McPhaden, An assessment of the XBT sampling network in the central Pacific Ocean, USTOGA4 Tech. Rept., University Corporation for Atmospheric Research, Boulder, Colo., 62 pp., 1985.

Kessler, W.S. and B.A. Taft, Dynamic heights and zonal geostrophic transports in the central tropical Pacific during 1979-1984, *J. Phys. Oceanogr., 17*, in press, 1985.

Legeckis, R.L., W. Pichel and G. Nesterczuk, Equatorial long waves in geostationary satellite observations and in multichannel sea surface temperature analysis, *Bull. Am. Meteorol. Soc., 64*, 133-139, 1983.

Levitus, S., Climatological Atlas of the World Ocean, NOAA Prof. Pap. 13, U.S. Govt. Printing Office, 173 pp., 1982.

McPhaden, M.J., A.J. Busalacchi and J. Picaut, Model validation study of the mean seasonal cycle in the tropical Pacific, Manuscript in preparation, 1987.

Meyers, G., Seasonal variation in transport of the Pacific North Equatorial Current relative to the wind field, *J. Phys. Oceanogr., 5*, 442-449, 1975.

Munk, W., Internal waves and small scale processes, in Evolution in Physical Oceanography, MIT Press, Cambridge, Mass., 264-291, 1981.

National Academy of Sciences, U.S. Participation in the TOGA Program--A Research Strategy, National Academy Press, Washington, D.C., 24 pp., 1986.

Picaut, J., R. Tournier and V. Fabre, Champs mensuel 1979-1985 de température, hauteurs dynamiques et courants géostrophiques, deduits de mesures XBT 0-400 m le long des trois rails moyens de navigation dans le Pacifique tropical, Manuscript in preparation, 1987.

Rebert, J.P., J.R. Donguy, G. Eldin and K. Wyrtki, Relations between sea level, thermocline depth, heat content and dynamic height in the tropical Pacific Ocean, *J. Geophys. Res., 90*, 11719-11725, 1985.

Roed, L.P. and O.M. Smedstad, 1984: Open boundary conditions for forced waves in a rotating fluid. *SIAM J. Sci. Stat. Comput.*, 5, 414-426.

Sadler, J.C. and B.J. Kilonsky, Deriving surface winds from satellite observations of low-level cloud motions, *J. Clim. Appl. Met., 24*, 758-769, 1985.

Weisberg, R.H., D. Halpern, T.Y. Tang and S.M. Hwang, M^2 tidal currents in the eastern equatorial Pacific Ocean, *J. Geophys. Res.*, in press, 1987.

White, W.B., G. Meyers and K. Hasunuma, Space/time statistics of short-term climate variability in the western North Pacific, *J. Geophys. Res., 87*, 1979-1989, 1982.

White, W.B., Meyers, G.A., J.R. Donguy and S.E. Pazan, Short-term climatic variability in the thermal structure of the Pacific Ocean during 1979-1983, *J. Phys. Oceanogr., 15*, 917-935, 1985.

Wunsch, C. and A.E. Gill, Observations of equatorially trapped waves in sea level variations, *Deep-Sea Res., 10*, 449-455, 1976.

MOUILLAGES CHAINES A THERMISTANCES A 165°E

I. MISE EN PLACE ET PREMIERS RESULTATS

Un prototype de bouée ATLAS a été réalisé au NOAA/PMEL de Seattle et mis en place à 2°S-110°W, dès novembre 1984. Cette bouée, ancrée par grande profondeur et munie d'une chaîne à thermistances, transmet ses informations, par moyennes journalières, en temps quasi-réel par le système ARGOS. La partie électronique de cette bouée assure l'acquisition des mesures de températures de l'air et de l'eau de 0 à 500m sur 11 niveaux. La correction des déplacements verticaux éventuels de la ligne de mouillage est assurée par des mesures de la pression à 300 et 500m. Les versions récentes de bouées ATLAS sont aussi équipées de capteur de vent. Ainsi ce système de mesures, mis en place dans la bande équatoriale du Pacifique, est très bien adapté pour permettre le suivi du phénomene El Nino et de ses précurseurs et étudier tout évènement dans le guide d'ondes équatoriales.

Profitant de la radiale bi-annuelle SURTROPAC-TOGA du NO Coriolis le long du méridien 165°E, nous avons établi une coopération avec S.P.Hayes du NOAA/PMEL et son équipe pour mettre en place, vérifier et renouveler chaque année un certain nombre de bouées ATLAS le long du méridien 165°E. Cette opération, dont le financement de départ a été assuré essentiellement par la NOAA, a débuté en juillet 1985. La transmission ARGOS des données de la bouée à 2°N a été intermittente, mais une sauvegarde sur cassette est aussi assurée dans l'ensemble électronique de la bouée. Celle à 2°S a fonctionné, avec quelques problèmes aux niveaux des derniers capteurs, jusqu'en janvier 1986, date d'une tentative de piratage par un navire de pêche. Par chance, le NO Coriolis assurait la campagne SURTROPAC 5 vers la même période. J.Marchand, électronicien du Groupe SURTROPAC, revenait juste d'un stage de trois semaines au NOAA/PMEL pour s'initier aux équipements électroniques de ces bouées ATLAS et à leurs techniques de mise à l'eau (rapport joint). Il a pu donc effectuer les réparations nécéssaires pour assurer la remise en route des transmissions ARGOS. Vers la mi-mai et, probablement par suite du cyclone qui a ravagé les Iles Salomon, les deux bouées ont cessé d'émettre. La campagne SURTROPAC 6 de juin-juillet 1986 a permis de récupérer seulement celle à 2°N et la cassette de données correspondantes et de remettre en place deux nouveaux mouillages. Cette même campagne du NO CORIOLIS a aussi servi à récupérer un mouillage courantométrique équatorial à 165°E mis en place en janvier 1986 par un bateau chinois dans le cadre d'une coopération TOGA américano-chinoise. Ainsi, 165°E se trouve être le rail le mieux suivi du programme TOGA. C'est pourquoi nous nous efforçons de développer ce réseau ATLAS le long de ce méridien.

En 1987, un financement direct du MRES a permis de rajouter un mouillage ATLAS à 5°S et, lors de la prochaine campagne du NO Coriolis SURTROPAC 9 de Janvier 1988, une bouée ATLAS à 5°N va être installée. Un financement attendu en 1987-88 de l'US-TOGA, du PNEDC et du MRES, va permettre de maintenir ces quatre mouillages à 165°E et probablement de les étendre par un cinquième à 8°N.

La Figure 1 est un exemple des informations collectées, de juillet 1985 à avril 1987, par la bouée ATLAS à 2°S-165°E: température de l'air et de la surface de la mer, profondeur de l'isotherme 20°C, tracé des isothermes et à partir de juillet 1986, composantes du vent. Toutes ces données de moyenne journalière des mouillages ATLAS le long du méridien 165°E sont récupérées chaque jour au NOAA/PMEL via le système ARGOS. Elles sont validées et pour les températures en profondeur, corrigées des éventuelles variations de profondeur dans la ligne de mouillage. L'ensemble de ces informations est ensuite regroupé par mois pour être expédié au Centre ORSTOM de Nouméa, via le système français de transmission de données par paquet TOMPAC du Pacifique Sud. Selon nos besoins, cette cadence de transmission peut être accélérée.

Parallèlement à ces mouillages situés dans la partie ouest du Pacifique Equatorial, et dans le cadre du programme américain EPOCS (Equatorial Pacific Ocean Climate Studies), d'autres mouillages ATLAS ont été mis en place le long des méridiens 170°W, 140°W, 125°W et 110°W de 1985 à 1987 (Figure 1). Malgré une amélioration des systèmes électroniques et des lignes de mouillages par l'équipe de S.P.Hayes, nous avons enregistré, lors de conditions météorologiques normales, de nouvelles pertes à 165°E qui peuvent être imputées aux navires de pêches. Nos mouillages agissent en effet comme des radeaux agrégatifs et le NO Coriolis a déja noté une longue ligne juste à proximité d'une ATLAS. Néanmoins, à la date de rédaction du présent rapport (Octobre 1987), dix bouées ATLAS du réseau TOGA-TAO (Thermal Array for the Ocean) sont opérationelles et transmettent 100% de leurs données. La bouée ATLAS à 5°N-165°E va être mise en place par le NO Coriolis en janvier 1988, celle à 0°-170W en mai 1988 et les deux mouillages ATLAS à 5°N-140°W et 9°N-140°W ainsi qu'un mouillage courantométrique à 7°N-140°W vont ête installés en juin 1988.

Les figures 3(a-c) illustrent parfaitement l'utilité de tels mouillages ATLAS pour appréhender El Nino. Dès novembre 1986 une série de coups de vent d'ouest, à l'équateur, semblent avoir initié ce phénomène. Il se traduit par un enfoncement des isothermes à 140°W à partir de décembre, suivi d'un relèvement à 165°E puis d'un enfoncement marqué à 110°W. Il semble donc que la région autour de 165°W soit un point nodal de cet évènement El Nino 1986-87. Comme attendu les variations de température de surface ont été plus marquées à 110°W qu'à 140°W et 165°E. On notera cependant une accroisement régulier de la température de surface à 140°W qui s'est poursuivi après avril 1987.

Parallèlement à ces descriptions d'El Nino qui ont été régulierement présentées par S.P.Hayes dans les "Climate Diagnostics Bulletin" et très commentées dans "ENSO-INFO", des analyses plus détaillées ont été entreprises à partir de ces séries temporelles uniques. En particulier nous avons estimé les variations temporelles des courants géostrophiques à l'équateur par l'utilisation de la dérivée seconde du champ méridien de hauteurs dynamiques. Ce dernier champ a été déduit des séries temporelles de température mesurées avec ces mouillages ATLAS et les capteurs de température des mouillages courantométriques équatoriaux à 110°W et 165°E (J.Picaut, S.P.Hayes et M.J.McPhaden, manuscrit en préparation).

D'autres études sont en cours ou envisagées, comme la relation entre la pente méridienne autour de l'équateur et les tensions de vent N-S, la recherche d'ondes mixtes de Rossby-gravité à 165°E et le recalage temporel des mesures effectuées par les croisières quadri-annuelles SUTROPAC et américano-chinoise le long du méridien 165°E.

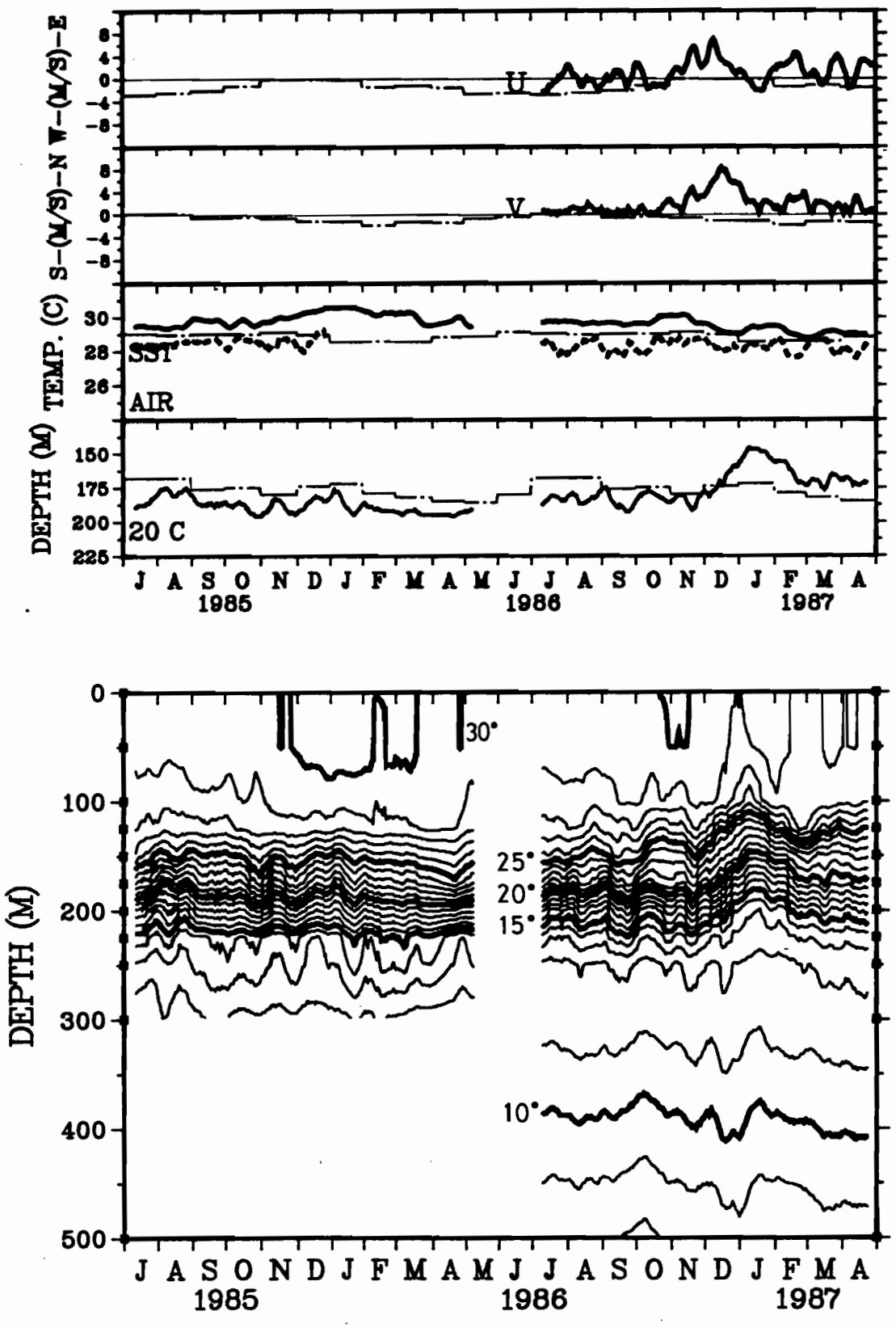

Figure 1. Exemple de tracés déduits des mesures de la bouée ATLAS à 2°S-165°E, de juillet 1985 à avril 1987.
Figure du haut: composantes U et V du vent (positives respectivement vers l'est et vers le nord), température de surface de l'eau (trait continu), température de l'air (trait discontinu) et profondeur de l'isotherme 20°C. Les courbes en trait discontinu alterné correspondent aux moyennes climatologiques.
Figure du bas: tracé des isothermes.

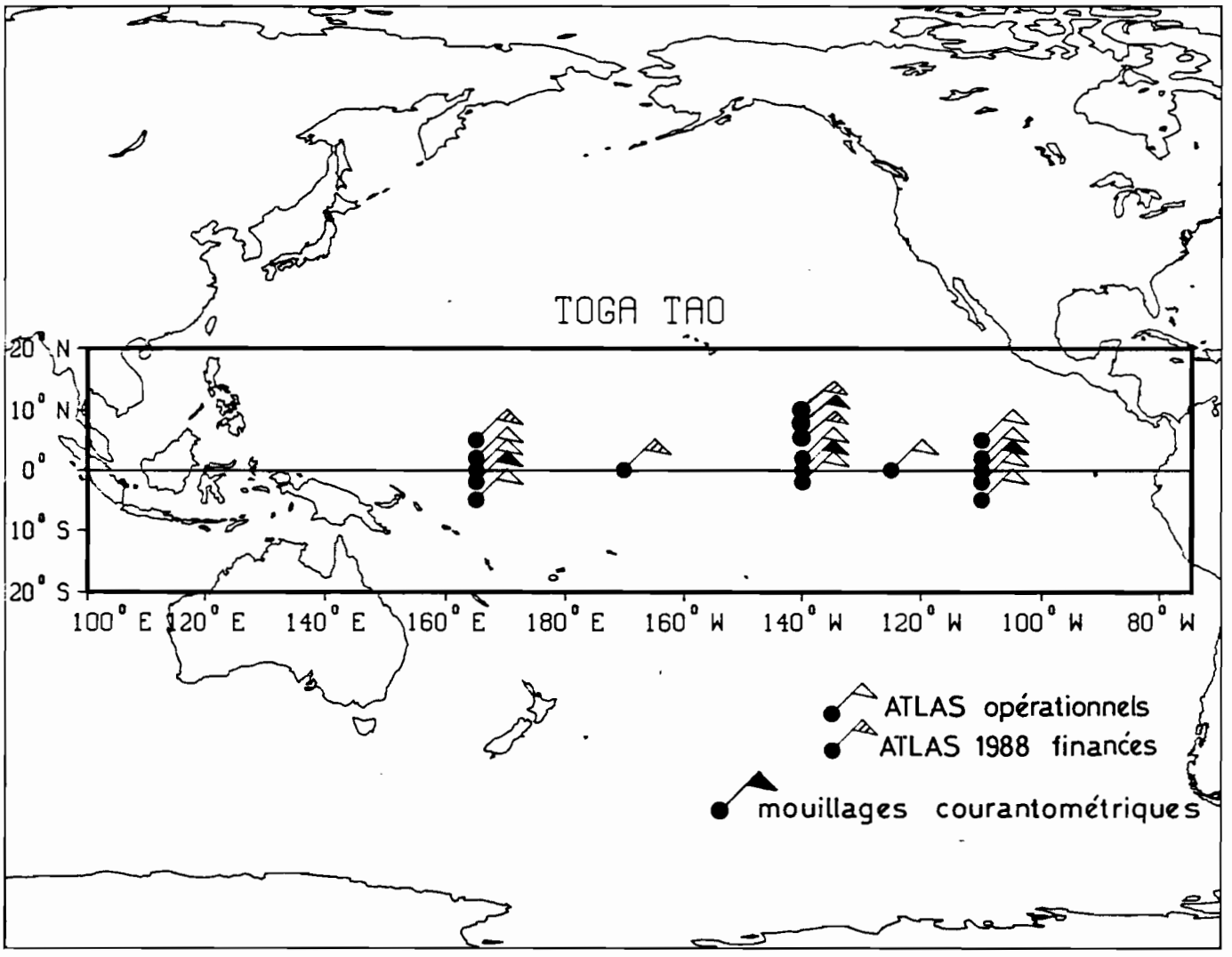

Figure 2. Position des mouillages ATLAS du réseau TOGA-TAO et des mouillages courantométriques.

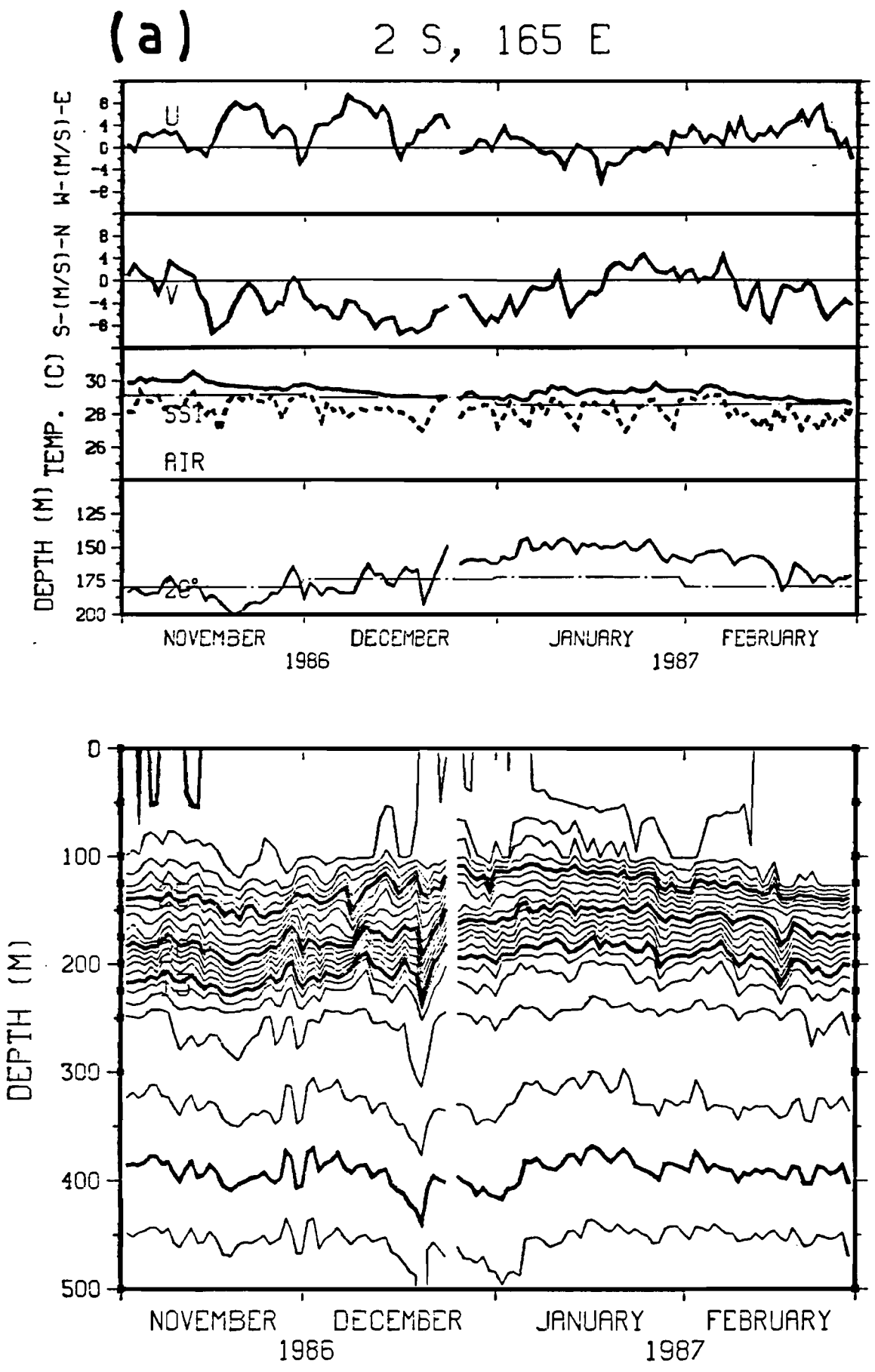

Figure 3. Mise en évidence de l'El Nino 1986-87 à travers les données ATLAS. (a) 2°S-165°E, (b) 2°S-140°W (c) 2°S-110°W.

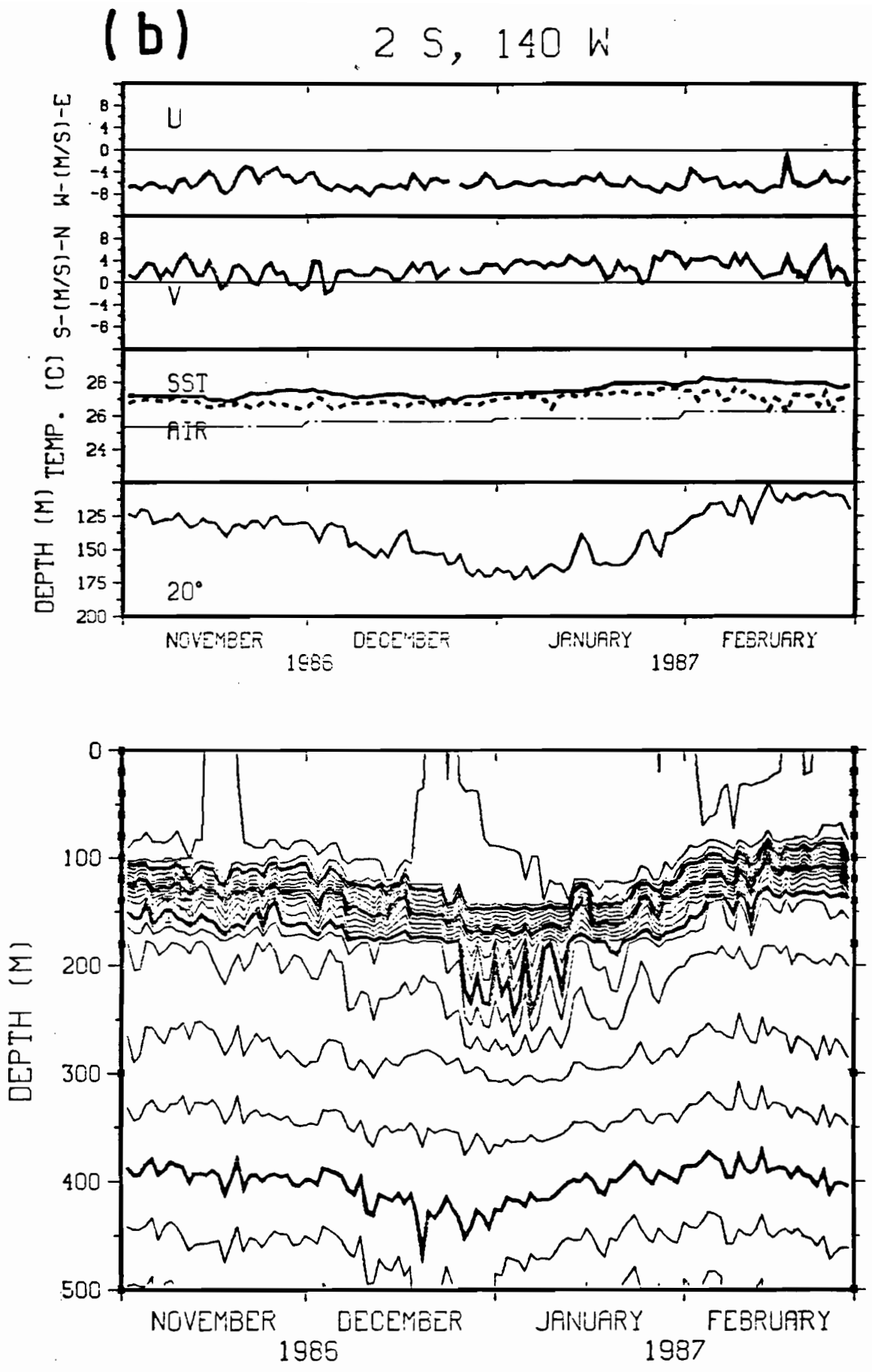
(b)
2 S, 140 W
U
V
SST
AIR
20°
DEPTH (M) TEMP. (C) S-(M/S)-N W-(M/S)-E
NOVEMBER
DECEMBER
JANUARY
FEBRUARY
1986
1987
DEPTH (M)

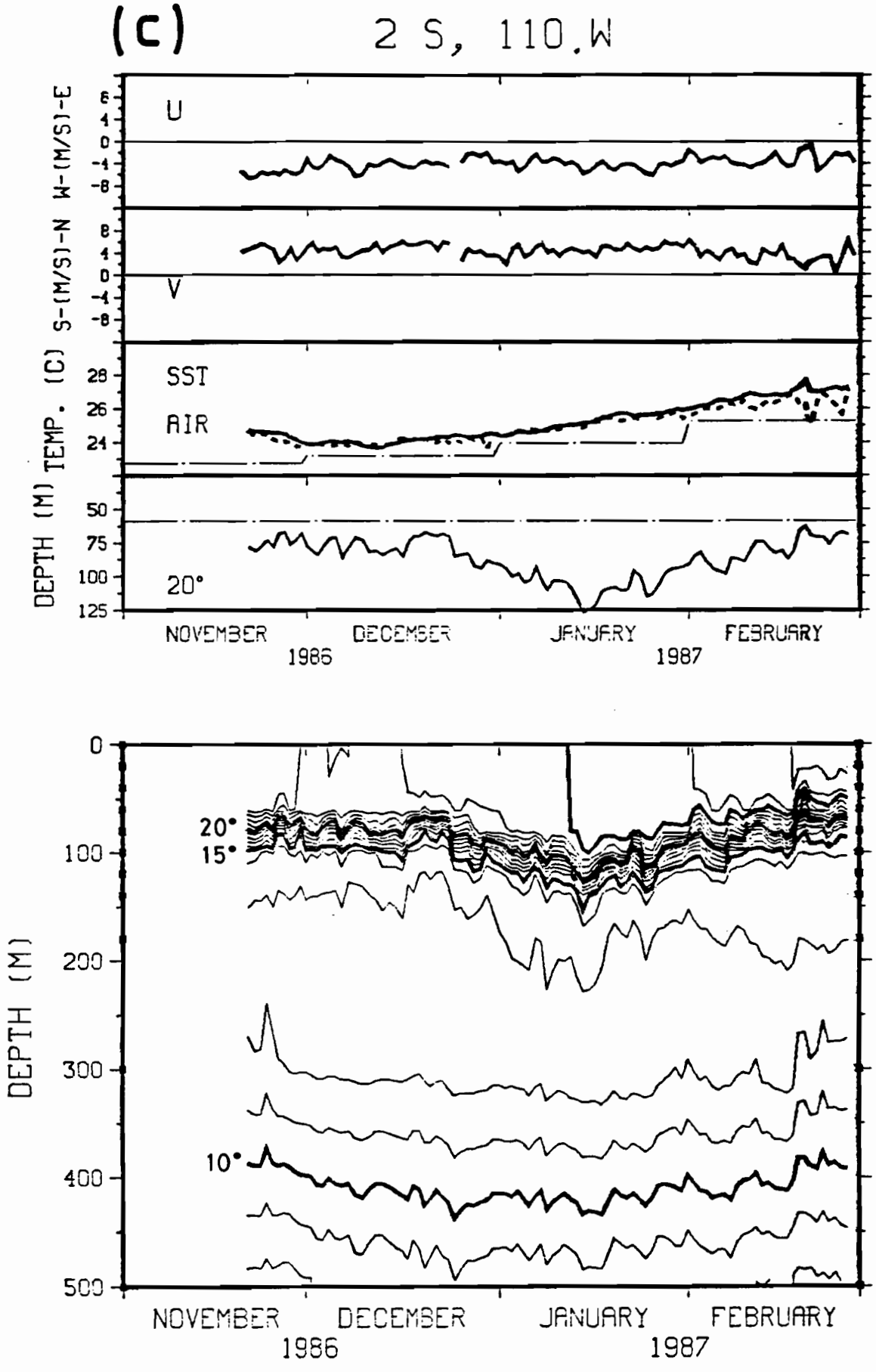
(C)
2 S, 110.W
U
V
SST
AIR
20°
DEPTH (M) TEMP. (C) S-(M/S)-N W-(M/S)-E
NOVEMBER
DECEMBER
JANUARY
FEBRUARY
1986
1987
20°
15°
10°
DEPTH (M)

II. RAPPORT DE STAGE AU NOAA/PMEL

1-21 décembre 1985

(J.Marchand)

Ce stage se situe dans le cadre du programme TOGA au titre des échanges scientifiques et techniques, notamment avec le PMEL/ NOAA (Pacifique Marine Environmental Laboratory), Seattle Etat de Washington. Il a porté sur l'initiation aux techniques du système chaînes à thermistances ancrées ATLAS (Autonomes Temperature Lines Acquisition). Les chaînes à thermistances ancrées permettent une surveillance continue de la structure thermique de l'océan, entre 0 et 500 m, dans la zone équatoriale. Elles viennent en complément du réseau de mesures XBT puisque déployées dans des zones non couvertes par le réseau. Le système ATLAS assure l'acquisition des mesures de vent, de températures de l'air et de l'eau, de la surface à 500 m, ainsi que de la pression à 300 et 500 m pour la correction des déplacements verticaux éventuels de la ligne de mouillage. Les données sont transmises en temps réel sur le réseau ARGOS. Ces données doivent permettre une étude du phénomènes d'El Nino et de ses précurseurs : variabilité thermique basse fréquence entre vent et contenu thermique de l'océan dans la région proche de l'équateur, contraintes locales et lointaines d'ondes équatoriales, relation du changement du contenu de chaleur de l'océan par interaction local air-mer et estimation de la circulation océanique, calcul des indices de transport géostrophique et comparaison continue des séries de mesures avec les modèles théoriques. Ce stage a été décidé à l'issue de la croisière SURTROPAC de juillet 1985, au cours de laquelle j'avais assisté les techniciens du PMEL/NOAA pour le mouillage des bouées ATLAS à 2°S, 2°N sur le 165°E, rail des croisières bi-annuelles SURTROPAC. Il était apparu opportun d'acquérir les connaissances nécessaires pour de ponctuelles interventions techniques mais surtout dans l'optique du projet ORSTOM/PMEL-NOAA pour le mouillage de deux ou quatre bouées ATLAS en complément de celles déployées en juillet 1985 avec le N.O. CORIOLIS.

Le stage s'est déroulé au Centre PMEL/NOAA de Seattle, du 1er au 21 décembre 1985. Il a eu pour objet l'étude de la réalisation des divers éléments constituants le système ATLAS, en particulier l'électronique, la préparation de l'équipement immergé et en rappel, la procédure de déploiement :

- câble d'acier : montage des cosses d'amarrage.
- câble électronique : coupe des longueurs pré-déterminées et préparation des liaisons mécaniques et électriques.
- cordes nylon : montages des cosses plastiques et épissures.
- test d'élongation des cordes nylon.

1 - Principe (fig.1) :

Le système est conçu autour d'une bouée toroïdale à ligne de mouillage tendue. Un câble électrique de 500 m de long, agrafé à la ligne, comporte dix capteurs de température et deux capteurs de pression. Sur la bouée une électronique à microprocesseur gère l'acquisition, la sauvegarde sur cassette et la transmission en temps réel sur réseau ARGOS, des données de température et de pression de la chaîne plus les températures de surface et de l'air, soit 14 données. La dernière version permet aussi la mesure de vent (vitesse et direction).

2 - Equipement de surface :

2.1. - la bouée toroïdale (fig. 2) d'environ 2,3 m de diamètre extérieur et de 80 cm de diamètre de couronne, est en fibre de verre passée sur une armature en acier inox, celle-ci comporte 3 traverses, espacées de 120°, dépassant les surfaces supérieures et inférieures de la bouée, et qui servent de points de fixation de la tour d'aluminium et du trépied d'amarrage de la ligne. De la mousse est injectée à l'intérieur de la bouée maintenant ainsi sa flottabilité en cas de dommage de la coque. La flottabilité de la bouée est supérieure à 3 tonnes.

2.2. - Une tour en aluminium, à 3 pieds et de 2,5m de hauteur comporte quatre plaques de contreplaqué marin. La plaque supérieure supporte le réflecteur radar sur la deuxième est fixé le support de l'antenne ARGOS. La troisième sert d'appui au tube électronique et celle du bas de protection contre le clapot. La tour est fixée avec des isolateurs en Derlin aux traversées supérieures de la bouée. Le capteur de température de l'air est fixé sur un des pieds de la tour, à environ 1,80m.

2.3. - Le module électronique :

2.3.1. - Un tube-conteneur en aluminium, traité comprend, de bas en haut le PTT (Plateform Terminal Transmitter) ARGOS, les batteries au lithium, les cartes CPU et E/S et l'enregistreur à K7. Les liaisons électriques entre l'électronique et les connecteurs extérieurs sont faites au travers de filtres RF (radio frequency). Le chapeau du tube comporte les connecteurs étanches de la chaîne à thermistances, des capteurs températures air et surface, de l'antenne ARGOS et du terminal, de plus un commutateur étanche permet la mise sous tension et le test du système (à partir d'une simple Télétype) sans ouverture du tube.

2.3.2. - La carte contrôleur, CPU, a été développé par le PMEL autour du micro-processeur 1806 RCA. Cette carte comporte le programme en EPROM et les circuits assurant :

- la commande de l'acquisition des données toutes les 10 minutes et le calcul de leur moyenne toutes les six heures.
- le contrôle de l'enregistreur Memodyne
- le contrôle des données vers le PTT
- la communication par RS 232 avec un terminal.

2.3.3. - La carte E/S comprend :

- le décodage d'adresse des E/S, selon la technique de topographie mémoire (memory-mapped)
- la base de temps générant les interruptions d'achantillonnage et de calcul de moyenne
- l'interfaçage et contrôle des chaînes de capteurs (il y a 2 chaînes de capteurs, voir 3.1.)
- la détection et conversion des données des capteurs
- la logique de commande et d'état des chaînes de capteurs.

3 - La chaîne à thermistances :

3.1. - Le câble électrique de 500 m a 3 conducteurs, un est commun et les 2 autres se partagent les capteurs en chaîne 1 et 2, ils assurent l'alimentation et la transmission des données des capteurs. La technique d'acquisition des données est celle du multiplexage temporelle. Les chaînes sont alimentées successivement, les capteurs transmettent leurs données l'un après l'autre durant 2 secondes selon la table de temps :

Capteurs	Chaîne	Délai en seconde (après mise sous tension)
temp. air	1	2
temp. surface	2	2
temp. 25 m	1	6
50 m	2	6
75 m	1	10
100 m	2	10
125 m	1	14
150 m	2	14
200 m	1	18
300 m	2	18
400 m	1	22
500 m	2	22
Pression 300 m	1	26
Pression 500 m	2	26

3.2. - L'électronique des capteurs est identique qu'il s'agisse de température ou de pression. Les circuits comprennent un régulateur de tension 5 Volt, une base de temps gérant les délais et la période de transmission, un convertisseur tension/fréquence asservi par le capteur et pilotant un interrupteur statique. L'électronique présente sur le câble l'alimentant, un signal série modulé en courant. La plage de mesure va de 8°C à 32°C pour la température de la pression atmosphérique à 750 psi pour la pression. Les capteurs et leur électronique sont montés à l'intérieur du tube en PVC qui est rempli de résine (fig.3).

4 - La ligne est composée d'un câble acier à couple de torsion compensé, gainé de plastique de 700 m de longueur gréé au trépied par une chaîne de 50 cm. A l'autre extrémité est fixé un émerillon de 5 tonnes, puis autant de corde de nylon pré-étiré , par longueur d'environ 500 m (à cause d'impératifs mécaniques de fabrication) qu'il est nécessaire pour le mouillage. La dernière longueur de nylon est reliée à l'ancre de 2,5 tonnes, par un émerillon de 3 tonnes et 10 m de chaîne de 1/2 pouce.

5 - Une attention particulière a été portée aux caractéristiques mécaniques : efforts de tension prévenus par test d'élongation, manilles et émerillons correctement dimensionnés, élimination des couples électriques par isolateur en Delrin entre chaque élément mécanique de métal différent. Il est à noter que le système de sub-surface est très résistant et insensible aux morsures des poissons. Il comporte en effet un câble métallique long de 700 m, un câble électrique ayant une double armature en acier et enfin le

le PVC des modules capteurs est très résistant. Le principe de deux chaînes de capteurs offre une sécurité de mesure en cas de problème sur l'une d'elle.

6 - Les techniques de réalisation du système ATLAS sont parfaitement maitrisées, facilitées, il est vrai par l'utilisation de matériels bien adaptés, et grâce à l'équipe bien structurée et très enthousiaste du PMEL. Le stage s'est d'autant mieux déroulé sur le plan technique, que j'ai été bien accepté par l'ensemble de l'équipe, cela est essentiel pour l'avenir de nos relations techniques avec le PMEL.

7 - A l'issue du stage et sur la demande de J. PICAUT du Groupe SURTROPAC de Nouméa nous avons discutés avec S. HAYES, responsable scientifique, et H. MILBURN responsable technique, des problèmes matériels et techniques que nous poseraient la réalisation de deux bouées à chaînes à thermistances sur financement français.

1. Le flotteur, armature acier et fibre de verre, ainsi que la tour aluminium et le trépied peuvent être réalisés à Nouméa.
2. L'électronique, les capteurs et le montage ne pouvant techniquement et matériellement pas être réalisés à Nouméa, seraient fournis par le PMEL, contre par exemple la prise en charge par TOGA France des frais ARGOS d'un montant équivalent.
3. La ligne du mouillage-câble métallique gainé, corde nylon, manilles, émerillons et autres accessoires, seraient achetés aux USA, par l'intermédiaire éventuel du PMEL.
4. Pour la préparation du matériel à Nouméa, le PMEL pourrait mettre à notre dispositon un technicien, l'autre solution serait de préparer l'équipement au PMEL, et serait certainement plus commode.
5. En ce qui concerne le déploiement des bouées, l'aide technique du PMEL nous serait assurée.
6. Les données, après réception pré-traitement seraient transmises par Télémail à Nouméa par moyennes journalières.
7. Dans l'hypothèse ou l'ORSTOM aurait le financement pour une ou deux chaînes à thermistances ATLAS pour 1987, le PMEL pourrait faire l'avance de deux systèmes complets pour la campagne de janvier 1987. Dans tous les cas il s'agirait de travailler en

étroite coopération avec nos partenaires américains, l'intérêt de l'ORSTOM étant complémentaire de celui du PMEL/NOAA.

Ces propositions seront réactualisées en fonction des moyens dont l'ORSTOM pourra disposer tant sur le plan financier, que matériel et humain.

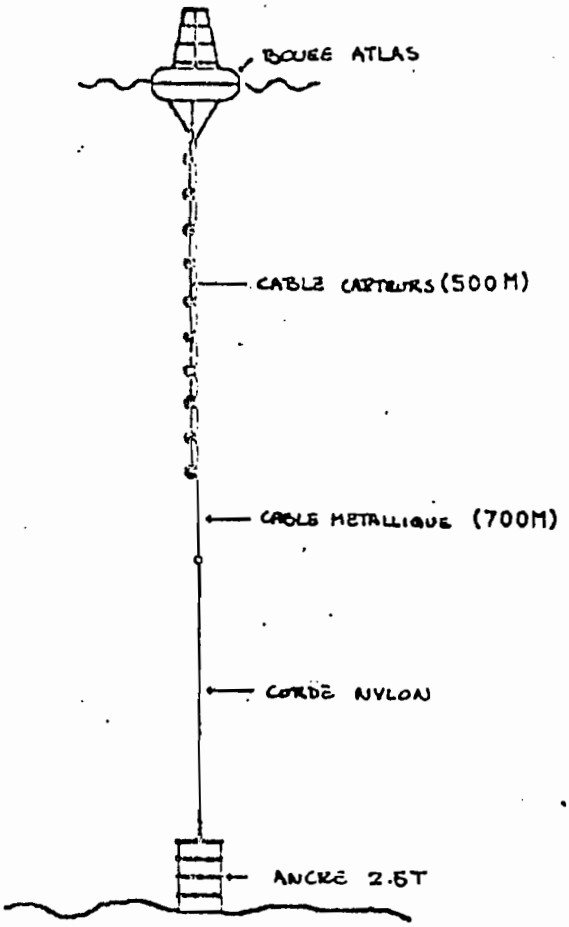

Figure 1

ATLAS . CHAINE A THERMISTANCES ANCREES

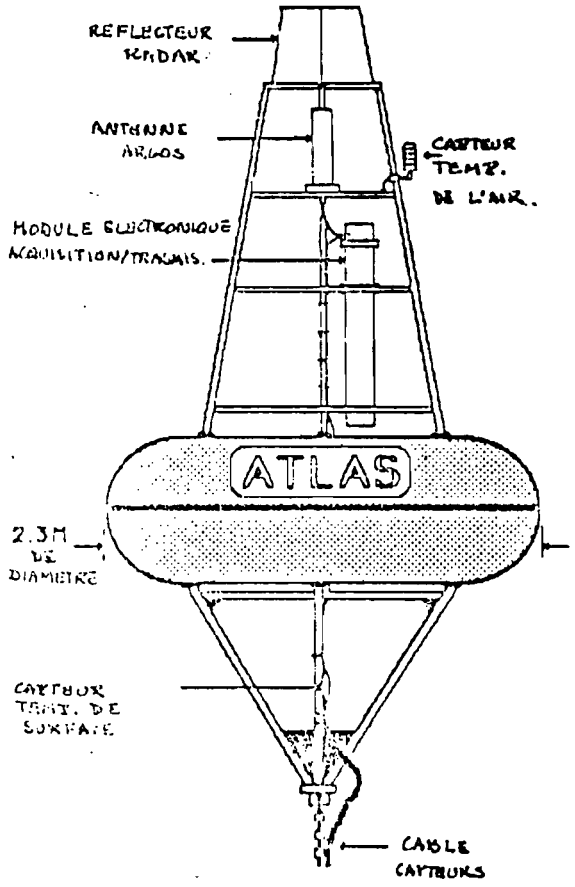

Figure 2

BOUEE ATLAS

Imprimé par le Centre ORSTOM
de NOUMEA

Novembre 1987